



HAL
open science

Nonintrusive Nocturnal Remote Monitoring of Vital Signs in Ambient Assisted Living Environments

Ibrahim Sadek Ibrahim Hussein Tahoun

► **To cite this version:**

Ibrahim Sadek Ibrahim Hussein Tahoun. Nonintrusive Nocturnal Remote Monitoring of Vital Signs in Ambient Assisted Living Environments. Systems and Control [cs.SY]. Université Montpellier, 2018. English. NNT : 2018MONTTS102 . tel-02152975

HAL Id: tel-02152975

<https://theses.hal.science/tel-02152975>

Submitted on 11 Jun 2019

HAL is a multi-disciplinary open access archive for the deposit and dissemination of scientific research documents, whether they are published or not. The documents may come from teaching and research institutions in France or abroad, or from public or private research centers.

L'archive ouverte pluridisciplinaire **HAL**, est destinée au dépôt et à la diffusion de documents scientifiques de niveau recherche, publiés ou non, émanant des établissements d'enseignement et de recherche français ou étrangers, des laboratoires publics ou privés.

THÈSE POUR OBTENIR LE GRADE DE DOCTEUR DE L'UNIVERSITÉ DE MONTPELLIER

En Informatique

École doctorale : Information Structures Systèmes I2S

Unité de recherche : Image and Pervasive Access Lab., CNRS UMI 2955, Singapour

Titre de la thèse

Télésurveillance Nocturne Non Intrusive De Signes Vitaux Dans Des Environnements D'assistance A L'autonomie A Domicile

Présentée par Ibrahim SADEK IBRAHIM HUSSEIN TAHOUN

Le 10 Avril 2018

Sous la direction de Mounir MOKHTARI, Zhang HAIHONG, Jit BISWAS

Devant le jury composé de :

[M. Timo JAMSA, Professeur, Faculté de Médecine, Université d'Oulu, Finlande]

[Rapporteur]

[M. David FOFI, Professeur, Université de Bourgogne, France]

[Rapporteur]

[M. Philippe FRAISSE, Professeur, Université de Montpellier, France]

[Examineur]

[M. Eric CAMPO, Professeur, Université de Toulouse, France]

[Examineur]

[M. Mounir MOKHTARI, Professeur, Institut Mines-Télécom, France]

[Directeur de thèse]



UNIVERSITÉ
DE MONTPELLIER

THESIS TO OBTAIN THE DEGREE OF DOCTOR OF PHILISHOPIY DELIVERED BY THE UNIVERSITY OF MONTPELLIER

Specialty Computer Science

Doctoral School: Information, Structure and Systems (I2S)
Research Unit: Image and Pervasive Access Lab, CNRS UMI 2955, Singapore

Thesis Title

Nonintrusive Nocturnal Remote Monitoring of Vital Signs in Ambient Assisted Living Environments

Presented by Ibrahim SADEK IBRAHIM HUSSEIN TAHOUN

On 10 April 2018

Under the Supervision of Mounir MOKHTARI, Zhang HAIHONG, Jit BISWAS

In front of a jury composed of:

[M. Timo JAMSA, Professor, Faculty of Medicine, University of Oulu, Finland]

[Reviewer]

[M. David FOFI, Professor, University of Burgundy, France]

[Reviewer]

[M. Philippe FRAISSE, Professor, University of Montpellier, France]

[Examiner]

[M. Eric CAMPO, Professor, University of Toulouse, France]

[Examiner]

[M. Mounir MOKHTARI, Professor, Institute Mines Telecom, France]

[Thesis Director]



UNIVERSITÉ
DE MONTPELLIER

Acknowledgments

First and foremost, I would like to thank all the people who supported and collaborated with me to achieve this work. I could not have made it without your help.

I would also like to extend my deepest gratitude to my thesis director, Professor. Mounir Mokhtari, the Image and Pervasive Access Lab's (IPAL) director, for giving me the opportunity to explore this work and for his expert advice, and encouragements. I would like to thank him for giving me the opportunity to interact and collaborate with scientists and industrial partners throughout meetings and demos. I would also like to thank him for the freedom and trust which he granted to me during my work.

I would like to give great thanks to Professor. Jit Biswas who gave me a lot of support and guidance throughout my thesis. Further, he assisted me a lot in my publications by giving advice and reviewing my papers. I would also like to thank him for initiating the collaboration between IPAL and Khoo Teck Puat (KTPH) hospital, Singapore.

Further thanks go to Professor. Bessam Abdulrazak for his interest in my research and also for his valuable contributions in my publications.

I would like to extend my appreciation to Dr. Edwin Seet for his role in data collection during our clinical study at KTPH. Moreover, I would also like to thank him for his contribution to my journal publication.

Special thanks go to Ms. Chia Audris for his valuable contribution and support during our clinical study. Without her support, we could not have completed the study.

Special thanks go to my colleagues at IPAL for their help and support during my stay, especially Dr. Thibaut Tiberghien, Dr. Joaquim Bellmunt, Martin Kodys, Antoine Demarasse, Fabien Clavier, Angela Saenz, Anssuya Etwaro. I also thank my fellow PhDers and my other colleagues.

I would like to thank my colleagues at the University of Montpellier for their help and support in my Ph.D. registration, especially Dr. Hamdi Aloulou, Firas Kaddachi, and Dr. Romain Endelin.

My Ph.D. was partially supported by A*STAR Graduate Academy (AGA). I would also like to give warm thanks to Prof. Zhang Haihong who accepted to be my co-supervisor and for his follow up throughout my research.

And last, but not least important, very special thanks go to my beloved wife Lamees, parents, who supported and encouraged me during stressful moments.

Abstract

Nonintrusive and long-term monitoring of human physiological functions are essential requirements for early diagnosis and prophylaxis due to many reasons, one of the most important being improving the quality of life. In this research, we focus on sleep monitoring as a substantial vector of quality of life. Sleep is a fundamental and vital physiological function. Getting enough quality sleep is necessary to a person's mental health, physiological well-being, quality of life, and safety. Sleep-disordered breathing, specifically obstructive sleep apnea can result in serious health issues, including hypertension and stroke.

The current approaches for diagnosing sleep disorders are burdensome, intrusive, and can affect the patient's sleep quality. As a result, there is a crucial need for less cumbersome systems to diagnose sleep-related problems. We propose to use a novel nonintrusive sleep monitoring system based on a microbend fiber-optic mat placed under the bed mattress. The sleep quality is assessed based on different parameters, including heart rate, breathing rate, body movements, wake up time, sleep time, night movement, and bedtime. The proposed system has been validated in a health and wellness environment in addition to a clinical environment as follows.

In the former case, the heart rate is measured from noisy ballistocardiogram signals acquired from 50 human volunteers in a sitting position using a massage chair. The signals are unobtrusively collected from a microbend fiber optic sensor embedded within the headrest of the chair and then transmitted to a computer through a Bluetooth connection. The heart rate is computed using the multiresolution analysis of the maximal overlap discrete wavelet transform. The error between the proposed method and the reference ECG is estimated in beats per minute using the mean absolute error where the system achieved relatively good results (10.12 ± 4.69) despite the remarkable amount of motion artifact produced owing to the frequent body movements and/or vibrations of the massage chair during stress relief massage. Unlike the complete ensemble empirical mode decomposition algorithm, previously employed for heart rate estimation, the suggested system is much faster. Hence, it can be used in real-time applications.

In the latter case, we evaluated the capacity of the microbend fiber optic sensor to monitor heart rate and respiration unobtrusively. In addition, we tested the capacity of the sensor in discriminating between shallow breathing and no breathing. The proposed sensor was compared to a three-channel portable monitoring device (ApneaLink) in a clinical setting during a drug-induced sleep endoscopy. Across all ten patients recruited for our study, the system achieved satisfactory results in the mean heart rate and the mean respiratory rate with an error of 0.55 ± 0.59 beats/minute and 0.38 ± 0.32 breaths/minute, respectively. Besides, the Pearson correlation coefficient between the proposed sensor and the reference device was 0.96 and 0.78 for heart rate and respiration, respectively. On the contrary, the proposed sensor provided a very low sensitivity ($24.24 \pm 12.81\%$) and a relatively

high specificity ($85.88 \pm 6.01\%$) for sleep apnea detection. It is expected that this preliminary research will pave the way toward unobtrusive detection of obstructive sleep apnea in real-time.

Following successful validation of the proposed system, we have successfully deployed our sleep monitoring system in thirteen apartments with mainly senior residents over six months. Nevertheless, in this research, we concentrate on a one-month deployment with three senior female residents. The proposed system shows an agreement with a user's survey collected before the study. Furthermore, the system is integrated within an existing ambient assisted living platform with a user-friendly interface to make it more convenient for the caregivers to follow-up the sleep parameters of the residents.

Keywords: Ballistocardiography; E-Health; Sleep apnea; Technology and services for assisted-living and elderly; Technology and services for home care; Vital signs

Résumé

En vue du diagnostic précoce et la prophylaxie, la surveillance des fonctions physiologiques humaines est exigée d'être essentiellement à la fois non intrusive et à long terme. Parmi nombreuses motivations, l'une des plus importantes est l'amélioration de la qualité de vie. Dans cette recherche, nous nous concentrons sur la surveillance du sommeil comme un vecteur substantiel de qualité de vie. Le sommeil est une fonction physiologique fondamentale et vitale. Avoir suffisamment de sommeil de qualité est nécessaire pour la santé mentale, pour le bien-être physiologique, pour la qualité de vie et pour la sécurité d'une personne. La respiration irrégulière pendant le sommeil, particulièrement l'apnée obstructive du sommeil, peut entraîner de graves problèmes de santé, y compris l'hypertension artérielle et accident vasculaire cérébral.

Les approches actuelles pour diagnostiquer les troubles du sommeil sont lourdes, intrusives et peuvent influencer sur la qualité du sommeil du patient. Il y a donc un besoin crucial de systèmes moins encombrants pour diagnostiquer les problèmes liés au sommeil. Nous proposons d'utiliser un nouveau système de suivi du sommeil non intrusif basé sur un tapis à fibre optique à microflexion placée sous le matelas de lit. La qualité du sommeil est évaluée en fonction de différents paramètres, y compris la fréquence cardiaque, le rythme respiratoire, les mouvements du corps, l'heure du réveil, la durée du sommeil, le mouvement nocturne et l'heure du coucher. Le système proposé a été validé dans un environnement de santé et de bien-être, en plus d'un environnement clinique comme suit.

Dans le premier cas, la fréquence cardiaque est mesurée à partir de signaux ballistocardiogramme bruités acquis de 50 volontaires en position assise à l'aide d'une chaise de massage. Les signaux sont recueillis discrètement à partir d'un capteur de fibre optique microflexible intégrée dans l'appui-tête de la chaise, puis transmis à un ordinateur par une connexion Bluetooth. La fréquence cardiaque est calculée à l'aide de l'analyse multi-résolution de la transformée discrète en ondelettes à chevauchement maximal. L'erreur entre la méthode proposée et électrocardiogramme de référence est estimée en battements par minute en utilisant l'erreur absolue moyenne où le système a obtenu des résultats relativement bons (10.12 ± 4.69) malgré la quantité remarquable d'artefact de mouvement produit en raison des fréquents mouvements corporels et/ou vibrations de la chaise de massage pendant le massage de soulagement du stress. Contrairement à l'algorithme complet de décomposition du mode empirique de l'ensemble, précédemment utilisé pour l'estimation de la fréquence cardiaque, le système proposé est beaucoup plus rapide. Par conséquent, il peut être utilisé dans les applications temps réel.

Dans ce dernier cas, nous avons évalué la capacité du capteur de fibre optique microflexible pour suivre la fréquence cardiaque et la respiration d'une manière discrète. En outre, nous avons testé la capacité du capteur dans la discrimination entre la respiration superficielle et pas de respiration. Le capteur proposé a été

comparé à un dispositif de surveillance portatif à trois canaux (ApneaLink) dans un milieu clinique au cours d'une endoscopie sous anesthésie. Parmi les dix patients recrutés pour notre étude, le système a obtenu des résultats satisfaisants quant à la fréquence cardiaque moyenne et quant à la fréquence respiratoire moyenne avec une erreur de 0.55 ± 0.59 battements/minute et de 0.38 ± 0.32 respirations/minute, respectivement. De plus, le coefficient de corrélation Pearson entre le capteur proposé et le dispositif de référence était de 0.96 et 0.78 pour la fréquence cardiaque et la respiration, respectivement. Au contraire, le capteur proposé a fourni une très faible sensibilité ($24.24 \pm 12.81\%$) et une spécificité relativement élevée ($85.88 \pm 6.01\%$) pour la détection de l'apnée du sommeil. On s'attend à ce que cette recherche préliminaire ouvre la voie vers la détection discrète de l'apnée obstructive du sommeil en temps réel.

Suite à la validation réussie du système proposé, nous avons déployé avec succès notre système de surveillance du sommeil pendant plus de 6 mois dans treize appartements habités principalement par les personnes âgées. Néanmoins, dans cette recherche, nous nous concentrons sur un déploiement d'un mois avec trois résidents seniors de sexe féminin. Le système proposé montre l'accord avec l'enquête utilisateur recueillie avant l'étude. En outre, le système est intégré dans une plateforme d'autonomie assistée existante avec une interface conviviale pour rendre plus commode pour les aidants le suivi des paramètres de sommeil des résidents.

Mots-clés: Balistocardiographie ; E-Santé ; Apnée du sommeil ; Technologie et services pour les personnes âgées et assistées ; Technologie et services pour les soins à domicile ; Signes vitaux

Publications

Papers in refereed journals

1. **Sadek, I.**, Seet, E., Biswas, J., Abdulrazak, B., Mokhtari, M., 2018. Noninvasive Vital Signs Monitoring for Sleep Apnea Patients: A Preliminary Study. *IEEE Access*, 6, pp.2506-2514. [Impact factor 3.244].
doi:10.1109/ACCESS.2017.2783939
2. **Sadek, I.**, Mokhtari, M., 2018. Nonintrusive Remote Monitoring of Sleep in Home-Based Situation. *Journal of medical systems*, Springer Nature, 42, 64. [Impact factor 2.456].
doi:10.1007/s10916-018-0917-6

Papers in refereed conferences

1. **Sadek, I.**, Biswas, J., Fook, V.F.S., Mokhtari, M., 2015. Automatic heart rate detection from FBG sensors using sensor fusion and enhanced empirical mode decomposition, in: 2015 IEEE International Symposium on Signal Processing and Information Technology (ISSPIT). IEEE, pp. 349–353.
doi:10.1109/ISSPIT.2015.7394358
2. **Sadek, I.**, Biswas, J., Yongwei, Z., Haihong, Z., Maniyeri, J., Zhihao, C., Teng, T.J., Huat, N.S., Mokhtari, M., 2016. Sensor data quality processing for vital signs with opportunistic ambient sensing, in: Proceedings of the Annual International Conference of the IEEE Engineering in Medicine and Biology Society, EMBS. Institute of Electrical and Electronics Engineers Inc., pp. 2484–2487.
doi:10.1109/EMBC.2016.7591234
3. **Sadek, I.**, Biswas, J., Abdulrazak, B., Haihong, Z., Mokhtari, M., 2017. Continuous and unconstrained vital signs monitoring with ballistocardiogram sensors in headrest position, in: 2017 IEEE EMBS International Conference on Biomedical and Health Informatics, BHI 2017. Institute of Electrical and Electronics Engineers Inc., pp. 289–292.
doi:10.1109/BHI.2017.7897262
4. **Sadek, I.**, Bellmunt, J., Kodyš, M., Abdulrazak, B., Mokhtari, M., 2017. Novel unobtrusive approach for sleep monitoring using fiber optics in an ambient assisted living platform, in: Lecture Notes in Computer Science (Including Subseries Lecture Notes in Artificial Intelligence and Lecture Notes in Bioinformatics). Springer Verlag, pp. 48–60.
doi:10.1007/978-3-319-66188-9_5

Contents

1	Introduction	1
1.1	Research Description	1
1.2	Current Healthcare Challenges	2
1.2.1	Growing Numbers of Elderly People	2
1.2.2	Prevalence of Chronic Diseases	4
1.2.3	Shortage of Caregivers	5
1.2.4	Rising Costs of Healthcare	5
1.3	Research Objectives of this Thesis	7
1.4	Structure of the Thesis	7
2	Background	9
2.1	Introduction	9
2.2	Cardiovascular System	10
2.3	Respiratory System	11
2.4	Physiology of Sleep	13
2.5	Sleep Monitoring	14
2.6	Polysomnography	15
2.7	Actigraphy	17
2.8	Consumer Sleep Tracking Devices	18
2.8.1	Wearable Sleep Tracking Devices	19
2.8.2	Sleep Tracking Apps on Smart-phones	20
2.8.3	Bed-Based Sleep Tracking Devices	22
2.9	Conclusion	25
3	Literature Review	27
3.1	Introduction	27
3.2	Ballistocardiography	28
3.2.1	Piezoelectric Polyvinylidene Fluoride-Based Sensors	31
3.2.2	Electromechanical Film-Based Sensors	35
3.2.3	Pneumatic-Based Sensors	40
3.2.4	Strain Gauges-Based Sensors	42
3.2.5	Hydraulic-Based Sensors	47
3.2.6	Fiber Optic-Based Sensors	50
3.3	Conclusion	53
4	System Design	55
4.1	Introduction	55
4.2	System Design	56
4.2.1	Suitable Sensor Selection	57
4.2.2	System Development	59

4.2.3	System Validation	60
4.2.4	UbiSMART Design	60
4.2.5	System Integration	61
4.3	Conclusion	62
5	Methodology	63
5.1	Introduction	63
5.2	Health and Wellness Application	64
5.2.1	Quality Processing of Fiber Optic Sensor Data	65
5.2.2	Application Specific Signal Data Quality	66
5.2.3	Data Processing	67
5.3	Clinical Application	82
5.3.1	Experimental Setup and Data Collection	86
5.3.2	Data Processing	88
5.4	Real-life Deployment	92
5.4.1	Data Collection	93
5.4.2	Data Processing	94
5.5	Conclusion	95
6	Results and Discussion	97
6.1	Introduction	97
6.2	Results of Health and Wellness Application	97
6.2.1	Wavelet Analysis Versus CEEMDAN Algorithm	102
6.3	Results of Clinical Application	105
6.3.1	Heart and Respiratory Rate Estimation	105
6.3.2	Sleep Apnea Event Detection	107
6.4	Results of Real-life Deployment	111
6.5	Conclusion	117
7	Conclusion and Future Directions	119
7.1	Conclusion	119
7.2	Future Directions	121
	Bibliography	123

List of Figures

1.1	Distribution of the world’s population by age and sex, 2017. Source: United Nations, Department of Economic and Social Affairs, Population Division (2017). <i>World Population Prospects: The 2017 Revision</i> . New York: United Nations.	3
1.2	Average annual rate of population changes for the world and by region, estimates, 1950 – 2015, and medium-variant projection, 2015 – 2100. Source: United Nations, Department of Economic and Social Affairs, Population Division (2017). <i>World Population Prospects: The 2017 Revision</i> . New York: United Nations.	4
1.3	An illustration of a sensor mat as an example of an IoT device in a medical setting.	6
2.1	Anatomy of the human heart.	10
2.2	A schematic view of the human respiratory system. Retrieved from Wikimedia Commons website: https://en.wikipedia.org/wiki/Respiratory_system	12
2.3	A sample hypnogram (defined by electroencephalogram) showing sleep cycles designated by increasing REM sleep.	13
2.4	An illustration of the location of the various electrodes and sensors used for monitoring sleep. Image courtesy: British Lung Foundation.	16
2.5	A 30-second epoch from the PSG. Image adapted from [Basner 2012].	17
2.6	Examples of wearable sleep tracker devices; (a) Zeo, (b) SleepImage, (c) Fitbit, (d) Lark, (e) WakeMate, (f) Jawbone, (g) BodyMedia SenseWear armband, (h) Hexoskin, and (i) ŌURA.	21
2.7	Examples of bed-sensor devices; (a) Emfit QS, (b) Beddit, (c) EarlySense, (d) Sleepspace Reston, (e) Withings Aura.	23
3.1	(a) Example of a typical BCG signal with letters used to designate the waves. The arrow indicates the position of the beginning of the electrical ventricular systole (QRS. complex of the electrocardiogram). Image adapted from [Starr 1939, Starr 1940, Pinheiro 2010b], (b) Aortic arch and force vectors coming from blood ejection by the left ventricle. Image adapted from [Eblen-Zajjur 2003].	28
3.2	Example of a typical electrocardiogram signal.	29
4.1	The deployable sensor mat and processing unit (Mat dimensions: 20 cm × 50 cm × 0.5 cm).	57
4.2	Longitudinal section of the microbend fiber-optic sensor.	58
4.3	Simplified view of UbiSMART AAL platform with sleep mat and its processing unit as a sensor.	61

4.4	UbiSMART user interface is organized in tiles and it provides following information: daily quantity of sleep (selected day) with updated bed occupancy status that changes the color of the icon and status line; aggregated week overview of sleep quantity; and heartbeat information.	62
5.1	Opportunistic remote monitoring of vital signs.	65
5.2	Screen capture of the labeling tool.	66
5.3	Flowchart of the quality processing system.	68
5.4	Two examples for informative and non-informative segments (sampling frequency: 50Hz).	69
5.5	BCG signal with a reference ECG signal. ECG is shown in 1 st row. However, BCG signal and its 6 th decomposition component are shown in 2 nd row (sampling frequency: 50Hz).	71
5.6	Intrinsic mode functions (DC1-DC9) of a typical BCG signal (Figure 5.5); the 6 th component shows a match with cardiac cycles (sampling frequency: 50Hz).	74
5.7	An example of a signal data quality processing (sampling frequency: 50Hz).	76
5.8	An example of a 60-second sleep signal (sampling frequency: 50Hz).	77
5.9	An example of a 60-second body movement signal (sampling frequency: 50Hz).	78
5.10	An example of a 60-second bed-exit signal (sampling frequency: 50Hz).	79
5.11	Example for three-level MODWT; $h_{\{.\}}$ is a high-pass filter, $g_{\{.\}}$ is a low-pass filter, $W_{\{.\}}$ is a wavelet coefficient, and $V_{\{.\}}$ is a scaling coefficients.	80
5.12	The flowchart of the proposed heart rate estimation method; BM: Body Movement, RR: Respiratory Rate, and MRA: Multiresolution Analysis.	80
5.13	Symlet-8 MODWT multiresolution decomposition of a BCG signal (sampling frequency: 50Hz).	81
5.14	The cepstrum of a 30-second ballistocardiogram signal; the heart beat interval (HBI) is 1.02 seconds.	82
5.15	The autocorrelation of a 30-second ballistocardiogram signal; the heart beat interval (HBI) is 1.64 seconds.	83
5.16	Drawing representing event and inter-event duration, as well as pre- and post-event amplitude (with upward deflection of flow during inspiration). Image adapted from [Jaimchariyatam 2013].	84
5.17	Sleep apnea sensor proposed by Zansors, LLC. Image adapted from [Jennifer 2017]	85
5.18	The positioning of the optical fiber mat on the operating room table.	86
5.19	Real deployment of the MFOS mat in the operating theatre of Khoo Teck Puat Hospital.	88
5.20	System components and operation of ApneaLink device (ApneaLink, ResMed, San Diego, California, USA).	89

5.21	Overall system flowchart; BM: Body Movement, HR: Heart Rate, and RR: Respiratory Rate.	90
5.22	An example of a 10-second body movement signal for patient No. 4.	91
5.23	An example of a 10-second sleep signal for patient No. 4.	92
5.24	The first, second, and third rows represent a typical 10-second time-window of the raw signal, the BCG signal along with the 4 th wavelet smooth coefficient, and the respiratory signal respectively; amplitude values were normalized between -1 and 1.	93
5.25	Overview of our unobtrusive monitoring in a living space.	94
5.26	Sleep mat integration at the three HDB apartments; (a) 1 st home with mat under sleeping rug, (b) 2 nd home with mat under bed mattress, (c) 3 rd home with mat under bed mattress.	95
5.27	Representation of a participant's night from our real-life deployment. Three typical signal shapes are labeled according to recognized conditions: <i>bed empty</i> , <i>bed motion</i> , <i>sleep</i> . Gantt diagram: Row "B" is the result of the signal processing from the bed sensor. Row "M" shows a very inaccurate detection using motion sensors (blank space indicates activity detection in other rooms out of scope). Row "S" indicates the participant's answer in the survey Table 5.3 about their waking and sleeping habits.	96
6.1	Bland-Altman plot between the reference ECG-derived heartbeat intervals to associated BCG-derived heartbeat intervals for Group1.	100
6.2	Bland-Altman plot between the reference ECG-derived heartbeat intervals to associated BCG-derived heartbeat intervals for Group2.	101
6.3	Box plots of the average MAE for CEEMDAN algorithm and wavelet methods regarding the average beats per minute across all 50 subjects.	103
6.4	BCG signal with the 4 th level smooth coefficient during a massage session (sampling frequency: 50Hz).	104
6.5	Box plots of the average MAE for best wavelet, FFT, cepstrum, and autocorrelation methods regarding the average beats per minute across all 50 subjects.	105
6.6	(a) Bland-Altman plot and (b) Pearson correlation plot of all patients regarding the HR measurement.	108
6.7	(a) Bland-Altman plot and (b) Pearson correlation plot of all patients regarding the RR measurement.	109
6.8	The first and second rows represent a 10-second time window of the BCG signal and the respiratory signal for patient No. 4.	111
6.9	Bland-Altman plot of waking-up time for resident No. 2; green <i>bigotimes</i> symbols represent Wednesday.	112
6.10	Bland-Altman plot of sleep time for resident No. 3 over deployment time.	113
6.11	Bland-Altman plot of waking-up time for resident No. 3 over deployment time.	114

6.12	Bland-Altman plot of total sleep time for the 2 nd resident over deployment time.	115
6.13	Bland-Altman plot of heart rate representation of resident No. 3 over deployment time.	116
6.14	Bland-Altman plot of breathing rate representation of resident No. 2 over deployment time.	116
6.15	Sleep disturbance distribution for resident No. 2 over deployment time; the moving average is computed using a time-window of three days.	117

List of Tables

3.1	Nomenclature of ballistocardiogram (normal displacement) signal [Scarborough 1956, Pinheiro 2010b].	30
3.2	Summary of unconstrained monitoring of vital signs using PVDF-based sensors. <i>WT</i> : wavelet transform, <i>N/A</i> : not available, <i>P. Infants</i> : premature infants, <i>M</i> : male, <i>F</i> : female, <i>HR</i> : heart rate, <i>HRV</i> : heart rate variability, <i>RR</i> : respiratory rate, <i>ACF</i> : autocorrelation function, <i>Min</i> : minutes, <i>Hrs</i> : hours, <i>Sec</i> : seconds, <i>CLC</i> : complete-linkage clustering, <i>TM</i> : template matching, <i>FREQ</i> : frequency, <i>CEP</i> : cepstrum, <i>PCA</i> : principal component analysis, <i>MAP</i> : maximum amplitude pairs, <i>AMDF</i> : adaptive-window average magnitude difference function, <i>ECG Sync</i> : electrocardiogram synchronization, <i>EMD</i> : empirical mode decomposition, <i>TH</i> : threshold, <i>CWT</i> : continuous wavelet transform, <i>Lab</i> : laboratory.	36
3.3	Summary of unconstrained monitoring of vital signs using EMFi-based sensors. <i>WT</i> : wavelet transform, <i>N/A</i> : not available, <i>M</i> : male, <i>F</i> : female, <i>HR</i> : heart rate, <i>RR</i> : respiratory rate, <i>ACF</i> : autocorrelation function, <i>Min</i> : minutes, <i>Hrs</i> : hours, <i>Sec</i> : seconds, <i>CEP</i> : cepstrum, <i>MAP</i> : maximum amplitude pairs, <i>AMDF</i> : adaptive-window average magnitude difference function, <i>EMD</i> : empirical mode decomposition, <i>TH</i> : threshold, <i>LT</i> : linear transform, <i>Lab</i> : laboratory.	41
3.4	Summary of unconstrained monitoring of vital signs using Pneumatic-based sensors. <i>N/A</i> : not available, <i>M</i> : male, <i>F</i> : female, <i>HR</i> : heart rate, <i>RR</i> : respiratory rate, <i>Min</i> : minutes, <i>Hrs</i> : hours, <i>Sec</i> : seconds, <i>STFT</i> : short-time Fourier transform, <i>Lab</i> : laboratory.	43
3.5	Summary of unconstrained monitoring of vital signs using Pneumatic-based sensors. <i>N/A</i> : not available, <i>M</i> : male, <i>F</i> : female, <i>HR</i> : heart rate, <i>RR</i> : respiratory rate, <i>Min</i> : minutes, <i>Hrs</i> : hours, <i>Sec</i> : seconds, <i>SWM/M</i> : sliding window minimum/maximum, <i>ECG Sync</i> : electrocardiogram synchronization, <i>PCA</i> : principal component analysis, <i>CCF</i> : cross-correlation function, <i>ED</i> : Euclidean distance, <i>HVS</i> : heart valve signal, <i>ACF</i> : autocorrelation function, <i>SE</i> : Shannon entropy, <i>EMD</i> : empirical mode decomposition, <i>Lab</i> : laboratory.	46
3.6	Summary of unconstrained monitoring of vital signs using Hydraulic-based sensors. <i>N/A</i> : not available, <i>M</i> : male, <i>F</i> : female, <i>HR</i> : heart rate, <i>RR</i> : respiratory rate, <i>Min</i> : minutes, <i>Hrs</i> : hours, <i>Sec</i> : seconds, <i>WPPD</i> : windowed peak to peak deviation, <i>CA</i> : clustering approach: <i>HT</i> : Hilbert transform, <i>STE</i> : short-time energy, <i>eFUMI</i> : extended function of multiple instances, <i>Lab</i> : laboratory.	49

3.7	Summary of unconstrained monitoring of vital signs using Hydraulic-based sensors. <i>N/A</i> : not available, <i>M</i> : male, <i>F</i> : female, <i>HR</i> : heart rate, <i>RR</i> : respiratory rate, <i>Min</i> : minutes, <i>Hrs</i> : hours, <i>Sec</i> : seconds, <i>BP</i> : blood pressure, <i>PPG Sync</i> : Photoplethysmography synchronization: <i>STFT</i> : short-time Fourier transform, <i>CEPS</i> : cepstrum, <i>Lab</i> : laboratory.	54
5.1	Features' mathematical equations.	70
5.2	Patients' demographic information.	87
5.3	Home situation and sleep habits of each resident.	95
6.1	10-fold cross validation mean accuracy for Group1 and Group2, (RF: ntrees = 50, SVM: RBF kernel, NN: 50 hidden neuron).	98
6.2	Accuracy results for testing Group2 Vs. Group1 (Experiment1) and testing Group1 Vs. Group2 (Experiment2).	98
6.3	Confusion Matrix of random forest classifier for testing Group1 Vs. Group2 (Experiment2).	99
6.4	The MAE for Group1 and Group2 before and after classification regarding the average beats per minute.	99
6.5	The mean and standard deviation (SD) of the MAE for MODWT and CEEMDAN regarding the average beats per minute across all 50 subjects.	102
6.6	The mean and standard deviation (SD) of the MAE for best wavelet, FFT, cepstrum, and autocorrelation methods considering the average beats per minute across all 50 subjects.	103
6.7	The mean absolute error of all 10 patients for the average beats per minute computed during the entire study.	106
6.8	The mean absolute error of all 10 patients for the average breaths per minute computed during the entire study.	106
6.9	Sensitivity and specificity of sleep apnea detection	110
6.10	Starting and ending of napping time for resident No. 3.	113

Introduction

Contents

1.1	Research Description	1
1.2	Current Healthcare Challenges	2
1.2.1	Growing Numbers of Elderly People	2
1.2.2	Prevalence of Chronic Diseases	4
1.2.3	Shortage of Caregivers	5
1.2.4	Rising Costs of Healthcare	5
1.3	Research Objectives of this Thesis	7
1.4	Structure of the Thesis	7

1.1 Research Description

Technological progress allows us to take better care of ourselves and our relatives with less effort. Furthermore, we observe an emergence of *Zero-Effort Technologies* (ZET) [Mihailidis 2011]. They represent technological solutions that provide a service without requiring any form of active participation of the user. Their main paradigm is to leverage on unobtrusive observations of daily activities and on smart use of available information. *Ambient Assisted Living* (AAL) platforms, which is a specific type of ZET, target improving the quality of life – of both the monitored person and their caregivers. Such a platform aims at empowering people who may be at risk without assistance, especially the elderly. It contributes to users’ autonomy in their own living space rather than leaving them completely dependent on others (e.g., a nursing home) [Sadek 2017b].

In this research, we focus on sleep monitoring as a substantial vector of quality of life. Sleep is one of the most important elements all human needs similar to oxygen, water, and food. Getting enough quality sleep is necessary to a person’s mental health, physiological well-being, quality of life, and safety. Humans spend a third of their life’s sleeping. As advised, among other things, by the *U.S. National Institutes of Health*, sleep deficiency can lead to fatal health problems. Currently, sleep assessments and evaluation tools are burdensome, expensive, and time-consuming. For these reasons, inexpensive, non-disruptive, and unobtrusive methods to monitor sleep and sleep quality are greatly needed. Healthcare systems worldwide are struggling with significant challenges, i.e., rapid growth in aging population, increased number

of people with chronic and infectious diseases, rising costs, and inefficiencies in health-care systems. As a response to these challenges, the healthcare community is seeking out novel noninvasive solutions that can improve the quality of healthcare for the patient while maintaining the cost of the service provided. This is where a massive use of Internet of Things devices (wearables, low-energy sensors, beacons, apps) is playing a major shift in the quality of life of the population. To achieve these goals, early diagnosis, prevention, and a more efficient disease management system are highly needed [Koenig 2008]. In the following section, we discuss in more detail the current challenges facing the healthcare systems.

1.2 Current Healthcare Challenges

Across the world, healthcare challenges can exist in different shapes and forms. Thereafter, it introduces tremendous pressure on the current system. Even though every country faces different challenges and encounters diverse effects, it is still feasible to identify overall global risk to current healthcare systems. These challenges are an essential starting point for the work ahead.

Population aging, the prevalence of chronic diseases, shortage of healthcare professionals, and the unexpected rise of healthcare costs, among other reasons, are the major challenges facing today's healthcare systems. For solving these issues, public and private sector players should collaborate together to find more innovative and cost-effective systems that can be deployed in out-of-hospital environments [Niewolny 2013]. Nowadays, clouds and the Internet of Things can help improve access to care, increase the quality of care and above all reduce the cost of care. The major challenges facing the healthcare communities are discussed in ensuing subsections.

1.2.1 Growing Numbers of Elderly People

Unlike earlier generations, people are living longer and healthier due to recent advances in medical science. The elderly populations are growing more rapidly than any other age group in just about every country around the world. The reasons for this are declining fertility rates and/or rising life expectancy. In general, the world's population is projected to increase by slightly more than one billion people over the next 13 years, reaching 8.6 billion in 2030, and to increase further to 9.8 billion in 2050 and 11.2 billion by 2100 (Figure 1.1 and Figure 1.2), more specifically the number of older persons in the world is projected to be 1.4 billion in 2030 and 2.1 billion in 2050, and could rise to 3.1 billion in 2100.

Over the next few decades, a further increase in the population of older persons is almost inevitable, given the size of the cohorts born in recent decades [United Nations 2017]. Typically, aging causes several limitations to older adults as a result of their cognitive decline, chronic age-related diseases in addition to weaknesses in physical activities, vision, and hearing. Since the number of older people who do require a special care has grown, too few specialists and resources are

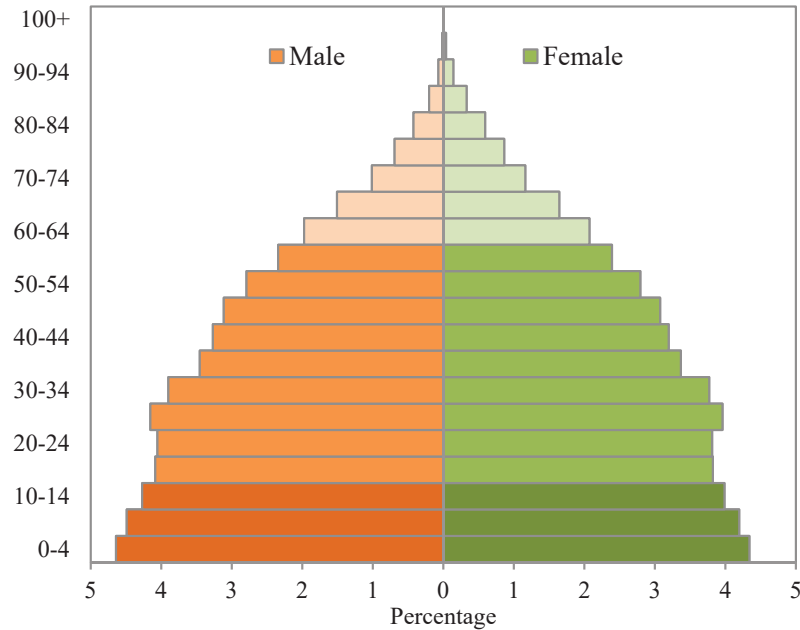


Figure 1.1: Distribution of the world’s population by age and sex, 2017. Source: United Nations, Department of Economic and Social Affairs, Population Division (2017). *World Population Prospects: The 2017 Revision*. New York: United Nations.

going to be available to address their needs. Many seniors prefer to stay alone in their homes. This phenomenon is referred to as *aging in place*, independent living at home, is denoted as the increased in the number of elders who remain in their own homes for the following years in their lives [Ricart 2017]. Providing a healthcare to elders living alone in their homes is a very challenging task given that fact that most of the elders might have a physical and/or cognitive decline.

Aging in place (defined as “remaining living in the community, with some level of independence, rather than in residential care” [Wiles 2012]) becomes possible thanks to advancements in sensor technology, wireless communications, and information technology. Long-term monitoring of physiological data in real-life environments such as users’ homes is essential to help manage health problems such as cardiovascular complications, diabetes, etc. Usually, recent modalities available to monitor physiological data can be divided into two main categories: non-wearable and wearable sensors. The non-wearable sensors can be integrated with home furnishings and structures, whereas the wearable sensors can be embedded in a form factor of, for instance, a wristwatch, bracelet, or ring, etc.

The benefit of these sensors is that they can monitor several variables from individuals in their own homes during their normal daily activities. In addition, they can observe trends in physiological data over an extended period of time as well as automatically alert healthcare professionals or caregivers in emergency

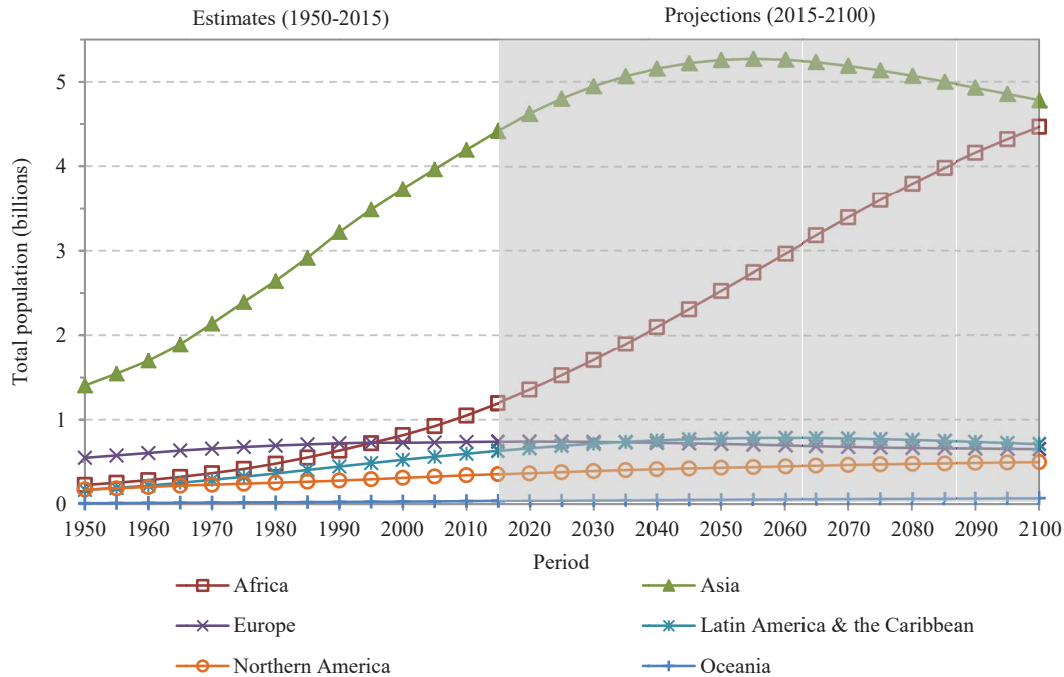


Figure 1.2: Average annual rate of population changes for the world and by region, estimates, 1950 – 2015, and medium-variant projection, 2015 – 2100. Source: United Nations, Department of Economic and Social Affairs, Population Division (2017). *World Population Prospects: The 2017 Revision*. New York: United Nations.

situations such as falls in case of older people [Korhonen 2003]. Although some older adults might have concerns about the intrusion of privacy and loss of autonomy when using remote healthcare monitoring devices, this method is preferred by older adults since it promotes independence with the added sense of protection in case something went wrong they could get an immediate assistance [Rashidi 2013, Liu 2016, van Hoof 2011].

1.2.2 Prevalence of Chronic Diseases

There will be an increase in age-related diseases, namely Alzheimer disease and Parkinson’s disease in which cure is not yet available. Consequently, the percentage of individuals unable to live independently is going to increase. As the population ages, there is an increasing concern about how we will pay for the quality of care for the elderly and how we will address the quality of care to our aging population [Rashidi 2013]. Hereafter, there is an immediate need to use low-priced measures to improve health in this group with the intention of preventing illness and disability later [Ricart 2017]. Moreover, there is a crucial need for self and remote monitoring of vital physiological parameters.

1.2.3 Shortage of Caregivers

The number of healthcare practitioners and caregivers trained to deal with aging populations will be limited. As a result, family members or relatives should informally replace the caregivers. Observing dependent individuals at home might cause some difficulties to family members such as higher levels of painfulness and physical health problems [Ricart 2017]. Well-designed and -implemented technology can extend the reach of caregivers, ultimately offsetting the rising cost of healthcare and the need for skilled caregivers. To give some examples, remote health monitoring technologies such as wearable devices and video teleconferences are now making it possible for monitoring to come to patients with disabilities rather than vice-versa.

The Internet of Things (IoT) technology enables and facilitates remote monitoring of patients who don't have ready access to effective health monitoring. Likewise, it also helps thoroughly reduce costs and promote health by increasing the availability and quality of care [Niewolny 2013, Islam 2015]. The IoT is a network of smart devices and other objects, integrated with electronics, software, sensors, and network connectivity that allows these objects to obtain and exchange data. The concept of IoT allows the healthcare professionals and caregivers to access a patient's medical history, vitals, lab results, medical and prescription histories either on-site or remotely via tablets or smart-phones. Additionally, patients can be monitored and advised from anywhere [Dimitrov 2016]. The IoT based solution can be utilized to record patient health data in a securely manner from several sensors, apply complicated algorithms to analyze the data and then distribute it through wireless connectivity with medical specialists who can make suitable health recommendations. Figure 1.3 shows an illustration of a sensor mat as an example of an IoT device in a medical setting.

1.2.4 Rising Costs of Healthcare

Healthcare costs are projected to continue to increase. Thus, the current paradigm of health care will become unsettled as the aging population is going to grow in the coming decades [Zheng 2014]. As an example, an elderly person might have the condition of sleep-disordered breathing (SDB). The SDB, better known as the obstructive sleep apnea (OSA) syndrome and associated cardiovascular complications are among the most common clinical disorders. The prevalence of OSA was determined to influence approximately 14% of men and 5% of women, in a population-based study employing an apnea-hypopnea index (AHI) cutoff of ≥ 5 events/h associated with clinical symptoms to define OSA [Kimoff 2016, Kapur 2017]. The gold-standard approach to diagnose OSA is known as polysomnography (PSG), the PSG test should be performed in a specialist sleep clinic for a complete overnight.

In principle, the sleep test includes many sensors placed on the patient body to record specific body functions such as the heart's electrical activity, brain's electrical activity, breathing, thoracoabdominal movement, blood oxygen saturation, body movement, etc. The PSG system provides accurate and real-time data. Nevertheless,

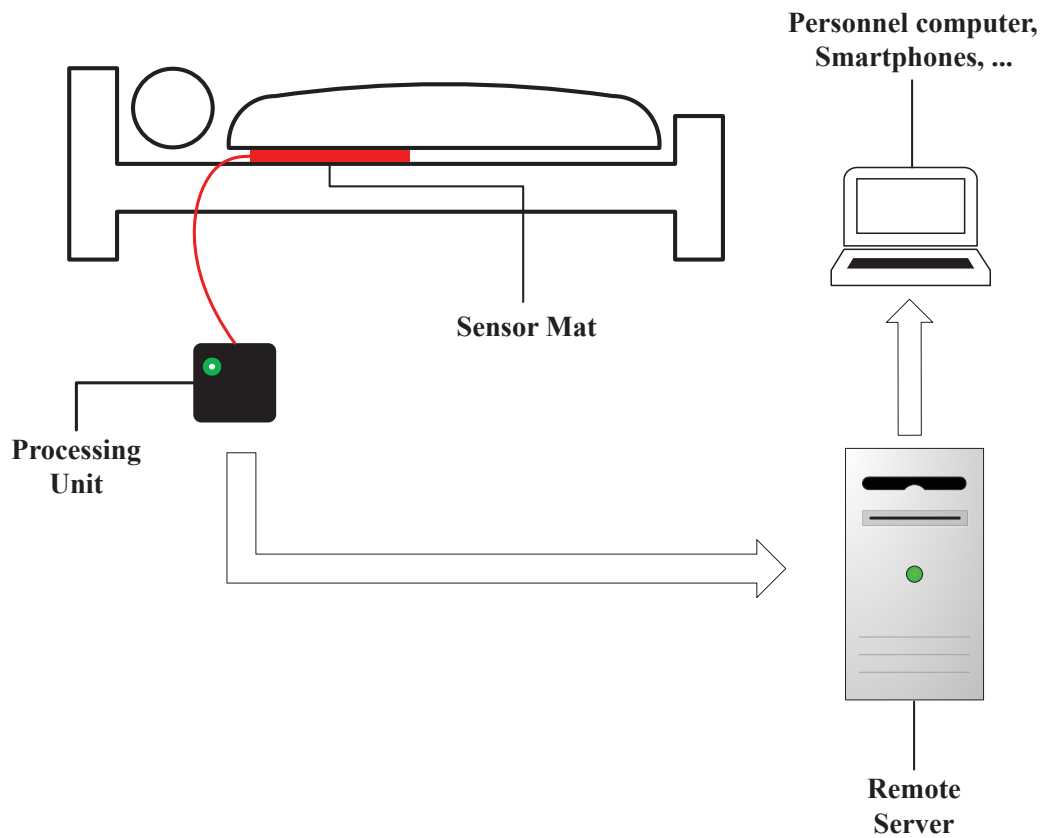


Figure 1.3: An illustration of a sensor mat as an example of an IoT device in a medical setting.

it introduces many limitations, i.e., complexity, invasiveness, excessive cost, and absence of privacy. Technological advancements in hardware and software enable noninvasive and unobtrusive sensing of vital signs. An alternative approach which may help diagnose OSA and other cardiovascular diseases is the ballistocardiography. The ballistocardiogram (BCG) signal records the mechanical activity originating from the rebound of the body, generated when the blood is pumped out of ventricles into the large blood vessel synchronous with each heartbeat [Park 2018]. During the 1900s, BCG signals were massively studied and numerous publications appeared in major scientific and clinical journals. Nevertheless, BCG signals were largely abandoned by the medical community as the measurement devices (e.g., moving table types) were very bulky and complex [Inan 2015].

Recently, BCG sensors such as the microbend fiber may be embedded in ambient locations such as mattresses, pillows, chairs, beds, or even weighing scales, to measure BCG. Some common BCG sensing technologies in literature are microbend fiber-optic sensors, fiber Bragg grating sensors, piezo-resistive fabric sensors, electromechanical film and polyvinylidene fluoride film-based sensors. One of the main advantages of the microbend fiber-optic sensor is that due to its immunity to electrical and

electromagnetic interference it is a very suitable tool to be implemented in the magnetic resonance imaging environment. Other advantages include small size, lightweight, and lower price. Additionally, the sensor is an appropriate choice for unconstrained and long-term monitoring of vital signs as it is highly sensitive to pressure changes induced due to the ballistic forces of the heart, while not required to be in close contact with the body [Sadek 2017a].

1.3 Research Objectives of this Thesis

1. Design and developing a robust system for remotely collecting vital physiological signs namely heart rate, respiration, and body movement unobtrusively from subjects in their beds.
2. Design and developing a robust system for remotely monitoring the quality of sleep unobtrusively from subjects in their beds.
3. Deploying and validating the proposed system in a clinical setting.
4. Deploying the proposed system in real-life environments such as users' homes.
5. Integrating the proposed system within an existing ambient assisted living platform known as UbiSMART.

1.4 Structure of the Thesis

This thesis is structured as discussed below:

1. **Chapter 1** describes the problem statement as well as general information about current healthcare challenges, namely growing number of older adults, the prevalence of chronic diseases, shortage of caregivers, and rising costs of healthcare. This chapter ends with the research aims and the thesis outline.
2. **Chapter 2** briefly describes the human physiology, including cardiovascular and respiratory systems. The sleep cycles are also discussed, which consist of rapid eye movement sleep and non-rapid eye movement sleep. At last, the chapter discusses the gold-standard for assessing sleep and some of the available sleep monitoring technologies. These devices could be wearables such as bracelets; smart-watches or non-wearables like bed-sensors that can be installed underneath the user's bed mattress.
3. **Chapter 3** gives a summary about ballistocardiography and how it has been evolved over time to reach an acceptable level for healthcare providers. This chapter also gives a comprehensive review of available sensors used in literature to analyze and interpret ballistocardiogram signals. These sensors include microbend fiber-optic sensors, piezo-resistive fabric sensors, electromechanical film and polyvinylidene fluoride film-based sensors, load cells, strain gauges, pneumatic, and hydraulic sensors.

4. **Chapter 4** covers the operating principle of the proposed sensor, i.e., microbend fiber-optic sensor. Likewise, it discusses our system development cycle. Furthermore, it presents how the proposed system is validated in health and clinical environments. Finally, it shows how the system is integrated within an existing Ambient Assisted Living platform.
5. **Chapter 5** discusses in detail the proposed methodology to analyze the data acquired by the optical fiber sensor. Various algorithms have been implemented such as empirical mode decomposition, wavelet analysis, frequency analysis, and autocorrelation function to analyze ballistocardiogram signals, and therefore interbeat intervals can be computed unobtrusively. Moreover, the data collection protocol for the two validation phases is also discussed. Wavelet analysis shows superior results compared with other algorithms. At last, the real-life deployment of the proposed system in user's homes is provided.
6. **Chapter 6** describes results and discussions about the proposed methodology to analyze the optical fiber data, in which a comparative study between various algorithms is provided. It also shows the suitability of the proposed sleep monitoring system for unobtrusive vital signs monitoring in a clinical setting. Moreover, it discusses in detail the results of our real-life deployment in three users' apartments in one month's time.
7. **Chapter 7** summarizes the main results, conclusions, limitation of the proposed system. In addition, it recommends some key factors to enhance the proposed methodology, and therefore it can provide continuous monitoring of physiological functions.

Background

Contents

2.1	Introduction	9
2.2	Cardiovascular System	10
2.3	Respiratory System	11
2.4	Physiology of Sleep	13
2.5	Sleep Monitoring	14
2.6	Polysomnography	15
2.7	Actigraphy	17
2.8	Consumer Sleep Tracking Devices	18
2.8.1	Wearable Sleep Tracking Devices	19
2.8.2	Sleep Tracking Apps on Smart-phones	20
2.8.3	Bed-Based Sleep Tracking Devices	22
2.9	Conclusion	25

2.1 Introduction

Sleep is a very significant biological function for the human being and is important to have a physical balance and a proper regime for decent quality of life. Inadequate quality and quantity of sleep can lead to a severe influence on an individual health. As a result, sleep analysis is a very important step towards the detection and diagnosis of sleep problems. Understanding cardiovascular and respiratory systems is essential for analyzing sleep and sleep cycles, this is because the active processes in the human body are different in sleep and wakefulness. Typically, analyzing a person's sleep requires an overnight sleep test or polysomnography that allows monitoring of several physiological functions a long with sleep cycles. Although the polysomnography or as known as the gold standard for sleep monitoring provides real-time and accurate information about sleep it is cumbersome, expensive, and time-consuming. Thus, the healthcare community is seeking out inexpensive and mobile devices that can support a long-term data collection and be accessible to most of the people. Actigraph is a very famous example that can be used for sleep analysis. The device is not as accurate as the polysomnography. However, the provided information which is based on the users' activity is very important for healthcare professionals to understand and analyze the sleep behavior of the

users. As the hardware and software technology is advancing very fast, several devices and mobile Apps have been developed for general healthcare monitoring, including sleep. These devices could be wearable such as bracelets or smart-watches or non-wearable like bed-sensors that can be installed underneath the user's bed mattress. We briefly explain the human physiology, including cardiovascular and respiratory systems in [Section 2.2](#) and [Section 2.3](#), respectively. The physiological aspects of sleep are discussed in [Section 2.4](#). Sleep monitoring and available sleep monitoring technologies are provided in [Section 2.5](#), [Section 2.6](#), [Section 2.7](#), and [Section 2.8](#), respectively. Finally, the chapter is concluded in [Section 2.9](#).

2.2 Cardiovascular System

The cardiovascular system is an extensive network which achieves two main tasks as follows. First, it transports oxygen and nutrients to body organs. Second, it eliminates waste products formed by the metabolism of nutrients from the tissue cells. It consists of the heart and the blood vessels that circulate blood throughout the entire body [[Tortora 2008](#)].

The heart, the primary organ of the cardiovascular system, is positioned somewhat to the left of the center of the chest, i.e., between the two lungs and is shielded by the rib cage. The adult heart is roughly the size of a large fist.

The human heart ([Figure 2.1](#)) consists of four chambers, i.e., two atria and two ventricles. The atria are the upper chambers that receive blood while the ventricles are the lower chambers that pump blood. The right atrium receives the blood

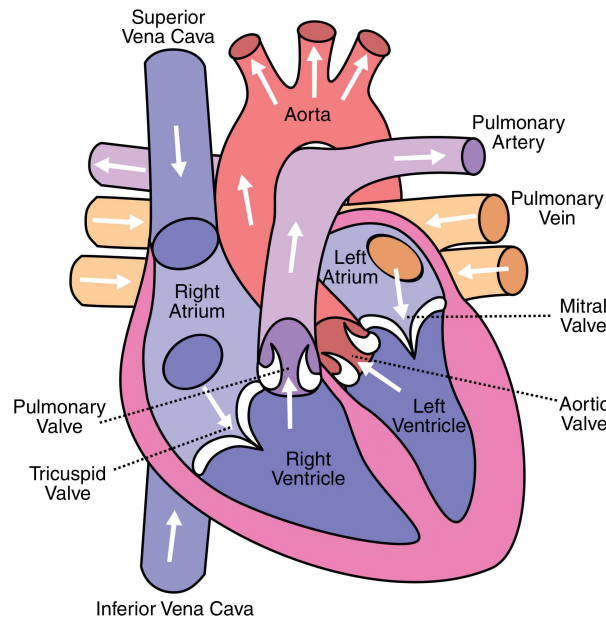


Figure 2.1: Anatomy of the human heart.

returning to the heart and then pumps it to the right ventricle. Next, the right ventricle pumps the deoxygenated blood to the lungs to be enriched with oxygen. Afterward, the blood is returned to the left atrium throughout the pulmonary veins. The left atrium contracts and sends the blood to the left ventricle. At last, the left ventricle sends the blood through the aorta into the circulatory network. The left ventricle requires a thick muscular wall so that it can pump the blood all the way around the body. The blood in the heart is kept moving in a forward direction thanks to a system of four one-way valves. During the time of contraction, the valves open to allow blood through, and close to prevent the blood flowing in the opposite direction when the chambers relax. Moreover, the valve system acts to sustain different pressure on the right and left sides of the heart.

The cardiac cycle, the electrical activity regulating the rhythmic contraction and relaxation of the heart's chambers, consists of two main phases, namely diastole, and systole. Diastole is the relaxation of the heart's muscles, and it takes up approximately two-thirds of the cycle. Systole is the contraction of the heart's muscles, in particular, the ventricles, which takes the remaining one-third of the cycle. During the time of diastole, the two atria contract following the impulse originated in the sinus node. As a result, the blood is propelled from the atria to the ventricles. During systole, the blood is ejected into the pulmonary artery and the aorta, respectively. The cardiac output (CO) is the amount of blood ejected from the left ventricle of the heart per minute. The cardiac output is the product of the heart rate (HR) multiplied by the stroke volume (SV) and is measured in liters per minute (L/m) as follows [Tortora 2008]:

$$\text{CO} = \text{HR} \times \text{SV} \quad (2.1)$$

The heart rate is the number of times the heart contracts or beats per minute (bpm). The stroke volume is the amount of blood ejected from the left ventricle with each heartbeat (one contraction and relaxation of the heart muscle) of the heart rate. It is measured in milliliters per beat (ml/beat); a decrease in the stroke volume is one of the early signs of the failing heart.

2.3 Respiratory System

The respiratory system or a.k.a., the ventilator system plays a key role in controlling homeostasis, i.e., balance between the multiple parts of the body's internal environment. The respiratory system is responsible for gas exchange in the body, delivering vital oxygen to the body and removing toxic carbon-dioxide. It can achieve such important tasks during different activity levels from unconscious sleep to consciousness levels of maximal endeavor [Story 2017]. A schematic view of the human respiratory system is shown in Figure 2.2. The respiratory system can be divided into two main parts: upper airways and lower airways. The upper airway consists of the nose, the paranasal cavities, i.e., sinuses, the pharynx, and part of the oral cavity. The function of the nose, paranasal cavities, and pharynx is to

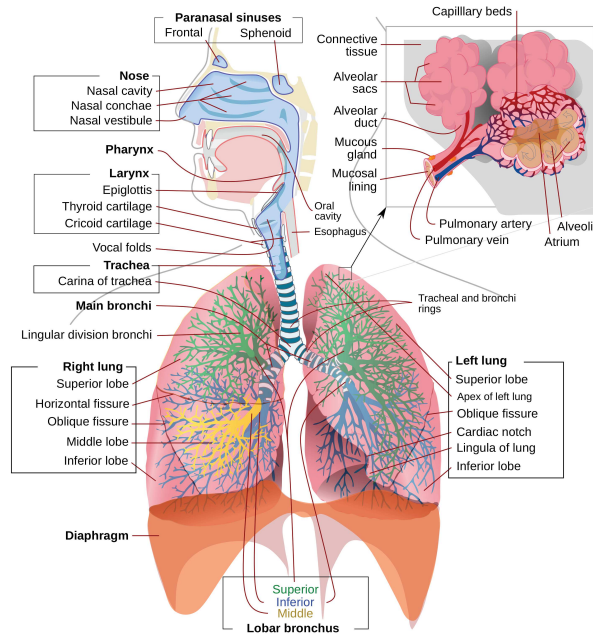


Figure 2.2: A schematic view of the human respiratory system. Retrieved from Wikimedia Commons website: https://en.wikipedia.org/wiki/Respiratory_system

warm, filter, and humidify the inspired air when it enters the respiratory tract. The filtering process is very important due to several reasons, among them clearing the inhaled air of dust and other debris and protecting the passage through the lungs against any potentially infectious foreign agents. The oral cavity is responsible for respiration as well as enabling sensation and smell. The main components of the lower airways encompass the larynx, trachea, and lungs. The larynx and trachea provide a channel for the pathway of air to the lungs whereas the lungs themselves receive the air and promote the gas exchange process [Rogers 2010]. The respiratory cycle consists of one respiration followed by one expiration. Ventilation (V) is the amount of air breathed in (inspiration) and out (expiration) during one minute. It can be computed by multiplying tidal volume (TV) and respiratory rate (RR) as follows:

$$V = TV \times RR \quad (2.2)$$

The tidal volume is the volume of air that enters or leaves during a single respiratory cycle. The respiratory rate is the amount of breaths per minute.

2.4 Physiology of Sleep

Knowing the basic principles of the sleep-wake cycle is very helpful to understand the importance of sleep. In human, the sleep-wake cycle involves approximately eight hours of nocturnal sleep and sixteen hours of daytime wakefulness. Two internal influences control the sleep-wake cycle, i.e., homeostasis and circadian rhythms. The homeostasis is the process of which the body maintains a steady state of internal conditions such as blood pressure, body temperature, and acid-base balance. In addition, the amount of sleep each night is also under the homeostatic control. The circadian rhythms are driven by the brain's biological clock, and it is referred to as cyclical changes. These cyclical changes are, for example, fluctuations in body temperature, hormone levels, and sleep that happen over a 24-hour period. In human, the biological clock contains a set of neurons in the hypothalamus of the brain known as the suprachiasmatic nucleus. In physiology and behavior, these 24-hour rhythms

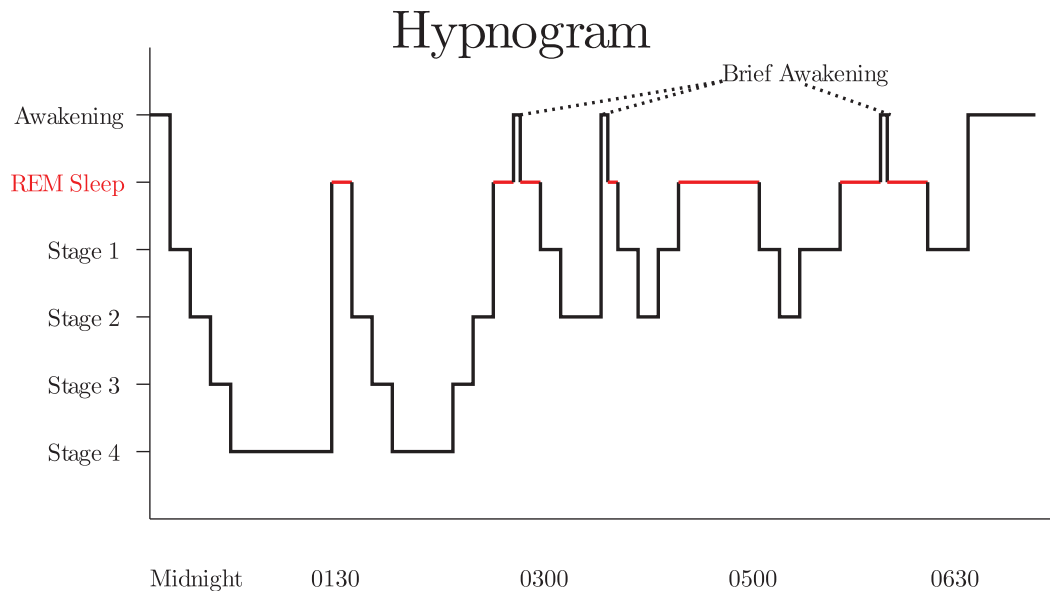


Figure 2.3: A sample hypnogram (defined by electroencephalogram) showing sleep cycles designated by increasing REM sleep.

are synchronized to the external physical environment and work/social schedules. Light and darkness, examples of the external signals, regulate the biological clock and help decide when we feel the need to wake up or go to sleep. Furthermore, the circadian clock helps promote wakefulness. On the one hand, whether it's night or day, the homeostatic system inclines to make us sleepier as time passes throughout the waking period. However, the circadian system inclines to keep us awake, provided that there is daylight, which encourages us to sleep once it becomes dark [Battle 2009]. Sleep can be divided into two general stages: non-rapid eye movement sleep (NREM) and REM (REM) sleep.

In the first stage, i.e., the NREM sleep, the physiological activities are reduced. When we get deeper into sleep, the brain activities become slower and have a greater amplitude as measured by the electroencephalogram. Moreover, the breathing and heart rate slow down, and blood pressure drops. The NREM sleep is further subdivided into four stages as follows [Battle 2009]:

1. **First Stage** is the period of time from being awake to falling asleep. The 1st stage is characterized by a reduction in brain waves and muscle activity. During this stage, people might encounter sudden muscle jerks headed by a falling sensation.
2. **Second Stage** is considered as a *light sleep* period, where the eye movements stop. During the 2nd stage, the brain activities become slower with sleep spindles, i.e., infrequent bursts of rapid waves. The sleep spindles are combined with uncontrollable episodes of muscle tone coupled with periods of muscle relaxation. Additionally, the heart rate decreases and body temperature drops.
3. **Third Stage** and **Fourth Stage** or a.k.a., *slow-wave sleep / deep sleep* is identified by slow brain waves (i.e., delta waves) scattered with smaller faster waves. During slow-wave sleep, the physiological activities decrease, and the body temperature falls even lower. In addition, the body becomes stationary. As eyes are not moving and the muscle's activity decreases, the sleep becomes deeper even though the muscles maintain their ability to work. Waking during the slow-wave sleep is very difficult. People will feel dizzy or disoriented for some minutes if they wake during these stages. Some children might undergo bed-wetting, sleepwalk, or night terrors during this stage.

The second stage, i.e., the REM sleep is a unique phase of sleep, where the brain waves become very intense. Similar to those in the waking state, brain activities become faster and desynchronized. In addition, breathing waves becomes more rapid, irregular, and shallow; the eyes move rapidly in different directions, and limb muscles become temporarily paralyzed. Furthermore, heart rate increases, and blood pressure rises. The most memorable and vivid dreams occur during this stage as well. It is also believed that the REM sleep plays a vital role to consolidate the memory, synthesize and organize the cognition, and regulate the mood [Battle 2009]. Figure 2.3 shows the electroencephalogram of a sleep cycle described by increasing REM sleep.

2.5 Sleep Monitoring

Sleep monitoring is described as the process of obtaining a qualitative sleep metrics by monitoring a person's sleep throughout the night. These metrics serves two functions. One is to formulate an objective view of the quality of a person's sleep. The other function is to determine the trends in sleep over time. Respiratory rate and body movements are considered the most related measurements for sleep monitoring

during the sleeping session. The respiratory rate and respiratory rate variability are used for REM sleep identification, while the movement metrics are utilized to discriminate between deep sleep, light sleep, and the waking stages of sleep. Several sleep parameters can also be extracted, for example, duration of a sleep period, the number of awakenings, duration of disturbed sleep periods, and the amount of time required to fall asleep. Monitoring quality of sleep can be performed using various devices that use a combination of sensors and sensor technology to examine the user's sleep patterns [Seebo 2017]. In the following sections, we discuss some of the common techniques used to monitor and assess the quality of sleep.

2.6 Polysomnography

The term polysomnography (PSG) or a.k.a., the gold standard for sleep quality monitoring, is a complete recording of the biophysiological variations that occur during sleep. In general, the PSG is an all-night test in a specialized sleep clinic. However, it might be performed during the day if this occurs to be the patient major sleep period, such as the patients with specific circadian rhythm disorders, where their regular bedtime is during the day.

Three main information can be inferred from the PSG study as follows. First, monitoring, staging and characterizing sleep. Second, identifying sleep-disordered breathing and its outcomes. Third, quantifying periodic limb movements during sleep. Furthermore, the PSG can also provide information about irregular behaviors during sleep, i.e., parasomnias [Koenig 2008]. During a PSG study, several sensors are mounted on various parts of the body in order to detect multiple physiological parameters in real-time (Figure 2.4). These physiological parameters can be detailed as follows:

- **Electroencephalography (EEG)** records the electrical activities of a person's brain using metal electrodes attached to the skin of the scalp to monitor three main regions of the brain such as frontal, central, and occipital, i.e., back. The EEG plays a vital role in determining the sleep stages of the patient.
- **Electrooculography (EOG)** monitors the eye movements, in which two leads are used and one is placed on the outside of each eye. The EOG also plays a role in determining the stages of sleep based on eye movements.
- **Electromyography (EMG)** measures muscle activities. Four electrodes might be used for the monitoring process such as two electrodes mounted on the chin and the other two placed on each leg close to the shin. The EMG can be employed to help diagnose sleep-related movement disorders such as restless leg syndrome, periodic limb movement disorder, and REM sleep behavior disorder.
- **Electrocardiography (ECG / EKG)** records the electrical activities of the heart using two to three electrodes on the person's chest.

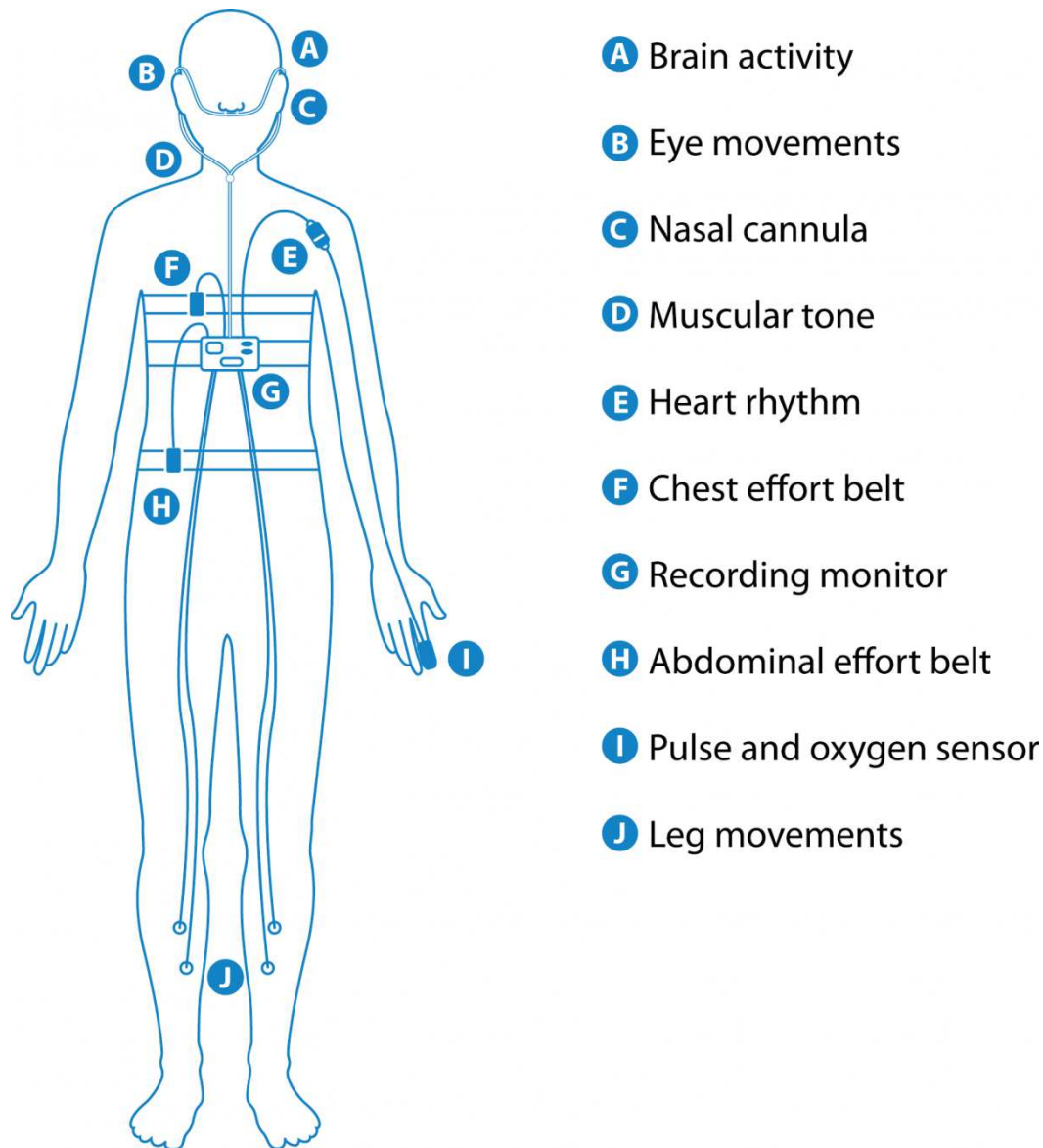


Figure 2.4: An illustration of the location of the various electrodes and sensors used for monitoring sleep. Image courtesy: British Lung Foundation.

- *Respiratory effort* measures the movements of the chest and abdominal wall. Two belts are used such as one belt around the chest and one around the diaphragm.
- A *nasal cannula/pressure transducer* is inserted into the nostrils to monitor changes in inhalation and exhalation as well as breathing rate.
- A *pulse oximeter* is placed on the patient's finger in order to measure

the blood oxygen saturation. The sleep-disordered breathing in particular sleep apnea can be detected based on the pulse oximeter, nasal cannula, and respiratory belts information. The sleep apnea happens when the person stops breathing for 10 seconds or longer during sleep. It can be further classified into three categories such as mild, moderate, and severe, based on the number of times in an hour that the person's breathing stops (apnea), or it becomes very shallow (hypopnea).

- **A sound probe** which can be utilized to detect the volume of snoring. It is also very helpful in discriminating between apnea events and hypopnea events.
- In addition to the above-mentioned modalities, the patient might be monitored on **a closed-circuit video system** and **an audio device**. This helps the technicians to record the different patient's behaviors and movements during sleep. Furthermore, it allows a smooth communication between the patient and technicians from different rooms.

Figure 2.5 shows a representative 30-second epoch from a sleep study [Basner 2012].

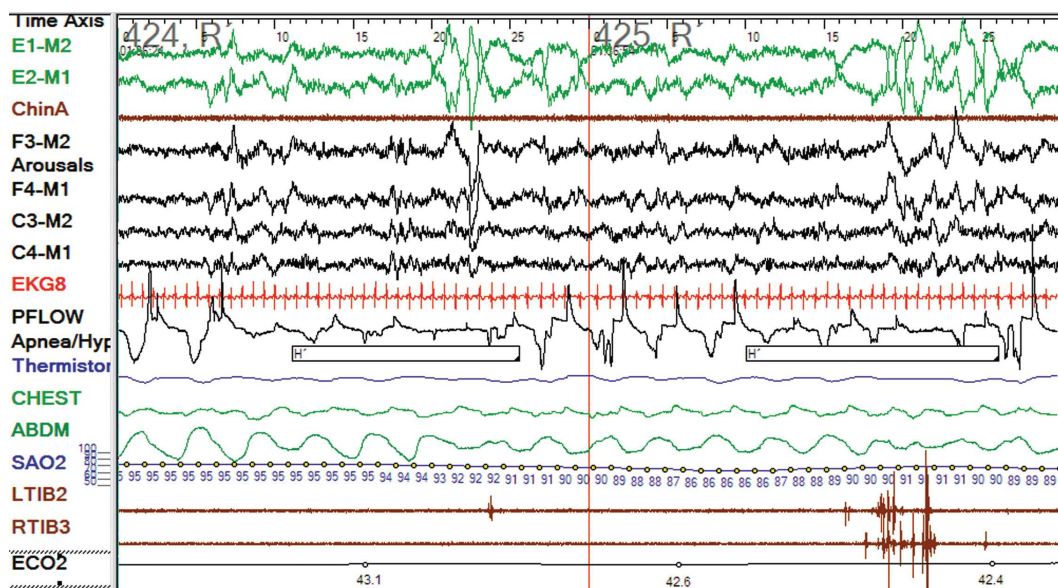


Figure 2.5: A 30-second epoch from the PSG. Image adapted from [Basner 2012].

2.7 Actigraphy

Actigraphy is the recording of human rest/activity cycles in a noninvasive manner. Typically, an actigraph unit is in a wristwatch-like package. The patient needs to

wear the unit for a week or more to measure entire motor activity. The movements that the actigraph unit receives are regularly recorded and some units also include light exposure. The data can be later read by a computer and interpreted offline; in some new sensors, the data are transmitted and analyzed in real-time. The current actigraphs use accelerometers that produce different values according to variations in orientation and the speed wherein the variation exists [Liu 2017b]. The objective is to sample these values multiple times a second and accumulate them over a period of time. At last, they are locally stored on the device and fetched at a later time. The actigraphs are able to record movements for many days, thanks to the accumulation of the data. As a result, they can provide a long-term data about circadian rhythms and the person's activity patterns. Previously, the data obtained from the analog actigraphs had to be manually scored through a very time-consuming process. However, the scoring process becomes fully automated by computer algorithms installed in digital actigraphs.

Patients can put the actigraphs either on the wrist or on the ankle so that the different limb movements can be tracked. The movement received from the ankle is very important in monitoring limb movements and/or restless syndrome. Actigraphs can provide very useful information about the sleep quality due to its longitudinal nature of data collection and its suitability to be used in the subjects' homes. Additionally, actigraphs allow researchers to conduct studies at nursing homes and assisted-living communities for both memory care and non-memory care residents. These studies can provide more information about the causes and signs of dementia along with a better understanding of the sleep modes of the residents and how their sleep requirements might deviate from people in other stages of life [Koenig 2008]. Although wearable sensors such as actigraphs can provide a long-term data collection about the user's sleep status, they might cause inconvenience to the daily lives of older adults. This is not always true, and it might depend on the level of education and the ability to learn and accept recent technologies.

2.8 Consumer Sleep Tracking Devices

In recent years, a lot of sensor technologies have been employed, particularly to monitor sleep-wake patterns together with the gold standard polysomnography and actigraphy; these sensor technologies are usually denoted as consumer sleep tracking devices.

In general, consumer sleep tracking devices are just like actigraphs because they allow the users to be mobile and sleep as normal while being monitored closely. Most of the commercially available sleep monitors pretend to help provide information about sleep duration, quality of sleep, enabling subjects to awaken only from light sleep. Typically, the data obtained from consumer sleep tracking devices are not intended for routine diagnosis of sleep disorders. However, technological advancements in hardware and software, accessibility, ready availability allows the public to adopt them for clinical purposes.

We summarize some of the consumer sleep tracking devices in following subsections [Kelly 2012, Russo 2015, Jeon 2015, Kolla 2016, Ong 2016]:

2.8.1 Wearable Sleep Tracking Devices

2.8.1.1 Zeo™

The device (Figure 2.6(a)) utilizes a headband to collect a combination of EEG and EMG signals from the forehead region. It classifies a 30-second epoch into light NREM, deep NREM, and REM sleep.

2.8.1.2 SleepImage™

The device (Figure 2.6(b)) records ECG signal, actigraphy, and body movements using a wire electrode attached to the chest with sticky pads. It helps provide knowledge about total time of sleep, quality of sleep, and the number of awakening that happen during sleep.

2.8.1.3 Fitbit™ and Fitbit Ultra™

The device (Figure 2.6(c)) is an activity tracker that can provide information about sleep based on movement. The device can discriminate between sleep and wake as well as provide information about total time of sleep, sleep latency, i.e., the length of time an individual can take to achieve the transition from full wakefulness to sleep and an arousal index.

2.8.1.4 Lark™

The device (Figure 2.6(d)) is a wrist-watch actigraphy that features a silent vibrating alarm. It also can give information about total sleep duration, sleep latency, a sleep quality index. The device needs to be connected to an iPhone.

2.8.1.5 WakeMate™

Another example of wrist-watch actigraphy is the WakeMate (Figure 2.6(e)). It can provide sleep information such as total sleep time, sleep latency, number of awakenings, and a quality of sleep. The sleep information can be transmitted to a smart-phone. Similar to other devices it has the smart-alarm feature to awaken the wearer at an optimal time within a time-window that ends in the final alarm setting.

2.8.1.6 Jawbone™ and Jawbone UP™

The device (Figure 2.6(f)) is a wrist-watch actigraphy (bracelet-like) that can connect to an iPhone. The sleep tracking is performed using bio-impedance sensors. It is claimed that the device can distinguish between light and deep sleep, although standard actigraphy does not allow such distinction. Furthermore, it is claimed that

the device can allow the wearer to awaken at an optimal time via a smart-alarm feature.

2.8.1.7 BodyMedia SenseWear armbandTM

This device (Figure 2.6(g)) employs several sensors such as the accelerometer, heat flux, temperature, a galvanic skin response to produce information about an individual sleep. Variation in heart rate, body temperature, and other recorded measures are utilized to report wake and sleep onset, and total time of sleep.

2.8.1.8 HexoskinTM

This device (Figure 2.6(h)) is a smart shirt with integrated sensors to measure heart rate and heart rate variability, the total time of sleep, and body movement.

2.8.1.9 ŌURATM

This device (Figure 2.6(i)) is a smart ring integrated with three types of sensors, i.e., infrared LEDs, 3D accelerometer and gyroscope, and body temperature sensor. The ring can provide various information such as sleep stages, heart rate variability, and body temperature [de Zambotti 2017].

2.8.2 Sleep Tracking Apps on Smart-phones

Nowadays, smart-phones become a fundamental part of our daily life, including the healthcare domain. A lot of people are using mobile Apps to help improve their health and fitness. As a result, the healthcare mobile Apps have grown exponentially. For instance, hundreds of Apps have been developed for sleep and sleep hygiene monitoring, and this number is projected to continue to increase year after year. Most of these Apps aimed to serve several functions, including but not limited to: a smart-alarm feature, sleep assistants, sound recording at the time of sleep, light sensor data, the usage of the phone, and the microphone to decide sleep/wake [Kolla 2016, Ong 2016]. Additionally, other Apps have been developed to help healthcare providers in screening some specific health problems such as repeated snoring and obstructive sleep apnea syndrome. It should be mentioned that insufficient publications are available to support the suitability of these Apps [Kelly 2012, Kolla 2016] for patients with sleep complaints. Unlike wearable sensors, smart-phone Apps are inexpensive to most of the users. However, they are very susceptible to motion artifacts because they need to be located on the subject's bed. These motion artifacts might arise from a bed partner and/or interference from blankets. As a result, the quality of the signal obtained by the phone's accelerometer can potentially be degraded. To recapitulate, either wearable sensors or Apps installed on smart-phones they tend to use 3-axis accelerometers to measure the user activity. The activity counts produced by the accelerometer are then used to decide whether the user is waking or asleep. Most of the validation studies between these



Figure 2.6: Examples of wearable sleep tracker devices; (a) Zeo, (b) SleepImage, (c) Fitbit, (d) Lark, (e) WakeMate, (f) Jawbone, (g) Body-Media SenseWear armband, (h) Hexoskin, and (i) ŌURA.

devices and the gold standard polysomnography or actigraphy have been performed against healthy people with no sleep problems. As a result, it is difficult to generalize their applicability to the patient suffered from sleep disorders. Overall, sleep trackers tend to overestimate total sleep time, sleep efficiency and underestimate wake up time after the onset of sleep. Another principal issue which has to be considered in selecting a sleep activity tracker is the Battery life and the frequency of recharging. To give an example, smart-watches are useful fitness and heart rate trackers. However, they don't have a long battery life that can last for the entire night. More specifically, smart-phones are not accurate enough to provide absolute sleep parameters and sleep staging, in addition, there is no proof that they can precisely awaken users from light sleep [Kelly 2012, Russo 2015, Jeon 2015, Kolla 2016, Ong 2016]. Some of the available Apps are discussed in the ensuing subsections:

2.8.2.1 Sleep Cycle AlarmTM App

This App utilizes the embedded accelerometer of the iPhone to recognize movements during sleep. Usually, the iPhone is to be placed nearby a person's headrest. The App can provide graphs representing total sleep time, a differentiation between light

sleep, deep sleep, and wake. Besides, it also has the smart-alarm feature.

2.8.2.2 Sleep Time™ App

This App can give a detailed information about wakefulness, light and deep sleep. Furthermore, it has the smart-alarm feature to help users wake up only during light sleep.

2.8.2.3 Toss N Turn™ App

This App can report information about sleep and wake time using the embedded accelerometer in the smart-phone in addition to light intensity, sound, details of phone usage, and charging status as well.

2.8.2.4 ApneaApp™: Sleep Apnea Detection on Smart-phones

This App uses the built-in microphone in a smart-phone to emit some kind of inaudible wave, that serves as a sonar system to detect amplitude changes during breathing. The phone is usually placed on a regular sideboard same as if the person is charging his/her phone and getting ready for sleep. The App is designed to detect normal breathing and abnormal breathing, which include hypopneas, obstructive and central sleep apnea. Although this App showed a good correlation with the gold standard polysomnography regarding the apnea-hypopnea index it has not been validated in a home-based environment [Kolla 2016].

2.8.2.5 SleepRate™

This App can support iPhones and Android phones. It can report information about the wake, sleep, REM, light non-REM, and deep non-REM. The App needs to be connected with a wearable polar heart sensor that can transmit up to 30 feet using a Bluetooth low energy device.

2.8.3 Bed-Based Sleep Tracking Devices

As we mentioned in [Section 2.7](#), the wearable devices might not be the optimal solutions for older adults, since these devices need to be placed on some parts of the body, such as wrists, arms, etc. The elderly people might forget to wear the devices. Other than that, these devices might annoy people that use them. Besides, it might be a sign of their condition defaming them in social communications [Kouroupetroglou 2014]. If we consider the educational background of the elderly people, it might also be difficult for them to use smart-phones. Alternatively, new sensors have been developed and become available for consumers that use nonintrusive technologies to detect subjects' vital signs and sleep patterns. These sensors are designed and packaged in a way to make them invisible to the subjects. For example, they can be easily integrated into ambient assisted living environments such as beds, pillows, chairs, or even in weighing scales [Zaunseder 2017].

In the following subsection, we discuss some examples of the commercially available devices, and more details will be provided in the next chapter (Chapter 3).

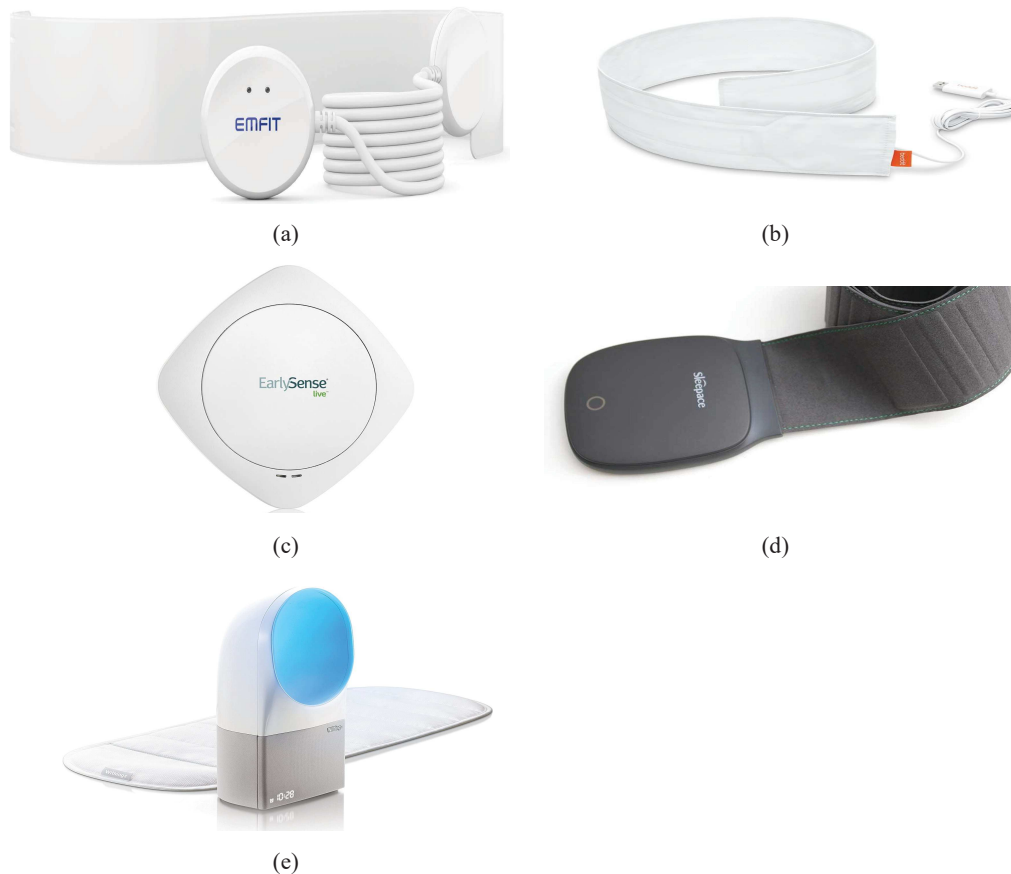


Figure 2.7: Examples of bed-sensor devices; (a) Emfit QS, (b) Beddit, (c) EarlySense, (d) Sleepace Reston, (e) Withings Aura.

2.8.3.1 Emfit QSTM

Emfit QS¹ depends on what is called ballistocardiography, i.e., the sudden ejection of blood into the great vessels with each heartbeat, breathing and movement analysis. The Emfit QS (Figure 2.7(a)) has an integrated data acquisition and cellular mobile data connectivity. The Emfit QS electronics consist of its own processor and memory for completely autonomous operation. The device has a web application that enables the users to track their sleep patterns. The user can place the device underneath the bed mattress. Consequently, the user will not notice it is there. Furthermore, the Emfit QS claims to report all three sleep stages, i.e., light, deep, and REM sleep,

¹Product website: <https://www.emfitqs.com/>

sleep time, in addition to a sleep score, which is a number consists of total sleep time, amount of REM and deep sleep, and the number of times awakened.

2.8.3.2 Beddit™ Smart Sleep Monitor

The Beddit² device uses several sensors, including piezo force sensor, capacitive touch sensor, humidity sensor, temperature sensor, and microphone (in the smart-phone) to provide similar information as Emfit Qs. However, since the device uses the sound information, it can record the snoring and total duration of snoring. The device is also installed under the bed mattress. The Beddit device (Figure 2.7(b)) needs to be connected to an iPhone only device via a Bluetooth connection. It also has the smart-alarm feature. The sleep information can be viewed through the Beddit mobile App.

2.8.3.3 EarlySense™ Mattress

The EarlySense³ device utilizes a piezoelectric sensor that can be placed under the bed mattress. The system (Figure 2.7(c)) can report information about heart rate, respiration, snoring, coughing, and movement. A recent study showed a good agreement between EarlySense and the gold standard polysomnography for sleep staging [Tal 2017]. Furthermore, the device provided promising results for sleep apnea detection [Davidovich 2016].

2.8.3.4 Withings Aura™

Withings Aura⁴ uses ballistocardiography to measure changes caused by respiratory rate, heartbeats and the body's movements during the night. It has been claimed that the device achieves this with clinical accuracy to evaluate the structure of the subject's sleep, as well as the existence in the bed and the number of wake-ups per night. It can discriminate an awake state from a sleep state, the periods in the bed sleeping - and awake, and measures the different sleep phases of your night. It uses the measurements from the sleep sensor to wake the subject at the best moment of his/her sleep cycle so that the subject wakes up refreshed. It provides the subject with an overview of his/her cardiovascular fitness and how well he/she recovered from stress and exercise by measuring your full-night resting heart rate. It also records his/her surrounding's temperature, luminosity, and sound level to provide he/she with full insights to enhance his/her sleep quality. The apparatus (Figure 2.7(e)) has two distinct parts. The first is a dock that transmits light and sound gradually along with sensors that measure temperature, luminosity and sound levels. The second is a pneumatic sensor under the mattress which measures heart rate, respiratory rate, and body movements.

²Product website: <https://www.beddit.com/>

³Product website: <https://www.earlysense.com/digital-health/>

⁴Product website: <https://support.health.nokia.com/>

2.8.3.5 Touch-Free Life CareTM System

The Touch-Free Life Care system⁵ is a bed-sensor that can broadcast information for remote monitoring. Like other devices, it can be located below any standard bed mattress and wirelessly transmits information such as respiration, heart rate, body movement, and quality score to PCs or mobile devices (iPhone only).

2.8.3.6 Sleepace RestonTM

The Sleepace Reston⁶ device is another example of bed-sensors. The device (Figure 2.7(d)) can provide vital signs such as respiration and heart rate as well as sleep cycle. The device is battery powered by a battery life up to 30 days. It needs to be connected to a smart-phone either Android or iPhone through a Bluetooth connection. It also claims a smart-alarm function to awaken the user from light sleep vs deep sleep. Users can follow up their sleep patterns using a mobile App.

2.9 Conclusion

In brief, this chapter discussed the cardiovascular and respiratory systems because they are fundamental parts of understanding sleep and quality of sleep. Next, we described the two main stages of sleep namely rapid eye movement sleep and non-rapid eye movement sleep. Afterward, we defined sleep monitoring and reviewed the most common sleep monitoring modalities namely polysomnography and actigraphy. Additionally, we mentioned some of the commercially available sleep tracking devices. In general, sleep tracking devices such as smart-watches, wearable bracelets, or Apps installed on smart-phones are mainly designed to help enhance the quality of life, extend independent living and reduce health professionals' necessary time and healthcare costs. Although they do not yet meet the standard criteria as independent devices for healthcare application, they can provide longitudinal information, which is impossible in typical approaches. Among these sleep tracking devices, the bed-based sensors are very promising and convenient types of sleep monitoring. The reason is that these devices are completely nonintrusive with no electrodes or wires mounted on the subject's body. Such devices are mainly depending on the movements of the body during sleep and respiration as well. In the next chapter, we will explain in detail the different methods and modalities being used to monitor human vital signs and sleep using the bed-sensor technologies. In our analysis, we aimed to use the nonintrusive technology like bed-sensors because the subjects do not have to wear them. Besides, they are affordable and ready-to-use devices.

⁵Product website: <http://bamlabs.com/>

⁶Product website: <http://www.sleepace.com/>

Literature Review

Contents

3.1	Introduction	27
3.2	Ballistocardiography	28
3.2.1	Piezoelectric Polyvinylidene Fluoride-Based Sensors	31
3.2.2	Electromechanical Film-Based Sensors	35
3.2.3	Pneumatic-Based Sensors	40
3.2.4	Strain Gauges-Based Sensors	42
3.2.5	Hydraulic-Based Sensors	47
3.2.6	Fiber Optic-Based Sensors	50
3.3	Conclusion	53

3.1 Introduction

Up until now in [Chapter 2](#), we have discussed in some detail the various products on the market today that can be employed to track different perspectives of sleep such as duration and quality of sleep. These products can be either wearable sleep trackers, such as smart watches and smart-phones or non-wearable sleep trackers such as in-bed sleep monitors. In this research, we prefer using the in-bed sleep monitors to the wearable sleep trackers as they are more convenient for elderly people. The in-bed sleep monitors are more likely to be suitable for older adults due to multiple reasons. For instance, as some of the older adults might have cognitive and memory impairments, they might forget to wear the device, or they might remove the device. Hence, the monitoring system may not work as intended [[Sanchez 2017](#)]. Additionally, the in-bed monitors are entirely nonintrusive, and they do not require any invasive electrodes or wires to be connected to the subject's body.

It is very important to monitor sleep and quality of sleep, especially for older adults because they spend more time in bed compared to younger adults. Insufficient sleep for older adults might cause depression, attention and memory problems, excessive daytime sleepiness, and experience more nighttime falls [[Cooke 2011](#)]. Typically, in-bed sensor technology is based on recording body movements, respiratory movements, and ballistocardiographic movements representing the mechanical activity of the heart [[Alihanka 1981](#)]. As it was previously mentioned in [Chapter 1](#), the recording of these physiological signals can be performed using multiple sensors, namely

microbend fiber-optic sensors, piezo-resistive fabric sensors, electromechanical film and polyvinylidene fluoride film based sensors, load cells, strain gauges, pneumatic, and hydraulic sensors [Inan 2015]. The first of these sensors was a static charge sensitive bed introduced by Alihanka *et al.* [Alihanka 1981]. The next sections will discuss, in more detail, ballistocardiography and the different techniques used in literature to analyze and interpret ballistocardiogram signals.

3.2 Ballistocardiography

Ballistocardiography (BCG) is a noninvasive technique for creating a graphical representation of the heartbeat-induced repeated motions of the human body. These repeated motions happen due to the rapid acceleration of blood when it is ejected and moved in the great vessels of the body during periods of relaxation and contraction, known as diastole and systole, respectively. In other words, BCG can provide information about the overall performance of the circulatory system; this is because BCG measures the mass movements, i.e., the mass of the circulating blood and the heart during the cardiac cycle [Pinheiro 2010b]. During atrial systole, when the

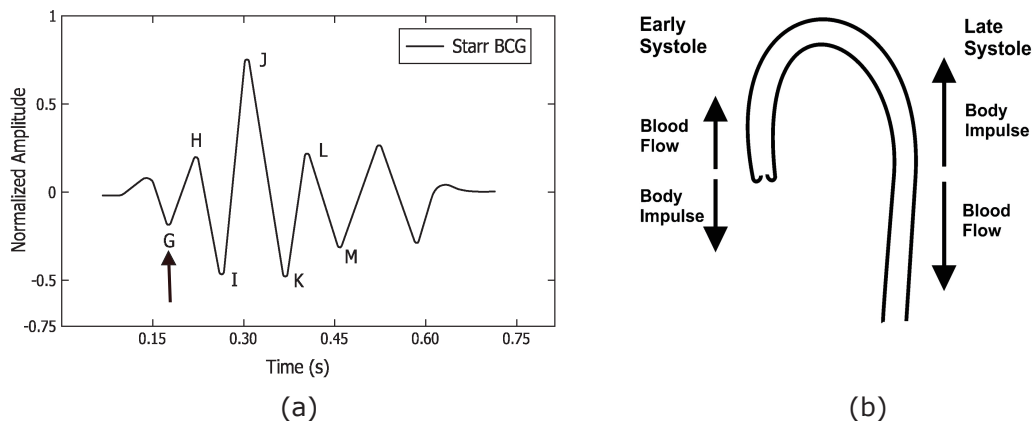


Figure 3.1: (a) Example of a typical BCG signal with letters used to designate the waves. The arrow indicates the position of the beginning of the electrical ventricular systole (QRS. complex of the electrocardiogram). Image adapted from [Starr 1939, Starr 1940, Pinheiro 2010b], (b) Aortic arch and force vectors coming from blood ejection by the left ventricle. Image adapted from [Eblen-Zajjur 2003].

blood is ejected into the large vessels, the center of mass of the body moves towards the head of the body. In other ways, when the blood moves towards the peripheral vessels and concentrates further away from the heart in the peripheral vessels, the center-of-mass moves towards the feet (Figure 3.1(b)). This shift comprises several components as a result of cardiac activity, respiration, and body movements. This

shifting of the center of mass of the body generates the BCG waveform since the blood distribution changes during the cardiac cycle [Vogt 2012].

More than 100 years ago, BCG failed to prove its functionality, and it did not start to be used in routine tasks for a few general reasons as follows. First, there had been insufficient standard measurement methods, i.e., different methods had resulted in slightly different signals. Second, the exact physiologic origin of the BCG waveform had not been well-understood. Furthermore, there had been insufficient clear guidelines for interpretation of the results, and therefore the medical community was unwilling to take risks. Third, there had been a dominant focus on some clinical diagnostic, for example, *myocardial infarction*, *angina pectoris*, *coronary heart disease*; these applications need a high level of specificity and reliability that the BCG had not reached. Fourth, the emergence of ultrasound and echocardiography methods that swiftly overhauled BCG and related methods for noninvasive cardiac and hemodynamic diagnostic [Giovangrandi 2011]. At the present time, BCG has

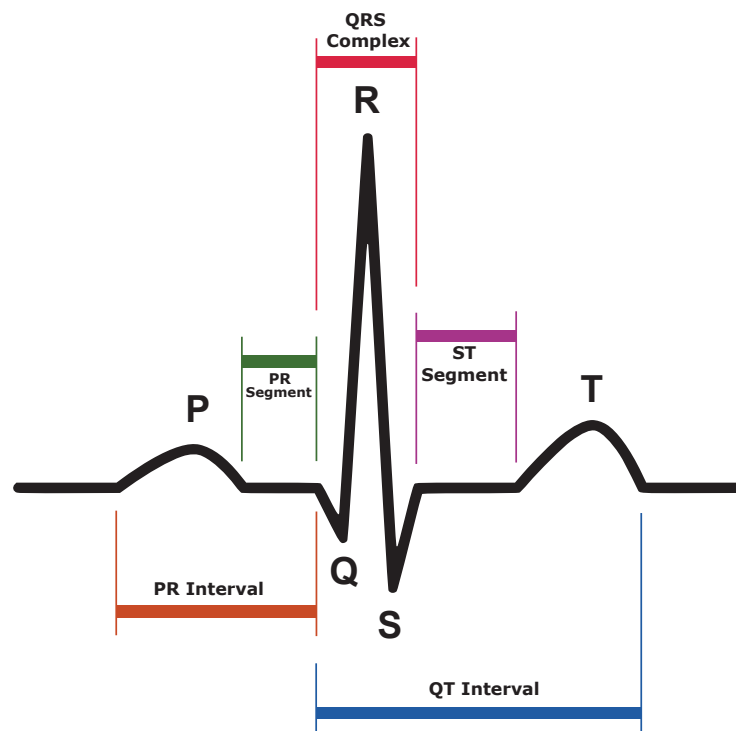


Figure 3.2: Example of a typical electrocardiogram signal.

been given a lot of interest thanks to the information technology revolution, including hardware technology as well as software and services. As described in [Chapter 1](#) and [Chapter 2](#), BCG sensors can be embedded in ambient environments without the need for medical staff presence. Consequently, it has an outstanding impact in current e-health systems. Ultimately, BCG helps reduce checkups' stress and the patient emotion and attention responses. [Figure 3.1\(a\)](#) shows an example of a typical BCG

signal, while [Figure 3.2\(b\)](#) shows an example of a typical electrocardiogram signal. The BCG waveforms may be grouped into three main groups, i.e., the pre-systolic (frequently disregarded), the systolic and the diastolic as given in [Table 3.1](#). The I and J waves are also quoted as ejection waves [[Pinheiro 2010b](#)]. To this extent,

Table 3.1: Nomenclature of ballistocardiogram (normal displacement) signal [[Scarborough 1956](#), [Pinheiro 2010b](#)].

<i>Pre-Systolic Group (See Figure 3.1(a))</i>
<ul style="list-style-type: none"> • F wave: (rarely seen) headward wave preceding G, related to pre-systolic events, not an after-vibration. • G wave: small footward wave which at times precedes the H wave.
<i>Systolic Waves (See Figure 3.1(a))</i>
<ul style="list-style-type: none"> • H wave: headward deflection that begins close to the peak of the R wave, maximum peak synchronously or near the start of ejection. • I wave: footward deflection that follows the H wave, occurs early in systole. • J wave: largest headward wave that immediately follows the I wave, occurs late in systole. • K wave: footward wave following J, occurs before the end of systole.
<i>Diastolic Waves (See Figure 3.1(a))</i>
<ul style="list-style-type: none"> • L and N waves: two smaller headward deflections which usually follow K. • M wave: footward deflection between L and N. • Smaller subsequent waves may be visible and are named in sequence.

the definition, formal limitations, and nomenclature of ballistocardiography were discussed. The formal limitations were mainly due to the complexity of the used system and misinterpretation of the obtained signals and its deformations. The field of ballistocardiography has been revived as a result of the numerous technological advancements, as, for example, the advent of microprocessors and laptop computers. All in all, ballistocardiography can be very useful in several applications such as monitoring of cardiac function and performance in addition to monitoring of sleep and sleep-disordered breathing [[Di Rienzo 2017](#), [Inan 2018](#)]. One of the most prominent features of ballistocardiography is the accessibility and ready-availability, which allows the system to be deployed in users' homes without affecting the users' privacy and daily activities. In what follows, we explain more in detail the various tools and algorithms exist in the literature to analyze and interpret ballistocardiography, wherein we look at what types of sensors that can be used for signal acquisition and what types of software algorithms that can be used to extract vital information such as heartbeat, respiration, and body movements.

3.2.1 Piezoelectric Polyvinylidene Fluoride-Based Sensors

The piezoelectric effect is the ability of some materials to produce an electric charge in response to applied mechanical stress. The polyvinylidene fluoride (PVDF) is an exciting piezoelectric material and is usually developed as a very thin and easily bent film. If a pressure force is applied to the film, it creates a mechanical bending and a shifting of positive and negative charge centers in the film, which then results in an external electrical field. The charge generated from PVDF is equivalent to the applied pressure. Therefore, PVDF is one of the suitable candidates for detecting the small fluctuations generated by different body parts [Xin 2016].

Wang *et al.* [Wang 2003] proposed to use a PVDF piezopolymer film sensor for unconstrained detection of respiration rhythm and pulse rate. The film sensor was placed under the bed-sheet at the location of the thorax to obtain the variations of the pressure on the bed attributable to respiratory movement and heartbeats. The authors used the wavelet multiresolution decomposition to compute the respiration and heartbeat. The output of the respiratory inductance plethysmography (RIP) and electrocardiography (ECG) were used as a reference for respiration and heartbeat, respectively. The objective of the wavelet analysis was to decompose the raw signal into low-frequency components and high-frequency components. Next, the component presenting a good agreement with either the respiratory movement or the heartbeat was selected. Afterward, the respiratory rate was computed directly based on a time-varying adaptive threshold. On the other hand, the heartbeat component was first squared to rectify it into unipolar, and then the envelope of the rectified signal was calculated using a moving average smoothing algorithm. At last, a time-varying adaptive threshold was also applied to the smoothed envelope to compute the heart rate. It should be noted that heart rate detection was very challenging because the pressure variations attributable to heartbeat on the bed was very weak, and the shape of the signal was not always uniform. Another study was proposed by Wang *et al.* [Wang 2007] to detect respiration rhythm and pulse rate of premature infants using PVDF sensor array. The system was tested in clinical environments on five premature infants (1 male and 4 females). The main challenge of the proposed system was frequent body movement of the infants and the weakness of the heartbeat vibration.

Niizeki *et al.* [Niizeki 2005] suggested using a PVDF sensor array for unconstrained monitoring of respiration and heart rate. The sensor array consisted of eight PVDF cable sensors and they were horizontally integrated with a textile sheet on a bed surface covering the upper half of the body. The cardiorespiratory signals, i.e., BCG and respiration were obtained using infinite impulse response digital filters. After extracting the cardiorespiratory signals, an optimal sensor selection search routine was applied to select the most appropriate sensor. The selection criterion was based on the magnitude of the power spectrum density (PSD). The autocorrelation functions of the cardiac and respiratory signals were computed using a 5-second and 15-second time segments for heartbeat and respiration, respectively. The outputs of the autocorrelation functions were smoothed and differentiated

using a Savitzky-Golay (5 adjacent points) algorithm and finally, the heart rate and respiration were computed by measuring the intervals between the peaks for the respective autocorrelation functions. A fixed threshold was used to determine if the subject changes posture during the measurement, in which the output from the PVDF cables was disturbed to a large extent. A charge-coupled device (CCD) camera was used to record the image of the body position during posture change as a time stamp. The proposed system was tested against thirteen healthy male subjects whose ages ranged from 21 to 49 years. ECG and pneumotachometer for measuring respiratory flow were used as a reference during the study. The study consisted of two phases, i.e., short-term recording for 10 minutes and an overnight study for 2 hours. For the overnight recording, only 7 subjects were involved. The proposed system had some limitations in particular susceptibility to motion artifacts caused by subject movements that might have led to the misidentification of the peak for autocorrelation functions.

Paalasmaa and Ranta [Paalasmaa 2008] applied an unsupervised learning approach on ballistocardiogram signals to compute heartbeat. The ballistocardiogram signals were collected from three subjects using a piezoelectric pressure sensor over 5 hours recording. To start with, feature vectors were extracted from the signal at possible heartbeat positions, i.e., the local maxima of the signal. Then, a complete-link clustering was applied to the feature vectors to look for a cluster with the highest density. The positions of the feature vectors of the densest cluster were found to match real heartbeat positions in the signal. An angular dissimilarity measure was adopted since it omits the differences in feature vector amplitudes. The sensor was located close to the patient's upper body so that it can register cardiac activity in a proper way.

Paalasmaa *et al.* [Paalasmaa 2012] introduced a sleep tracking web application, which was based on measurements from a piezoelectric film sensor placed under the mattress topper. The raw data coming from the sensor was sent to a web server for analysis and extracting information. This information includes heart rate, respiration, sleep staging, and stress reactions. The heart rate was computed by creating a heartbeat template using complete-link clustering [Paalasmaa 2008], then the heart rate intervals were detected by selecting those intervals that minimize a predetermined residual error. The sleep staging was carried out by utilizing heart rate variation, respiration variation, and activity information. The proposed approach was validated against a 40-patient group at a sleep clinic. The added value of this work is the suitability of the system for long-term monitoring of sleep and the web application for sleep analysis at home. A more comprehensive study was introduced by Paalasmaa *et al.* [Paalasmaa 2015] to compute heart rate from ballistocardiogram signals acquired with piezoelectric film sensor. At first, a model for the heartbeat shape was adaptively deduced from the signal using a hierarchical clustering approach. Afterward, interbeat intervals were identified by detecting positions where the heartbeat shape best matches the signal. The proposed method was verified with overnight recordings from 46 subjects in different settings, i.e., sleep clinic, home, single bed, and double bed.

Chen *et al.* [Chen 2009b] advised to use four piezoelectric sensors to detect heart rate and respiration. One sensor was placed under the pillow, whereas the other three were placed under the mattress close to the back, hip, and calf level positions. The data was collected from five healthy subjects at age of twenties during a 2-hour's nap in a sleep lab. ECG and nasal thermistor signal were employed as heart rate and respiration references. Heart rate and respiration were computed based on the multiresolution analysis of the wavelet decomposition in which the Cohen–Daubechies–Feauveau biorthogonal wavelet was selected as the basis function to design the decomposition and reconstruction filters. The 6th level approximation waveform was similar to the respiratory rhythm, while a combination of the 4th and 5th scale coefficients were found to be suitable for heart rate detection. The authors were able to measure both vital signs from the four positions. However, the overall optimal position was found in the back. That makes sense because the more the sensor is closer to the thorax, the more accurate the recovered signals are.

A wheelchair-based system for monitoring the cardiac activity of its user was proposed by Pinheiro *et al.* [Pinheiro 2012]. The signals were collected from piezoelectric film sensors and micro-electromechanical systems accelerometers installed in the seat and backrest of the chair. The system also included photoplethysmography (PPG) sensors in the armrests. The data from the sensors were sent via Wi-Fi to a laptop with a data acquisition board for deeper analysis. ECG recordings were used to validate the proposed system. The system was tested in different situations, namely unmoving wheelchair, tiled floor motion, and treadmill tests. In the last two situations, the ballistocardiogram signals collected from the piezoelectric sensors were completely corrupted by motion artifacts. On the other hand, the accelerometer was much more insensitive to wheelchair motion. The analysis was done on seven subjects using the fast Fourier transform. Subsequently, the prominent peak was selected within a specific frequency range for heart rate estimation. In a summary, getting informative ballistocardiogram signals from the piezoelectric sensors in a motion situation was almost impossible. However, it was more convenient to get informative signals from the accelerometers and the PPG sensors.

A multichannel approach was proposed by Kortelainen *et al.* [Kortelainen 2012] to extract heart rate and respiration information using eight PVDF sensor channels located in the upper position of the bed. The heart rate was estimated by averaging the signal channels in the frequency domain, in which a sliding time window was utilized to compute the cepstrum of each signal channel. However, the respiratory rate was computed from the first principal component of a principal component analysis (PCA) model applied to the low-pass filtered bed sensor signal. The assumption was that the first principal component will give the signal with the maximum variance, and as a result shall improve the sensitivity for the extraction of the respiration. Twenty-eight patients were recruited for the study and they were suspected to have diverse kinds of sleep problems. Frequency domain averaging was better than simple averaging over all the sensor channels. The extracted information, i.e., heart rate, respiration, and movement might have been used for further sleep analysis.

The same pressure bed sensor assembly with eight PVDF sensors was applied for sleep apnea detection in [Guerrero 2013]. The respiratory signal was computed by two methods. The first method was to apply a Hilbert transform to the bed sensor signal and then smooth the signal with a low pass filter. The second method was similar to Kortelainen *et al.* [Kortelainen 2012] by adopting the PCA approach. At last, the amplitude baseline of the respiratory signal was estimated as the mean value of the preceding 100 seconds. An apnea event was detected if the ratio with the baseline was less than a selected percentage threshold value for a period of at least 10 seconds. The authors applied their methodology to twenty-five patients out of twenty-eight patients recruited in [Kortelainen 2012]. The system showed a good agreement with the reference polysomnography. However, the authors used the simplified reduced respiratory amplitude index (RRAI) instead of the standard apnea-hypopnea index (AHI). In another study, Brüser *et al.* [Brüser 2015] have implemented three different methods using the same sensor set to measure the heart rate in a noninvasive way. Initially, the heart rate was computed using a sliding window cepstrum analysis [Kortelainen 2012]. Secondly, the heart rate was computed using a Bayesian fusion approach, in which three estimators were calculated from each sensor channel such as adaptive-window autocorrelation, adaptive-window average magnitude difference function, and maximum amplitude pairs. For each channel, these three estimator outputs were then combined using a Bayesian fusion method to obtain an overall estimate. In other words, Bayesian fusion approach was applied to 24 estimates. At last, the heart was estimated based on the aforementioned approach. However, for each channel separately. In general, the multichannel based approaches improved the robustness of heartbeat interval estimation over a single sensor. More specifically, Bayesian-based method slightly outperformed the cepstrum-based method.

Martin-Yebra *et al.* [Martín-Yebra 2015] extracted heart rate variability indices from ballistocardiogram signals and then evaluated their correlation with electrocardiogram-derived ones. The ballistocardiogram signals were acquired by a piezoelectric 3D-force plate in supine and standing positions, in a group of 18 healthy subjects (11 females). For each position, the data collection was performed during 5 minutes. Furthermore, subjects were asked to stay quiet to avoid any motion artifacts. The ballistocardiogram waves, i.e., (H, I, J, K) were detected by synchronizing ballistocardiogram signals with ECG signals. Although the proposed approach provided a good match with the reference ECG, it is very difficult to generalize this approach for real-life deployment as the data collection was conducted for a very short time and the detection part was achieved by adapting information from the ECG signals.

Katz *et al.* [Katz 2016] measured cardiac interbeat intervals using a contact-free piezoelectric sensor placed beneath the mattress under the tested subjects. The data was collected from 25 home sleep recordings of 14 healthy subjects in a two-in-bed setting. The authors applied three algorithms to the collected ballistocardiogram signals as follows. First, interbeat intervals were found by decomposing the signal into multiple components using an empirical mode decomposition filter and then

locating the candidate peaks within a localized search area. Second, after locating potential interbeat intervals, a binomial logistic regression model was applied to classify each interbeat interval into one out of three groups based on morphological properties of the ballistocardiogram signal. Finally, an additional algorithm was implemented to get discrete interbeat interval distribution maps during the night recording, considering interbeat interval data from overlapping 15 minutes windows. The preceding three algorithms demonstrated the effectiveness of the proposed system for heart rate variability analysis. Sela *et al.* [Sela 2016] used the same piezoelectric sensor to detect left ventricular ejection for 10 subjects (6 males and 4 females), where the lower body of each subject was enclosed in a negative pressure chamber. The negative pressure chamber regulates and controls the blood pressure of the participants. This study demonstrated the ability of the system to identify internal bleeding condition among patients at risk, namely individuals after an accident or surgical operation.

Alvarado-Serrano *et al.* [Alvarado-Serrano 2016] measured beat-to-beat heart rate from subjects sitting in a common office chair. The authors used a piezoelectric sensor fixed to the bottom side of the seat to collect ballistocardiogram signals from seven subjects (5 males and 2 females). Continuous wavelet transform with splines was implemented to detect beat-to-beat intervals in which an optimal scale was selected to reduce noise and mechanical interferences. Thenceforth, learning and decision phases were applied to the selected scale to detect potential J-peaks. In the learning phase, the first four heartbeats in the ballistocardiogram signal were found to define initial thresholds, search windows, and interval limits. The learned parameters were then utilized to determine the next heartbeat and were readopted after each heartbeat detected to adhere to the heart rate and signal-amplitude changes. A similar study was proposed by Liu *et al.* [Liu 2017a]. However, two PVDF film sensors were installed in the seat cushion and foot insole.

Choe and Cho [Choe 2017] used a piezoelectric sensor installed between a bed-frame and a mattress for unconstrained monitoring of heart rate. The data was collected from 7 male subjects sleeping in a supine sleeping position where the sensor was placed under the subject's back. In total, they collected ballistocardiogram signals for about 5 hours from all subjects, in which subjects were not moving during data acquisition. The data was first smoothed using a moving mean absolute deviation, then the J-peaks were detected within a specific search region using an adaptive thresholding technique. The authors achieved satisfactory results with the reference ECG. However, this method may not be applicable in real-life applications because the data was not collected in a typical sleep sitting and the motion artifacts were not considered as well. Table 3.2 summarizes the unconstrained monitoring of vital signs using the PVDF-based sensors.

3.2.2 Electromechanical Film-Based Sensors

The electromechanical film (EMFi) material is a plastic film that can transform mechanical energy into an electrical signal and the other way around. Basically, it

Table 3.2: Summary of unconstrained monitoring of vital signs using PVDF-based sensors. *WT*: wavelet transform, *N/A*: not available, *P. Infants*: premature infants, *M*: male, *F*: female, *HR*: heart rate, *HRV*: heart rate variability, *RR*: respiratory rate, *ACF*: autocorrelation function, *Min*: minutes, *Hrs*: hours, *Sec*: seconds, *CLC*: complete-linkage clustering, *TM*: template matching, *FREQ*: frequency, *CEP*: cepstrum, *PCA*: principal component analysis, *MAP*: maximum amplitude pairs, *AMDF*: adaptive-window average magnitude difference function, *ECG Sync*: electrocardiogram synchronization, *EMD*: empirical mode decomposition, *TH*: threshold, *CWT*: continuous wavelet transform, *Lab*: laboratory.

	Method	Subjects (M, F)	Deployment	Duration	Outcome
[Wang 2003]	WT	N/A	Lab	N/A	HR, RR
[Wang 2007]	WT	5 P. Infants (2 M and 3 F)	Hospital	10 Min	HR, RR
[Niizeki 2005]	ACF	13 M	Home	10 Min, 2 Hrs	HR, RR
[Paalasmaa 2008]	CLC	3 N/A	Lab	330 Min	HR
[Paalasmaa 2012]	CLC, TM	40 N/A	Sleep clinic	Overnight	HR, RR
[Paalasmaa 2015]	CLC, TM	60 N/A	Sleep clinic, home	Overnight	HR
[Chen 2009b]	WT	5 N/A	Lab	2 Hrs	HR, RR
[Pinheiro 2012]	FREQ	21 N/A	Wheelchair	5 Min	HR
[Kortelainen 2012]	CEP, PCA	6 N/A, 15 M, 13 F	Hospital	Overnight	HR, RR
[Guerrero 2013]	PCA	15 M, 13 F	Hospital	Overnight	Apneas
[Brüser 2015]	ACF, MAP, AMDF	15 M, 13 F	Hospital	Overnight	HR
[Martín-Yebra 2015]	ECG Sync	17 M, 11 F	Lab	5 Min	HRV
[Katz 2016]	EMD	14 N/A	Home	Overnight	HR
[Sela 2016]	N/A	6 M, 4 F	Lab	84 Min	LVET
[Alvarado-Serrano 2016]	CWT	5M, 2 F	Chair	100 Sec	HR
[Liu 2017a]	Adaptive TH	7 M	Lab	45 Min	HR
[Choe 2017]	CWT	6 N/A	Lab	67 Min	HR

is a flexible and thin bi-axially oriented polypropylene film covered with electrically conductive layers, which are enduringly polarized. EMFi has a static charge reaching hundreds of Volts. When a pressure is applied to the film, a charge is created on its electrically conductive surfaces and this charge can be measured as a current or voltage signal, usually with a charge amplifier. As a result, the EMFi serves as a sensitive motion sensor [Alametsä 2004]. Alametsä *et al.* [Alametsä 2004] suggested to use EMFi sensors for obtaining ballistocardiogram signals from certain places of the body. The authors installed EMFi sensors in a chair and in smaller pieces in a few positions on the body (arm, leg, and chest). The ballistocardiogram signals were collected from a few people and the duration of the recordings was relatively short. This study demonstrated the potential of the EMFi material in monitoring the changes in cardiac function. In another study, Koivistoinen *et al.* [Koivistoinen 2004] evaluated the ability of the EMFi sensors for measuring ballistocardiogram signals. The authors installed two EMFi sensors in the seat and backrest of a normal chair, and the data was collected from two young subjects (1 male and 1 female) for 5 minutes. After visual inspection versus the reference ECG, it was found that the acquired waveforms closely simulate those reported in the literature. Equivalent results were also reported by Junnila *et al.* [Junnila 2005, Junnila 2006], which presented the suitability of the EMFi sensors for extracting ballistocardiogram signals.

A smart mattress was developed by Koivistoinen *et al.* [Kortelainen 2007] to detect interbeat intervals in a nonintrusive way from six male subjects. The mattress consisted of 160 EMFi electrodes distributed throughout the mattress that enabled signal acquisitions from multiple locations. Two methods were implemented to detect interbeat intervals, i.e., a pulse method and an adaptive window cepstrum method. In the former, signals from all channel were high pass filtered and then squared. After that, these squared values were averaged between all channels and low-pass filtered the result. At last, the beginning of each heart rate was tracked in the generate pulse train signal. In the latter, the window length of the cepstrum was selected using the pulse method as the first estimator of the heart beats. Then, signals from all channels were averaged in the frequency domain. An interpolation was used to detect more accurate location for the selected cepstrum maximum value. Moreover, the motion artifacts were eliminated based on the signal variance using a sliding time window. Although the cepstrum-based method provided better results than the pulse method, its computational efficiency was not as good as the adaptive window method.

Aubert *et al.* [Aubert 2008] adopted a single EMFi sensor to provide heart rate, breathing, and an activity index representing body movements. The recommended system was validated utilizing data collected from 160 subjects (58 males and 102 females) for a total of 740 hours. Part of the data was collected in a sleep laboratory from patients (i.e., sleep apnea, insomnia, and other sleep disorders) who underwent a full polysomnography and the other part was collected at home from healthy subjects. Body movements were first isolated from the sensor data based on the signal amplitudes and energy, and their time derivatives. Thereafter, heart rate

was measured using a sliding window autocorrelation method, in which the optimal window length had to span 3 to 5 consecutive beats. The respiratory rate was estimated based on the local peaks, troughs, and zero-crossings, constrained to rules ensuring physiological validity in terms of duration and amplitude. Across the 60 subjects, the vital signs were computed over epochs of 30 seconds and the average values were computed and compared to the reference ECG and thorax belt, respectively. The recommended system achieved satisfying results compared to the reference devices.

Kärki and Lekkala [Kärki 2008] used EMFi and PVDF sensors in the measurements of heart rate and respiration. The objective of the study was to determine if there were differences between the results of both sensors. ECG was used as a reference for heart rate and a thermistor for respiration rate. Heart rate and respiration were measured using power spectral density (PSD). The two sensors were embedded inside a textile pocket and the pocket itself was integrated into clothing. They were positioned underneath a commercial heart rate belt on the left side of the sternum. Preliminary results showed that both sensors provided reliable results in the measurements of heart and respiration rates. However, the PSD was not robust enough because the peak in the spectrum might get wider and multiple peaks might have appeared. Another study was proposed by Kärki and Lekkala [Kärki 2009] to determine heart rate with EMFi and PVDF materials. The EMFi and PVDF sensors were grouped together to form a single structure. The data was collected from 10 subjects (5 males and 5 females) over 60 seconds recording (sitting and supine positions), where the sensor structure was placed under the legs of a chair and bed. These preliminary results demonstrated that the heart rate can be measured at home just by sitting on a chair or lying in a bed.

Pinheiro *et al.* [Pinheiro 2009] introduced a low-cost system to measure blood pressure variability and heart rate variability. A single EMFi sensor was installed in the seat of a normal office chair to measure ballistocardiogram signals while a finger PPG was used to estimate arterial oxygen saturation (SpO₂). For validation, ECG was acquired using three chest leads. Using LabVIEW, heart rate and heart rate variability were determined by an adaptive peak detection algorithm. The pulse arrival time was estimated as the time difference between ECG and PPG maximum peaks, and when considering BCG-PPG relation, the I-valley (Figure 3.1(a)) was the reference. The designed system was appraised using data collected from five healthy volunteers over 10 minutes recording. The preliminary study demonstrated that heart rate variability can be measured using the correlation between BCG and PPG. The PSD was exploited to measure the heart rate. In another study, Pinheiro *et al.* [Pinheiro 2010a] collected ballistocardiogram signals by placing an EMFi sensor in the backrest of a wheelchair's, beneath the lining. Two modulation-based schemes were carried out for heart estimation, i.e., a sliding power window and an all-peak detector. The objective was to find all local maxima and local minima, then a spline interpolation and a moving power window were employed to compute a modulating signal. At last, a fast Fourier transform was applied to the output of each method in order to measure the average heart rate from the signal's fundamental frequency.

This system was evaluated using data gathered from six normal subjects (4 males and 2 females) during 125 seconds.

Brüser *et al.* [Brüser 2013] proposed an unsupervised approach to determine inter-beat intervals using an EMFi sensor. The sensor was fixed underside of a thin foam overlay which was thus located on top of the mattress of a typical bed. The system was evaluated on over-night recordings from 33 individuals (14 males and 19 females). Three estimators were implemented, namely autocorrelation function, average magnitude difference function, Maximum amplitude pairs in order to compute the local interval length using a sliding time window. Ideally, this window contained two events of interest. The values of the local interval length were constrained by two thresholds, i.e., T_{\min} and T_{\max} . The body movements were detected based on the maximum amplitude range of each time-window. The information from the three estimators was then applied to a probabilistic Bayesian method to estimate the inter-beat intervals in a continuous manner. Although the proposed method achieved very satisfactory results, the main limitation existed in the implicit hypothesis that two successive heart beats in the BCG have an unknown but similar morphology. This assumption may not always hold true.

In the same way, Zink *et al.* [Zink 2015] used an EMFi sensor to detect heartbeat cycle length in patients suffered from atrial fibrillation and sinus rhythm. The sensor was placed under the bed-sheet and data was collected from 22 patients (15 M, 7 F) during and after cardioversion. Cardioversion is a medical procedure that returns a normal heart rhythm in people with certain types of abnormal heartbeats, namely arrhythmias. In another study, Zink *et al.* [Zink 2017] employed the EMFi sensor to measure heartbeat in patients suffered from sleep-disordered breathing. Twenty-one patients (19 males, 2 females) were recruited for the study and underwent a standard full-night polysomnography. A quality-index was proposed based on the three estimators previously discussed in [Brüser 2013] that allowed to identify segments with artifacts and to automatically exclude them from the analysis. The proposed system provided good correlation of beat-to-beat cycle length detection with simultaneously recorded ECG.

Pino *et al.* [Pino 2015] used two EMFi sensors installed in the seat and backrest of a normal chair in order to measure heart rate. Ballistocardiogram data were collected from 54 individuals, whereas 19 of them were measured in a laboratory (1 minute) and the rest in a hospital waiting room (2 minutes). Firstly, empirical mode decomposition and wavelet analysis were (Deabuchie 6) implemented to reconstruct ballistocardiogram signal. Secondly, the J-peaks of the ballistocardiogram signal was detected using a length transform analysis. The body movements were eliminated using a moving time window. Then, for each time-window two thresholds were computed, i.e., $T1 = (\max + \min)/2$ and $T2 = \text{mean} + 1.1 * \text{std}$, if $T1$ was greater than $T2$, the current window was marked as a body movement. The wavelet analysis was preferred to reconstruct the signal as it produced a higher effective measurement time. A similar approach was also proposed by Pino *et al.* [Pino 2016]. However, they increased the size of the dataset to 114 people. Of those, 21 were gathered in a school (2 minutes), 42 in homes (2 minutes), and 51 in a hospital waiting area. It is

difficult to assess the robustness of this system because the data was collected in a very short time and in a controlled environment as well.

In a recent study, Alametsä and Viik [Alametsä 2018] presented the stability of ballistocardiogram signal during 12 years' time, on which the data was gathered from a single person in a sitting position using EMFi sensors. Several other signals were recorded as well such as ECG, ankle pulse signal, and the carotid pulse signal from the neck near the carotid artery. All measurements lasted about 2 to 3 minutes with a sampling frequency of 500 Hz. In a conclusion, ballistocardiogram research may be recommended for examining long-term changes in heart operation and to reveal variations in it. Table 3.3 summarizes the unconstrained monitoring of vital signs using the EMFi-based sensors.

3.2.3 Pneumatic-Based Sensors

The idea of the pneumatic system is to deploy a thin air-sealed cushion between the bed and mattress. Thereafter, when a person rests in the bed, the forces originated because of the heartbeat, respiration, snoring and body movements affects the air in the cushion through the mattress. This slight human movement causes a pressure and therefore variations in pressure are measured by a supersensitive pressure sensor [Chow 2000, Watanabe 2004].

Watanabe *et al.* [Watanabe 2005] used the aforementioned pneumatic system to measure heartbeat, respiration, snoring, and body movements in a noninvasive manner. The three bio-signals, namely heartbeat, respiration, and snoring were detected using a band-pass filter with different cutoff frequencies. Following, windowed Fast Fourier transform algorithm was applied to measure heart rate and respiration. However, the relative magnitude of snoring was calculated by the standard deviation of the filtered snoring signal and the relative magnitude of body movements was calculated as the standard deviation of the envelope of the sensor output signal. The authors validated the proposed system using data collected from 15 subjects (12 males and 3 females) over 15 nights. Preliminary results showed good agreement against reference devices, namely ECG, belt-type respirometer, and a snoring detection microphone. The body movements were identified and recorded by a CCD camera. In another study, Kurihara and Watanabe [Kurihara 2012] acquired data from 10 subjects (20 seconds each) to measure heart rate and respiration. In this study, a condenser microphone was used as a reference for heart rate, respiration and signal-to-noise ratio. Validation results demonstrated that the pneumatic system was more susceptible to environmental noise, for example, opening and closing the door than the reference condenser microphone.

Chee *et al.* [Chee 2005, Shin 2006] recommended to use a balancing tube between two air cells to improve the effectiveness of posture changes during data collection. Balancing tube with a high air resistance aimed at equalizing the pressure of each air cell within a certain time constant. More precisely, it performed the role of a high-pass filter to eliminate body motion. The air-mattress system consisted of 19 air cells, in which measurements can be performed between any pair of cells.

Table 3.3: Summary of unconstrained monitoring of vital signs using EMFi-based sensors. *WT*: wavelet transform, *N/A*: not available, *M*: male, *F*: female, *HR*: heart rate, *RR*: respiratory rate, *ACF*: autocorrelation function, *Min*: minutes, *Hrs*: hours, *Sec*: seconds, *CEP*: cepstrum, *MAP*: maximum amplitude pairs, *AMDF*: adaptive-window average magnitude difference function, *EMD*: empirical mode decomposition, *TH*: threshold, *LT*: linear transform, *Lab*: laboratory.

	Method	Subjects (M, F)	Deployment	Duration	Outcome
[Kortelainen 2007]	Visually	1 M, 1 F	Lab	5 Min	BCG
[Kortelainen 2007]	CEP	6 M	Lab	Overnight	HR
[Aubert 2008]	Adaptive TH, ACF	58 M, 102 F	sleep Lab, Home	Overnight	HR, RR
[Karki 2008]	PSD	N/A	Lab	60 Sec	HR, RR
[Kärki 2009]	PSD	5 M, 5 F	Lab	30 Sec	HR, RR
[Pinheiro 2009]	PSD	5 N/A	Lab	10 Min	HR, BP
[Pinheiro 2010a]	PSD	4 M, 2 F	Lab	125 Sec	HR
[Brüser 2013]	ACF, MAP, AMDF	14 M, 19 F	Clinic	Overnight	HR
[Zink 2015]	ACF, MAP, AMDF	15 M, 7 F	Hospital	N/A	HRV
[Zink 2017]	ACF, MAP, AMDF	19 M, 2 F	Hospital	Overnight	HR
[Pino 2015]	EMD, WA, LT	54 N/A	Lab, Hospital	1 Min, 2 Min	HR
[Pino 2016]	EMD, WA, LT	114 N/A	Home, Hospital	2 Min, 2 Min	HR

However, the authors collected data from the two cells situated on the backside of the chest and abdominal region. Signal was collected from a single subject laying on the air mattress where ECG and nasal airflow signal were collected simultaneously. Although the balancing tube helped eliminate body motion, it affected the sensitivity of the measurement. Heart rate was measured by finding the maximum peak of the BCG signal between the two R-R peaks of the ECG signal. On the other hand, the respiratory rate was measured by windowed fast Fourier transform, i.e., short-time Fourier transform (STFT). Preliminary results showed good match against reference devices. Nevertheless, the proposed system might not be a preferred choice for large-scale deployment due to its complexity. In another study, Shin *et al.* [Shin 2010] applied the same air mattress for uncontaminated measurement of heart rate and respiration. In which, a total of 13 healthy male subjects were involved in the validation study, i.e., four hours study. The authors measured the heart rate from the R-peaks of the ECG, while the respiratory rate was measured manually. In addition, the authors asked three subjects to simulate sleep apnea (breath-holding) five times each for 10 to 15 seconds. Thereafter, the apneas were detected based on the variance of the respiratory signal with a moving window technique. Table 3.4 summarizes the unconstrained monitoring of vital signs using the pneumatic-based sensors.

3.2.4 Strain Gauges-Based Sensors

Brink *et al.* [Brink 2006] implemented four force sensors under bed-frames to unobtrusively record heartbeat, respiration activity, and body movements. Each force sensor consisted of a reflex light barrier sandwiched between two aluminum plates. When a force is applied to the sensor, the two aluminum plates are squeezed together slightly and the distance between them decreases. The reflex light barrier senses the distance between the two plates and converts it into a voltage signal, which is analogous to the ballistic forces of the heart. This voltage signal is then pre-amplified and passed through a low-pass filter to eliminate ripple and noise. In this preliminary study, heartbeat and respiration were detected by finding local minima or maxima in the signal within a sliding window. To evaluate the robustness of the force sensors, the signals were acquired from four subjects (2 males and 2 females) and in different conditions, i.e., three types of single beds, three types of frames, two types of mattresses. In total, seventy-two conditions were evaluated. In each condition, subjects were asked to sleep in a relaxed supine position on the bed. The signals were collected during 5-minute recording from the four force sensors. Additionally, ECG signals were also collected as a reference. Preliminary results showed that the proposed system can be an acceptable tool for computerized and unattended sleep-data collection over a lengthy period.

Inan *et al.* [Inan 2009] collected ballistocardiogram signals using strain gauges within a modified commercial scale. The signals were collected from twenty-one subjects (11 males and 10 females), on which participants were asked to stand as quiet as possible on the scale for 45 seconds while BCG and ECG were concurrently

Table 3.4: Summary of unconstrained monitoring of vital signs using Pneumatic-based sensors. *N/A*: not available, *M*: male, *F*: female, *HR*: heart rate, *RR*: respiratory rate, *Min*: minutes, *Hrs*: hours, *Sec*: seconds, *STFT*: short-time Fourier transform, *Lab*: laboratory.

	Method	Subjects (M, F)	Deployment	Duration	Outcome
[Watanabe 2005]	STFT	12 M, 3 F	Lab	Overnight	HR, RR, SI
[Kurihara 2012]	STFT	10 N/A	Lab	20 Sec	HR, RR
[Chee 2005, Shin 2006]	ECG Sync, STFT	1 N/A	Lab	N/A	HR, RR
[Shin 2010]	ECG Sync, STFT	13 M	Lab	4 Hrs	HR, RR

recorded. In this study, the measured ballistocardiogram signals from all subjects closely resemble those reported in the literature. Besides, the system was able to provide beat-to-beat cardiac output monitoring. Additionally, ballistocardiogram measurements were found to be repeatable over 50 recordings collected from the same subject over a three-week period. The proposed solution was more susceptible to motion artifacts because the signals were acquired in a standing position. Hence, it might not be suitable for older adults who cannot stand as tranquil on the scale. In order to eliminate floor vibrations, Inan *et al.* [Inan 2010a] proposed a seismic sensor, i.e., geophone, located in proximity to the modified scale that served as the noise reference. An adaptive algorithm was then implemented to filter the output of this sensor and cancel the vibrations from the measured ballistocardiogram signal. Signals were collected from a healthy volunteer while another person stomped around the scale, hence producing increased floor vibrations. Furthermore, signals were also collected from another volunteer standing inside a parked bus while the engine was functioning. This research established that ballistocardiogram recording is feasible in almost all environments, including ambulances and other transport vehicles, as long as the vibrations are not so significant to rail the electronics or lead to a distorted version of the ballistocardiogram force to be coupled to the scale.

In the same way, Inan *et al.* [Inan 2010b] evaluated the electromyogram signal collected from the feet of the subject during ballistocardiogram recording as a noise reference for standing ballistocardiogram measurements. As the lower-body electromyogram signal can be collected directly from the footpad of the modified scale, the proposed system is self-contained and can automatically eliminate motion artifacts. In another study, Wiard *et al.* [Wiard 2011] used a motion sensor instead of electromyogram sensors to record body motions and to serve as a noise reference. The added value of the motion sensor was to provide a minimum delay between the motion-related noise in the measured signal and the noise detected by the motion sensor. This minimum delay provided the time resolution needed to flag single heartbeat events, hence maximizing the refinement of the approach.

Brüser *et al.* [Bruser 2011] introduced an unsupervised learning approach to measuring heartbeat in a noninvasive manner. Ballistocardiogram signals were recorded by strain gauges in a Wheatstone bridge configuration attached to the slat under the mattress of a hospital bed. A high-pass filter was applied to the raw data in order to remove low-frequency respiratory components. Next, a set of features, representing the fundamental morphology of the heartbeat, were extracted from a 30-second time segment. Afterward, the principal component analysis was applied in order to reduce the dimensionality of the feature vectors. Additionally, a k-means clustering algorithm was adopted to identify clusters of feature vectors. This training step resulted in a list of estimated heartbeat locations. The parameters obtained during the training step were thus manipulated to locate heartbeats in the remaining ballistocardiogram signal by merging the results of three independent indicator functions, i.e., cross-correlation, Euclidean distance, and heart valve signal. Finally, the estimated heartbeat locations were exploited to provide an improved list of beat-to-beat periods. Signals were captured from sixteen healthy subjects

(9 males and 7 females) during thirty minutes switching their positions every 7.5 minutes (left lateral, supine, right lateral, prone). This method produced good agreement with the reference ECG. However, the primary limitation was the training step as it had to be repeated whenever subjects enter the bed or adjust their posture with regard to the ballistocardiogram sensor.

Nukaya *et al.* [Nukaya 2012] provided a contact-free method for unobtrusive measuring of heartbeat, respiration, body movement, and position change. The authors collected the pressure data using four piezoceramics transducers set beneath bed supports. The proposed system was able to detect previous bio-signals without the need for a preamplifier, accordingly without any voltage source. This is because the sensing devices were distortion sensors that operate without an electrical power supply, i.e., they produce voltage according to the time derivative of the distortion.

Vehkaoja *et al.* [Vehkaoja 2013] introduced dynamic pressure sensors for detecting heartbeat intervals of an individual sleeping on a bed. The pressure sensors were composed of EMFi material and located under the bed supports. In this study, individual heartbeats were not observed. However, the intervals in which the correlation between two successive signals segment maximized. Ballistocardiogram signals were collected from nine subjects (5 males, 4 females) during 1-hour recording. The beat-to-beat intervals provided by this approach can be adopted in determining frequency domain heart rate variability that is most frequently used in the assessment of sleep quality.

Lee [Lee 2016] *et al.* proposed to use load cells, installed under bed supports, to measure heart rate and respiration for infants. Four infants (5 to 42 months) were involved in the study and a total of 13 experiments were carried out between 10 to 178.8 minutes. Initially, heart rate and respiratory components were extracted using band-pass filters of various cutoff frequencies. For the heart rate component, a first-order differentiation filter was applied, thus a nonlinear transformation, i.e., a Shannon entropy was applied to the differentiated signal to obtain only positive peaks. Additionally, a moving average filter was employed to flatten out the spikes and noise bursts. At last, heart rate was measured by finding local peaks in an optimum signal. For the respiration component, as the band-pass filtered signal contained residual baseline drift, a detrending algorithm based on empirical mode decomposition was adopted to get rid of such unwanted trend. Similar to heart rate, local peaks were detected in the detrended signal and therefore the respiratory rate was measured. A signal quality index was developed to choose the optimum signal out of the four load cells' signals. The quality processing procedure was developed based on calculating a threshold value computed from an autocorrelation function and a power spectral density function. The proposed system achieved acceptable results compared to the reference ECG and respiratory belt. Table 3.5 summarizes the unconstrained monitoring of vital signs using the strain gauges-based sensors.

Table 3.5: Summary of unconstrained monitoring of vital signs using Pneumatic-based sensors. *N/A*: not available, *M*: male, *F*: female, *HR*: heart rate, *RR*: respiratory rate, *Min*: minutes, *Hrs*: hours, *Sec*: seconds, *SWM/M*: sliding window minimum/maximum, *ECG Sync*: electrocardiogram synchronization, *PCA*: principal component analysis, *CCF*: cross-correlation function, *ED*: Euclidean distance, *HVS*: heart valve signal, *ACF*: autocorrelation function, *SE*: Shannon entropy, *EMD*: empirical mode decomposition, *Lab*: laboratory.

	Method	Subjects (M, F)	Deployment	Duration	Outcome
[Brink 2006]	SWM/M	2 M, 2 F	Lab	5 Min	HR, RR
[Inan 2009]	ECG Sync	11 M, 10 F	Lab	45 Sec	HR
[Bruser 2011]	PCA, K-means CCF, ED, HVS	9 M, 7 F	Lab	30 Min	HR
[Vehkaoja 2013]	ACF	5 M, 4 F	Lab	1 Hrs	HR
[Lee 2016]	SE, EMD, SWM/M	Infants (3 M, 1 F)	Home	10 - 178.8 Min	HR, RR

3.2.5 Hydraulic-Based Sensors

The concept of the hydraulic sensor is to measure the change in pressure applied to a liquid-filled tube. For example, Heise *et al.* [Heise 2010] designed a hydraulic based-sensor for unrestrained monitoring of heart rate and respiration. Preliminary data were collected from two individuals (1 male and 1 female). Participants were instructed to lie on a bed for approximately 10 minutes. During the 10 minutes, they were asked to lie on the back, on the right side, on the back again, on the left side, and on the back once more (2 minutes each position). In this preliminary research, heartbeat signal was extracted by detecting the difference between the most negative and the most positive points within a moving window. After that, a low-pass filtered was applied to reduce the effect of noise and smooth the signal. A fixed threshold was employed to detect a body motion. Finally, the heart rate was measured by adopting the autocorrelation function. However, the respiratory rate was measured by low-pass filtering the signal and then subtracting the DC bias. Afterward, the zero-crossings were counted to provide the breaths per minute. Preliminary results approved that the hydroponic sensor was effective at extracting heart rate and respiration against the reference devices, namely a piezoresistive device worn on the subject's finger and respiration band wrapped around the subject's torso. In a different study, Heise *et al.* [Heise 2011] have validated the sensor using data collected from five subjects (3 males and 2 females) and have confirmed stability of the signal processing algorithms using real and synthesized signals.

Rosales *et al.* [Rosales 2012] deployed four hydraulic transducers under the bed mattress, covering the upper part of the body in order to measure heart rate in a nonrestrictive way. Each transducer was connected to a pressure sensor to record the pressure forces applied to it. In this preliminary study, heartbeats were computed using a clustering-based approach as follows. Every five seconds, body motions were eliminated based on the variance of the transducers' signal. Following body motions removal, the transducer's signal was band-pass filtered to remove respiratory components and filtered once more using an average filter to smooth the signal prior to feature extraction. Afterward, three features were extracted from every 5-second time window based on the IJK points of the ballistocardiogram signal. In addition, the extracted features were classified into two groups using k-means clustering algorithm. The first group, i.e., the smallest cluster was assigned to the heartbeat class. Then, the second group, i.e., the largest cluster was assigned to the non-heartbeat group. In conclusion, the heartbeats' (J-peaks) locations were compared to a reference signal obtained from a piezoresistive device worn on the subject's finger. Data were acquired from four subjects (2 males and 2 females) during 6 minutes (supine position). Although such clustering-based approach might have provided good results it might only be applicable to specific situations. Furthermore, to think the presented method to be applied in practical applications, manually labeling (training) data is, however, a restricting property.

A similar study was proposed by Su *et al.* [Su 2012]. Nonetheless, the heart rate was measured using the Hilbert transform and the fast Fourier transform

(30-second window). In this study, ballistocardiogram signals were acquired from five subjects (3 males and 2 females) during 2.5 minutes in a supine position. This approach provided a lower error rate compared with the windowed peak to peak deviation (WPPD) method introduced by Heise *et al.* [Heise 2010]. Although results were consistent with the reference device, ballistocardiogram signals were assumed relatively stationary. This assumption is not always true because typically heartbeats are not uniform in time [Heise 2013].

In another study, Lydon *et al.* [Lydon 2015] proposed a new algorithm to detect heart rate using the four hydraulic transducers. As a first step, a band-pass filter was implemented to remove the respiration component as well as high-frequency noise. Next, the data from the four transducers were separated into 0.3-second (30 samples) segments and the short-time energy profiles were computed for each segment. As a result, four heart rate values were generated for each transducer by locating the local peaks. Moreover, a single heart rate value was selected based on the DC level of each transducer's signal. Typically, a higher DC level in the obtained transducer's signal means that the transducer makes better contact with the body and therefore gives a more stable ballistocardiogram signal. Hence, the transducer with the highest DC level was chosen for heart rate measurement. Finally, outliers were eliminated by following whether the estimated heart rate value was more than 15 beats per minute from the moving average heart rate value. Validation data were collected from two groups, i.e, three subjects (2 males and 1 female) during 10 minutes recording and four older adults (4 males) in a typical home environment. This approach provided slightly better results compared to the clustering-based approach provided by Rosales *et al.* [Rosales 2012].

In order to address the uncertainty inherent in a ballistocardiogram signal, for instance, misalignment between training data and ground truth, improper collection of the heartbeat by some transducers, Jiao *et al.* [Jiao 2016] applied the Extended Function of Multiple Instances (eFUMI) algorithm to ballistocardiogram signals generated by the four hydraulic transducers. The objective of the eFUMI was to learn a personalized concept of heartbeat for a subject in addition to several non-heartbeat background concepts. Following the learning step, heartbeat detection and heart rate estimation can be applied to test data. The limitation of this algorithm is the need for sufficient training data, which might not be always available.

Rosales *et al.* [Rosales 2017] applied the clustering-based approach [Rosales 2012] and the Hilbert transform approach [Su 2012] to ballistocardiogram signal collected from four male senior residents. The signals were collected from residents over a two to four months period under in-home living conditions. However, the analysis was done only over five minutes of initial recordings. The Hilbert transform approach was able to produce more stable heart rate estimates compared to the clustering-based approach. The latter approach was more susceptible to motion artifacts. Table 3.6 summarizes the unconstrained monitoring of vital signs using the hydraulic-based sensors.

Table 3.6: Summary of unconstrained monitoring of vital signs using Hydraulic-based sensors. *N/A*: not available, *M*: male, *F*: female, *HR*: heart rate, *RR*: respiratory rate, *Min*: minutes, *Hrs*: hours, *Sec*: seconds, *WPPD*: windowed peak to peak deviation, *CA*: clustering approach, *HT*: Hilbert transform, *STE*: short-time energy, *eFUMI*: extended function of multiple instances, *Lab*: laboratory.

	Method	Subjects (M, F)	Deployment	Duration	Outcome
[Heise 2010]	WPPD	1 M, 1 F	Lab	10 Min	HR, RR
[Heise 2011]	WPPD	3 M, 2 F	Lab	10 Min	HR, RR
[Rosales 2012]	CA	2 M, 2 F	Lab	6 Min	HR
[Su 2012]	HT	3 M, 2 F	Lab	2.5 Min	HR
[Lydon 2015]	STE	2 M, 1F 4M	Lab Home	10 Min Overnight	HR HR
[Jiao 2016]	eFUMI	4 N/A	Lab	10 Min	HR
[Rosales 2017]	CA, HT	4 M	Home	Overnight	HR

3.2.6 Fiber Optic-Based Sensors

In existing literature, unobtrusive vital signs monitoring is achieved either by microbend fiber-optic sensors (MFOS) or fiber Bragg grating sensors (FBGS). The principle of the MFOS is that if an optical fiber is bent, insignificant amounts of light are lost through the fiber walls. This reduces the amount of received light and is a function of bend pressure [Lagakos 1987, Berthold 1995, Luo 1999, feng Hu 2016]. The FBG is an optical fiber that serves as a filter for a specific wavelength of light. The principle of the FBGS is to detect the reflected Bragg wavelength shift owing to changes in temperature, strain, or pressure [Moghadas 2010, Poeggel 2015]. Fiber Bragg gratings are commonly used optical fiber sensors for measuring temperature and/or mechanical strain. Though, the excessive cost of the interrogation systems is the most significant obstacle for their large commercial application [Díaz 2017].

Chen *et al.* [Chen 2009c, Chen 2012] described the effectiveness of the MFOS for noninvasive monitoring of heart rate and breathing rate. For heart rate, ballistocardiogram signals were gathered from several subjects in sitting position and breathing normally. Preliminary results have proved that the ballistocardiogram waveforms closely simulated those reported in the existing literature. For breathing rate, nine volunteers were involved in the study in which respiratory signals were collected during sleep. The system has shown a good match with the reference respiratory device. Deepu *et al.* [Deepu 2012] introduced a smart cushion integrated with MFOS for real-time heart rate monitoring. The cushion can be placed on the seat or back of a chair for data collection. In this study, five subjects were involved, and signals were collected during 5-minutes. Several steps were applied to the cushion's signals in order to unobtrusively measure the heart rate. Initially, low and high-frequency noises were suppressed using a band-pass finite impulse response (FIR) filter. Next, a cubing operation was applied to the filtered signal to enhance the amplitude swing while keeping the signal sign intact. Afterward, momentary upswing or downswing was removed by applying a moving average filter. Furthermore, the resultant signal was smoothed by utilizing the absolute value and averaging over a predefined time window. At last, the J-peaks were recognized by using a cone detection and comparing to an adaptive threshold. The proposed system achieved satisfactory results compared to the reference pulse oximetry device.

Chen *et al.* [Chen 2013] studied the possibility of measuring blood pressure using ballistocardiography and photoplethysmography (PPG). The concept was to calculate the time delay between the peaks of the ballistocardiography and the corresponding PPG peaks. Ballistocardiogram signals were collected from five healthy subjects in a sitting position using a cushion integrated with MFOS, whereas PPG signals were collected from a finger pulse oximeter. Preliminary results have shown that blood pressure might be measured using optical devices. However, the proposed approach was very challenging because it required a calibration procedure for each subject prior to measurement.

Lau *et al.* [Lau 2013] evaluated the effectiveness of the MFOS for respiratory monitoring and respiratory gating in the magnetic resonance imaging (MRI) envi-

ronment. Respiratory gating is the process of reducing cardiorespiratory artifacts by synchronizing magnetic resonance data acquisition to the cardiac or respiratory cycles. Unlike electrical sensors, fiber-optic sensors are immune to electromagnetic and radio-frequency interference. Twenty healthy subjects (10 males and 10 females) were involved in the study and they underwent T2-weighted half-Fourier single-shot turbo spin-echo MRI of the liver with synchronous breathing rate monitoring on a 1.5 Tesla magnetic resonance scanner. The breathing rate was detected by applying a band-pass filter and hence detecting local peaks in the time domain. This study presented that the MFOS were able to detect comparable breathing rate to the reference respiratory bellows and produce liver MRI images of good diagnostic quality compared to the navigator-acquired scans. Chen *et al.* [Chen 2014b] reported related results using data collected from eleven healthy subjects (6 males and 5 females) during MRI.

A similar study was provided by Dziuda *et al.* [Dziuda 2013a]. However, authors used FBG sensors rather than MFOS. Three healthy volunteers (2 males and 1 female) were included in the study and physiological data were collected during 95 minutes. Both heart rate and breathing rate were measured by finding local maxima after applying band-pass filters of different cutoff frequencies to the sensor data. Similar to the MFOS, the FBG sensor did not introduce any artifacts into MRI images. Furthermore, the system achieved comparable results to the reference devices, i.e., carbon electrodes and pneumatic bellows, respectively. Dziuda *et al.* [Dziuda 2013b, Dziuda 2014, Krej 2015, Dziuda 2015] reported similar results using data collected during MRI examination.

Zhu *et al.* [Zhu 2013] demonstrated the effectiveness of the MFOS for unobtrusive measurement of heart rate in a headrest position. Three healthy individuals were enrolled in the study in which an optical sensor mat was placed on the headrest of a massage chair. The participants were instructed to complete predefined series of tasks, i.e., rest, cognitive test battery, and relaxing massage session. In this preliminary study, the analysis was done only during rest periods for a total of six minutes. A band-pass filter was applied to the sensor data to remove low-frequency respiratory signals. Afterward, heart rate was computed using short-time Fourier transform. The proposed system achieved a relatively good agreement against the reference ECG.

Chen *et al.* [Chen 2014a] reported the results of using the MFOS in a clinical trial for unobtrusive monitoring of heart rate and respiration during sleep. During the study, data were collected from twenty-two subjects using the optical fiber sensor and also from the standard polysomnography as a reference. At the beginning, large body movements were eliminated using a moving time window. In which, a segment was identified as a body movement if the difference between the maximum and the minimum in the moving window was larger than a fixed threshold. Next, respiratory and heartbeat components were separated from the sensor's signals using band-pass filters of different cutoff frequencies. In the former, the signals were smoothed using a moving-average filter and hence the baseline was obtained by another moving-average filter of a larger window size. After subtracting the

signals and the baseline, they were further smoothed using Savitzky–Golay method. Finally, local peaks were detected, and breathing rate was computed. In the latter, all local peaks of the heartbeat signals were detected, and heart rate was computed accordingly. Consequently, incorrect heart rate values were eliminated by applying a histogram-based method, in which the group with the highest occurrence was selected and reported as final heart rate results. Results were promising. However, the proposed approach was prone to motion artifacts.

Zhu *et al.* [Zhu 2014] proposed to measure heart rate using ballistocardiogram signals collected from FBG sensor mat. The sensor mat consisted of three FBG sensor arrays or channels and each array contained six sensors. The arrays were located under the pillow, upper chest, and lower chest. In this study, ten subjects were enrolled, and signals were collected during 20 minutes such as 10 minutes of supine posture and 10 minutes of sideways posture. ECG signals were collected along with the fiber-optic signals as a reference. The signal from each sensor array was transformed from time domain into cepstrum domain. After that, the signal from the six sensors of the same arrays was fused by employing cepstrum. Finally, the heart rate was measured from the fused signal by recognizing peaks in the cepstrum. This study demonstrated that the heart rate can be measured from distinct locations. However, the best results were achieved from sensor arrays at chest position. In another study, Zhu *et al.* [Zhu 2015] used the same system to compute breathing rate and the system was tested against twelve subjects.

Fajkus *et al.* [Fajkus 2017a] introduced to measure heart rate and respiration using FBG sensors encapsulated inside a polydimethylsiloxane polymer (PDMS). The FBG sensors were embedded within a thoracic elastic strap to record cardiorespiratory signals. In this preliminary analysis, the authors collected data from 10 individuals (6 males and 4 females) during few minutes. Heart rate and breathing rate were detected by adopting two methods, i.e., identifying the periodic cycles in the time domain and applying the FFT to obtain the dominant frequency. The proposed system achieved comparable results to the reference ECG. However, it was susceptible to large body movements. In another study, Fajkus *et al.* [Fajkus 2017b] assessed the effectiveness of using FBG sensor encapsulated inside a PDMS and FBG sensor glued on a plexiglass pad for heart and respiratory rate monitoring. In this preliminary study, the authors collected data from 10 subjects (7 males and 3 females) and result shown that the FBG sensor encapsulated into PDMS was more accurate than FBG sensor encapsulated in plexiglass pad.

Chethana *et al.* [Chethana 2017] reported the use of FBG sensor for monitoring cardiac and breathing activities. Cardiorespiratory signals were collected from four subjects (2 males and 2 females) for 60 seconds, on which the FBG sensor was placed on the pulmonic area on the chest of the subjects. Results have been evaluated against an electronic stethoscope which recognizes, and records sound pulses generated from the cardiac activity. Nedoma *et al.* [Nedoma 2017] evaluated the effectiveness of the FBG sensor against fiber interferometric sensor for heart rate measurement. The former measured the heart rate through ballistocardiography, while the latter measured the heart rate through Phonocardiography. Cardiac signals

were obtained from six individuals (3 males and 3 females) using the two sensors for 60 minutes. Primary results have shown that the fiber interferometric sensor was more accurate than the FBG sensor. [Table 3.7](#) summarizes the unconstrained monitoring of vital signs using the fiber optic-based sensors.

3.3 Conclusion

This chapter provided the definition and the nomenclature of ballistocardiography. In addition, it discussed in detail the different modalities reported in existing literature for unobtrusive monitoring of vital signs, namely heart rate, breathing rate, and body movements. These modalities include piezoelectric polyvinylidene fluoride sensors, electromechanical film sensors, pneumatic sensors, load cells, hydraulic sensors, and fiber-optic sensors. In general, the output of these sensors is a composite signal that is composed of cardiac activities, respiratory activities, and body movements. Hence, these three signals should be separated from each other so that vital signs can be measured. The separation process is usually performed by applying a band-pass filter of specific cutoff frequencies according to the signal of interest. In other cases, the separation process can be performed by adopting a decomposition algorithm such as empirical mode decomposition algorithm and wavelet multiresolution analysis. It should be noted that, vital activities cannot be detected during body movements and hence they should be eliminated prior to the measurement process. Following the separation process, i.e., obtaining cardiac signals and respiratory signals, several algorithms can then be implemented for vitals measurements. As discussed in previous sections, these algorithms include but not limited to simple peak detector, autocorrelation function, fast Fourier transform, cepstrum analysis, wavelet multiresolution analysis, empirical mode decomposition, power spectrum analysis, and clustering-based approaches. The clustering-based approaches are not very effective because the training step should be repeated whenever the data collection protocol has been changed. Moreover, the ballistocardiogram morphology varies between and within subjects, and the shape of the signal is highly dependent on subject's postures, i.e., sleeping or sitting. Furthermore, the raw signal is noisy and nonstationary due to body movement, induced respiratory efforts, and the characteristics of the sensing system itself. As previously mentioned in [Chapter 1](#), the microbend fiber-optic sensor will be used to record cardiorespiratory signals due to its high sensitivity to ballistic forces of the heart as well as its immunity to electrical and electromagnetic interference. The ensuing chapter will show in more detail the theory of the microbend fiber-optic sensor in addition to the proposed system to analyze and interpret the cardiorespiratory signals obtained from the optical fiber sensor.

Table 3.7: Summary of unconstrained monitoring of vital signs using Hydraulic-based sensors. *N/A*: not available, *M*: male, *F*: female, *HR*: heart rate, *RR*: respiratory rate, *Min*: minutes, *Hrs*: hours, *Sec*: seconds, *BP*: blood pressure, *PPG Sync*: Photoplethysmography synchronization: *STFT*: short-time Fourier transform, *CEPS*: cepstrum, *Lab*: laboratory.

	Method	Subjects (M, F)	Deployment	Duration	Outcome
[Chen 2009c]	Visually	N/A	Lab	N/A	HR
[Chen 2012]	Visually	9 N/A	Lab	N/A	RR
[Deepu 2012]	Peak Detector	5 N/A	Lab	5 Min	HR
[Chen 2013]	PPG Sync	5 N/A	Lab	N/A	BR
[Lau 2013]	Peak Detector	10 M, 10 F	MRI	N/A	RR
[Chen 2014b]	Peak Detector	6 M, 5 F	MRI	N/A	HR, RR
[Dziuda 2013a]	Peak Detector	2 M, 1 F	MRI	95 Min	HR, RR
[Dziuda 2013b]	Peak Detector	8 M, 4 F	MRI	60 Min	HR, RR
[Dziuda 2014]	Peak Detector	1 M	MRI	19 Min	HR
[Krej 2015]	Peak Detector	6 M, 2 F	MRI	82 Min	HR
[Zhu 2013]	STFT	3 N/A	Lab	6 Min	HR
[Chen 2014a]	Peak Detector	22 N/A	Hospital	Overnight	HR, RR
[Zhu 2014, Zhu 2015]	CEPS	10 N/A	Lab	20 Min	HR, RR
[Fajkus 2017a]	Peak Detector, FFT	6 M, 4 F	Lab	N/A	HR, RR
[Chethana 2017]	Visually	2 M, 2 F	Hospital	1 Min	HR, RR
[Nedoma 2017]	Peak Detector	3 M, 3 F	Lab	60 Min	HR, RR

System Design

Contents

4.1	Introduction	55
4.2	System Design	56
4.2.1	Suitable Sensor Selection	57
4.2.2	System Development	59
4.2.3	System Validation	60
4.2.4	UbiSMART Design	60
4.2.5	System Integration	61
4.3	Conclusion	62

4.1 Introduction

In the preceding chapter, we mentioned several algorithms for analyzing and interpreting cardiorespiratory signals obtained from in-bed monitors. To wrap up, these algorithms can be broadly grouped into three categories: time-domain algorithms, frequency-domain algorithms, and wavelet-domain algorithms. A summary of these algorithms is given below to highlight which category of algorithms will be used in our analysis.

In the first place, time-domain algorithms are mainly focused on detecting local maxima or local minima using a moving window, and therefore finding the interval between the dominant J-peaks of ballistocardiogram signal. However, this approach has many limitations because of the nonlinear and nonstationary behavior of the ballistocardiogram signal. The implication is that the ballistocardiogram signal does not display consistent J-peaks, which can usually be the case for overnight, in-home monitoring, particularly with frail elderly. Additionally, its accuracy will be undoubtedly affected by motion artifacts.

In the second place, frequency-domain algorithms do not provide information about interbeat intervals. Nevertheless, they can provide information about heart rate variability. This is usually done by taking the fast Fourier transform or the inverse Fourier transform of the logarithm of the estimated spectrum, i.e., cepstrum of the signal using a sliding window. Thereafter, the dominant frequency is obtained in a particular frequency range. The limit of these algorithms is that the peak in

the spectrum may get wider and multiple peaks may appear, which might cause a problem in measuring the vital signs.

Finally, the objective of wavelet-domain algorithms is to decompose the signal into different components, hence the component which shows an agreement with the vital signs can be selected. In other words, the selected component contains only information about the heart cycles or respiratory cycles, respectively. Interbeat intervals can be found easily by applying a simple peak detector. An empirical mode decomposition is an alternative approach to wavelet decomposition, and it is also a very suitable approach to cope with nonlinear and nonstationary signals such as cardiorespiratory signals. Apart from the above-mentioned algorithms, machine learning approaches have been implemented for measuring heartbeats. However, manual labeling of training data is a restricting property. Furthermore, the training step should be repeated whenever the data collection protocol has been changed.

In the following sections, the operating principle of the microbend fiber-optic sensor is discussed in more detail ([Section 4.2.1](#)). Likewise, we discuss our system development cycle ([Section 4.2.2](#)). Furthermore, we present how the proposed system is validated for health and clinical applications ([Section 4.2.3](#)). At last, we show how the system is integrated within an existing Ambient Assisted Living platform ([Section 4.2.4](#) and [Section 4.2.5](#)).

4.2 System Design

This section aims to explain how the optical fiber data is analyzed and interpreted so that relevant information can be obtained. The optical fiber mat can provide different information such as heart rate, breathing rate, body movements, as well as sleep parameters. The sleep parameters involve waking up time, sleep time, the total time of sleep, sleep interruptions, i.e., frequent body movements and bed exits. To achieve these goals, first and foremost, we need to understand the nature of cardiorespiratory signals. In fact, cardiorespiratory signals are nonlinear and nonstationary signals that represent the functions of the cardiovascular and respiratory system, respectively. Typically, the acquisition of such signals requires sensors or electrodes that are attached to the body. For example, electrocardiography requires a minimum of two electrodes mounted on the body to record the electrical activities that occur in the heart during polarization, depolarization, and repolarization. Another example is the photoplethysmography that requires a sensor worn on the finger to estimate arterial blood oxygen saturation (SpO₂). Since before-mentioned sensors are fixed to the skin, the motion artifacts of skin movements are greatly minimized. However, when it comes to non-contact cardiac and respiratory activity monitoring, the situation is completely different. To explain, in our case the optical fiber mat can be placed under the bed mattress or on the seat or the backrest of a chair; hence, the acquired signals are more prone to motion artifacts compared to standard medical sensors.

We explain the principles of operation of the optical fiber sensor in [Section 4.2.1](#). Moreover, we provide an explanation of how the raw data is compiled and analyzed, as

well as how the proposed methodology is validated in [Section 4.2.2](#) and [Section 4.2.3](#), respectively.

4.2.1 Suitable Sensor Selection

As we discussed in [Chapter 1](#) and [Chapter 3](#), the microbend fiber-optic sensor¹ (MFOS) is selected for unobtrusive acquisition of cardiorespiratory signals. It is because the sensor is particularly sensitive to pressure fluctuations induced by the ballistic forces of the heart, and it does not require close contact with the body. It is also relatively small, lightweight, and affordable, and then it is a suitable candidate for long-term monitoring of vital signs without disturbing patient's comfort. In contradistinction to electrical sensors, optical sensors are immune to electromagnetic and radio frequency interference. Hence, they are useful for real-time monitoring of physiological signals during magnetic resonance imaging. The proposed optical fiber

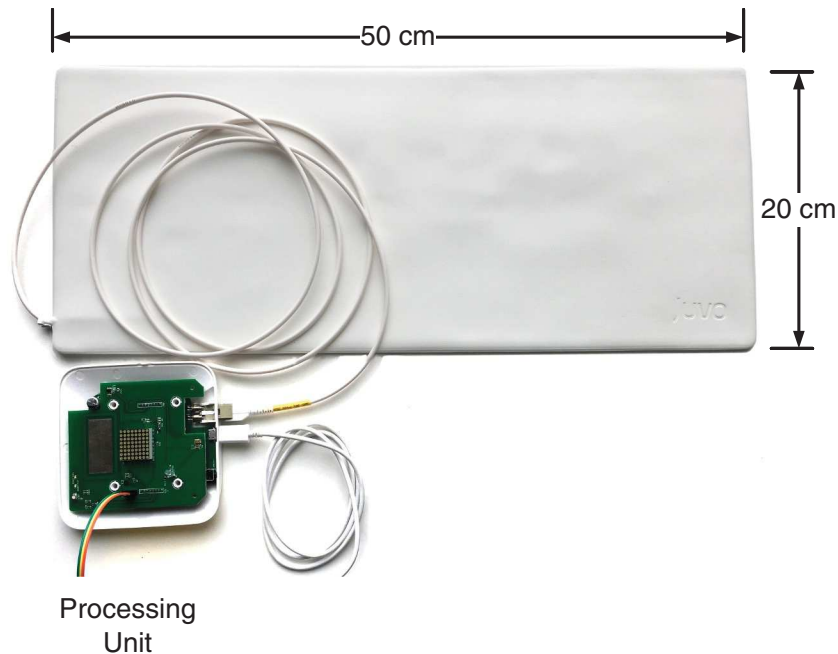


Figure 4.1: The deployable sensor mat and processing unit (Mat dimensions: 20 cm × 50 cm × 0.5 cm).

system consists of a sensor mat integrated with microbending multimode fiber and a processing unit as shown in [Figure 4.1](#). The processing unit contains a Micro-SD card, digital electronics for signal manipulation, and a Wi-Fi signal transmission module. By way of introduction, the fundamental principle of the MFOS is based on the light intensity modulation induced by microbending in multimode fibers,

¹The system hardware is commercialized by Juvo Labs company in Singapore (patented by A*STAR). Our contribution focused on the software part development by denoising and analyzing raw data from the mat

which is used as a transduction mechanism for detecting pressure. A 10-meter loop of graded-index multimode fiber is sandwiched between two layers of tuned grating structures that subject the fiber to mechanical perturbation when there is a pressure applied as shown in Figure 4.2. The pressure causes the transmission modes in the multimode fiber to be coupled into the loss mode, reducing the amount of light received by the photodetector. Thereupon, the detected light is converted to current by the photodetector, which is, in turn, converted into a voltage using a transimpedance amplifier. The signal is filtered via a 20 Hz low-pass filter and then digitized by a 16-bit analog-to-digital converter with a sampling frequency of 50 Hz.

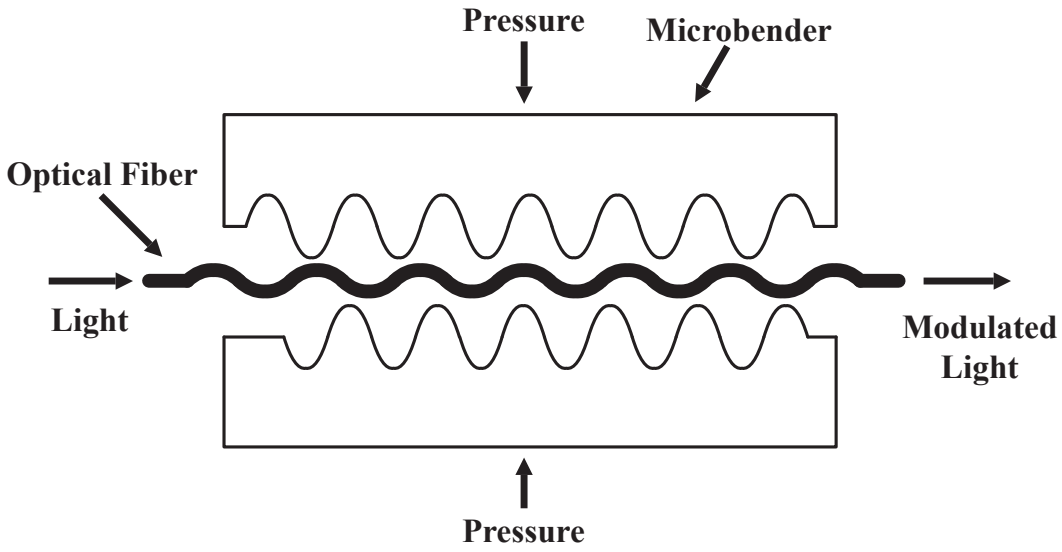


Figure 4.2: Longitudinal section of the microbend fiber-optic sensor.

Secondly, the presented sensor is constructed by using a typical graded-index multimode fiber with a core diameter of $100 \mu\text{m}$ and numerical aperture (N.A.) of 0.272 as the sensing fiber [Chen 2012, Lau 2013, Chen 2014b]. The sensor mat is manufactured to a dimension of $(20 \text{ cm} \times 50 \text{ cm} \times 0.5 \text{ cm})$, which facilitates its portability and inclusion into cushions, pillows, chairs, beds, etc. The sensor mat applies a force ΔF or a pressure ΔP to the bent multimode fiber and causes the amplitude of the fiber deformation X to change by an amount of ΔX . This takes place in response to breathing-generated body movement and heart rhythm-generated body movement. The transmission coefficient T for the light moving through the bent multimode fiber is altered by an amount ΔT as follows.

$$\Delta T = \left(\frac{\Delta T}{\Delta X} \right) \Delta F \left(k + \frac{AY}{l} \right) \quad (4.1)$$

where k is the force constant of the bent fiber, A is the cross-sectional area, Y is Young's modulus, and l is the microbender gap. Typically, detection of cardiores-

piratory signals is dependent on modulation in optical transmission. Regarding high-sensitivity pressure sensor application, Equation (4.1) is formulated as follows.

$$\Delta T \cong \frac{\Delta T}{\Delta X} A_p k^{-1} \Delta P \quad (4.2)$$

where A_p is the area of the deformer and ΔP is the variation in pressure. In order to achieve a maximum microbend sensitivity, the optical fiber should be constructed such that the spatial frequency Λ of the microbenders for graded-index multimode fiber complies with the following approximate relationship:

$$\Lambda = \frac{2\pi \cdot a \cdot n_0}{\text{NA}} \quad (4.3)$$

where a is the radius of the fiber core, n_0 is the refractive index of the core, and NA is the numerical aperture of the fiber. The loss in microbending develops because the guided modes are coupled to radiation modes. Equation (4.3) applies to graded-index multimode fiber. Alternatively, step-index multimode fiber can also be employed for construction of the sensor mat. In this condition, the spatial frequency Δ of the microbenders is obtained as follows.

$$\Lambda = \frac{\sqrt{2}\pi \cdot a \cdot n_0}{\text{NA}} \quad (4.4)$$

Efficient coupling between the guided modes and radiation modes can be accomplished with the spatial frequency Λ provided by Equation (4.3) and Equation (4.4) for graded-index and step-index multimode fibers, respectively. Nonetheless, the first group, i.e., graded-index multimode fibers is better than the second group, i.e., step-index multimode fibers because the first group has resonance condition, in which the microbending loss is precisely peaked whereas the second group does not have the resonance condition. As a result, the first group is decided for development of the sensor mat [Chen 2012, Lau 2013, Chen 2014b].

4.2.2 System Development

In light of the foregoing consideration, motion artifacts occurred due body movements or other environmental factors should be isolated and filtered out before the input signal is further processed. After that, cardiac and respiratory signals can be extracted from the filtered signal using a band-pass filter of different cutoff frequencies. Once the two main signals are separated, appropriate algorithms should be implemented so that heart and breathing rate can be measured.

In this research, various techniques have been adopted to analyze the data collected from the optical fiber mat. Initially, we applied machine learning algorithms to classify fiber-optic data into informative and non-informative signals based on their heart rate information. After that, we computed the heart rate from the informative signals using Complete Ensemble Empirical Mode Decomposition with Adaptive Noise (CEEMDAN) algorithm. This algorithm is a modified, improved algorithm for the Empirical Mode Decomposition algorithm. Preliminary results

were promising. However, the CEEMDAN algorithm required high processing time. Therefore, this approach did not meet our needs, and it was not suitable for real-life deployment. Secondly, instead of using machine learning algorithms to get informative signals, we designed a signal quality algorithm based on the signal variance that can automatically isolate motion artifacts and bed-exit events. The motion artifact is a large variation in the amplitude of the fiber-optic signal, which is sufficient enough to destroy valuable information in the signal. However, the bed-exit event is the standard fiber-optic signal that originates when there is no any pressure applied to the sensor. Thirdly, we implemented the multiresolution analysis of the Maximal Overlap Discrete Wavelet Transform (MODWT) instead of the CEEMDAN algorithm to measure the heart rate. The MODWT provided slightly inferior results to CEEMDAN algorithm. However, it required shorter processing time, so that it was more suitable for our real-time applications. Fourthly and finally, we tested the effectiveness of other algorithms such as fast Fourier transform, cepstrum, and autocorrelation function.

4.2.3 System Validation

We validated the proposed system for two different applications, i.e., health and wellness application as well as clinical application. In the former application, we collected data from fifty subjects, where the optical fiber mat was placed on the headrest of a massage chair. This application was very challenging because of the motion artifacts caused by movement of the chair and body movement as well. The objective of this study was to evaluate the effectiveness of the optical fiber mat to detect heart rate in a noisy environment. In the latter application, we collected data from ten subjects during a drug-induced sleep endoscopy. Data acquisition was carried out in the operating theatre of Khoo Teck Puat Hospital (KTPH), Singapore. The objective of this study was to check the performance of the optical fiber mat for unobtrusive monitoring of heart and breathing rate for sleep apnea patients. Furthermore, we also assessed the capability of the mat for unobtrusive apnea detection. After the validation procedures were completed successfully, we deployed our system in a real-life environment, i.e., user's home. The proposed system has been successfully deployed in three apartments of senior female residents over thirty days. Furthermore, the sleep monitoring system has been integrated within an existing Ambient Assisted Living (AAL) platform, better known as UbiSMART (Ubiquitous Service Management and Reasoning architecture) [Tiberghien 2011].

We briefly explain our AAL platform in Section 4.2.4, and we present the integration of the fiber-optic sensor into the platform in Section 4.2.5.

4.2.4 UbiSMART Design

UbiSMART is a web-enabled AAL platform intended for large-scale deployments following the approach presented by Bellmunt *et al.* [Bellmunt 2015]. Key features [Aloulou 2016] are *plug & play* ability, privacy protection as there is no sound

and no image recording, easy interaction for end-users, and generic architecture. This AAL platform is able to transform any environment into a smart space in five minutes, enabling an unobtrusive assessment of indoor as well as outdoor activities of dependent people in their home environment. The purpose of UbiSMART is to detect the *Activities of Daily Living* (ADL), and to provide rich services in the right context through appropriate channels. The framework is composed of three

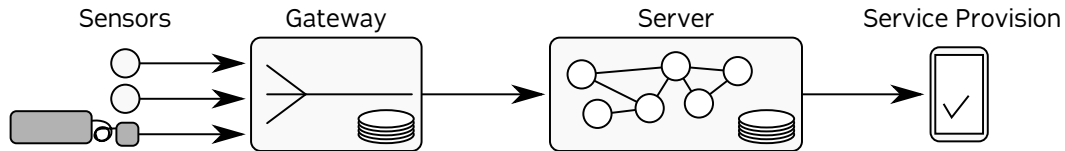


Figure 4.3: Simplified view of UbiSMART AAL platform with sleep mat and its processing unit as a sensor.

main parts (Figure 4.3), in data flow order: 1) **Gateway**, “smart home in a box” – sensors (motion sensors, contact sensors and the newly integrated bed sensor for sleep monitoring) and a gateway (Raspberry Pi); 2) **Server** – receives formatted inputs from the gateway, and processes them using semantic reasoning following the approach presented by Aloulou and Bellmunt *et al.* [Aloulou 2012, Bellmunt 2016]; 3) **Service Provisioning** – responsive user interfaces on the web or on hand-held devices that allow users to receive notifications or interact with the platform.

4.2.5 System Integration

The sleep mat equipment is considered as another sensor that contributes to the knowledge base of the AAL platform. We explain its integration into the existing system following the data flow from the source to the presentation.

4.2.5.1 Collection

The bed sensor-processing unit is wired to our *Gateway* (Raspberry Pi). Voluminous raw data is read and stored on a micro SD-card for a deeper off-line analysis. Simultaneously, the data is preprocessed to generate high level events, such as *bed empty*, *bed motion*, *sleep*. Currently, it operates on a time window of 10 seconds. For each time window, an event is produced. The events are then sent to the *Server* as a structured sensor data using Message Queuing Telemetry Transport (MQTT) protocol over an Internet connection [Bellmunt 2016].

4.2.5.2 Reasoning

Server handles the received structured information (event). The bed sensor will appear in the *home description* interface as available for association to a house. If confirmed, this association is stored in the knowledge base (KB). Any subsequent events are then inserted into the KB of the associated house, allowing to the reasoning engine to be aware of bed occupancy with respect to our ontology. Coupled with

the information from other sensors and sources, it provides an accurate contextual information. In parallel, the raw data is processed every 5 minutes to extract information about the occupant's respiratory effort and heart rate. This information is also inserted into the KB.

4.2.5.3 Presentation

Service provisioning through our simple responsive web interface *Life Tiles* Figure 4.4 allows us to give the user an instant feedback about bed occupancy and continuously updated information about the occupant's respiratory effort and heartbeat. Other indicators show aggregated information about activities out of the scope of this thesis.

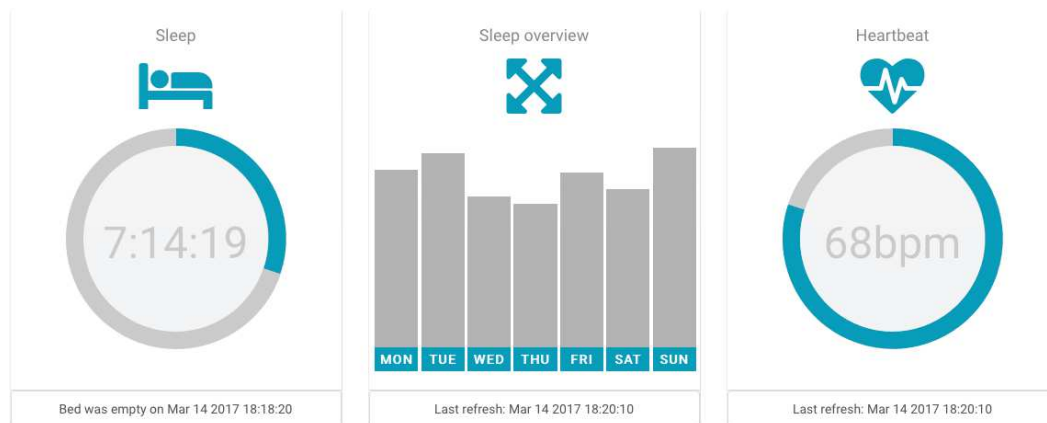


Figure 4.4: UbiSMART user interface is organized in tiles and it provides following information: daily quantity of sleep (selected day) with updated bed occupancy status that changes the color of the icon and status line; aggregated week overview of sleep quantity; and heartbeat information.

4.3 Conclusion

In this chapter, we discussed the working operation of the microbend fiber-optic sensor. We also provided an overall summary of the proposed system and how the system is validated in two different applications. Besides, we explained our current Ambient Assisted Living platform, i.e., UbiSMART and we presented how the microbend fiber-optic sensor is integrated within the platform. In the next chapter, we provide a step-by-step explanation of how our proposed system is validated for health and wellness application as well as clinical application. In which, we describe the data collection protocol for each application and we illustrate the algorithms used to process the sensor data.

Methodology

Contents

5.1	Introduction	63
5.2	Health and Wellness Application	64
5.2.1	Quality Processing of Fiber Optic Sensor Data	65
5.2.2	Application Specific Signal Data Quality	66
5.2.3	Data Processing	67
5.3	Clinical Application	82
5.3.1	Experimental Setup and Data Collection	86
5.3.2	Data Processing	88
5.4	Real-life Deployment	92
5.4.1	Data Collection	93
5.4.2	Data Processing	94
5.5	Conclusion	95

5.1 Introduction

Our aim in this chapter is to provide a detailed description of the methods used to process the data collected from the microbend fiber-optic sensor. To start with, we show how we validated the system using data acquired from a massage chair, in which several classifiers were adopted to label the data into informative and non-informative classes based on their heart rate information, and then we measured the heart rate using Complete Ensemble Empirical Mode Decomposition with Adaptive Noise algorithm (Section 5.2). Second, we illustrate the signal quality algorithm (Section 5.2.3.4), which substitutes the manual labeling process. Furthermore, we explain the multiresolution analysis of the Maximal Overlap Discrete Wavelet Transform as an alternative to the empirical mode decomposition algorithm (Section 5.2.3.5). Even more, we introduce the fast Fourier transform, cepstrum, and autocorrelation function for the sake of comparison with the wavelet approach (Sections 5.2.3.6 and 5.2.3.7). Third, we discuss how we validated the system in a clinical environment for unobtrusive monitoring of vital signs and sleep apnea events as well (Section 5.3). After all, we describe our real-life deployment, where three senior female residents were involved in our study and the sleep data was collected over a one-month period in a home-living situation (Section 5.4).

5.2 Health and Wellness Application

In several application domains, sensor networks provide enormous potential for information collection and processing [Kapadia 2009]. In this study, we focused on a new kind of sensing technology known as Opportunistic Ambient Sensing¹ (OAS). OAS can be used to provide applications and services that fit into the active and healthy lifestyle of end users and to unobtrusively extract reliable and meaningful data about their physiological parameters [Acampora 2013]. Although mobile phone-based applications are perhaps the most convenient, they lack the sensitivity and the proximity needed for the measurement of important vital signs such as heart rate (HR) and breathing rate (BR). Ambient sensors that are placed in the environment away from physical contact with the user, such as cameras, infrared motion sensors and other types of electromagnetic sensing devices, lack the proximity or physical contact needed for reliable detection of vital signs [Sadek 2016].

The microbend fiber-optic sensor (FOS), thanks to its high sensitivity to ballistic effects of human vital signs, is a sensor that is suitable for opportunistic ambient sensing. This sensor is a suitable option for nonintrusive long-term monitoring of vital signs for its high sensitivity to pressure changes caused by body movement, and simultaneously not required to be in close contact with the body. A cushion with embedded sensors, for example, is able to unobtrusively, yet with ample accuracy, capture vital signs of the user for those durations where the user is directly in contact with the sensor and motion artifacts are limited. A major challenge is dealing with the quality of the FOS signals. There are two basic approaches to monitoring quality in physiological data obtained from sensors, i.e., signal oriented and aggregate oriented. The first [Schumm 2010] is an exact approach, attempting to detect and track statistical properties of signal morphologies or event occurrences (or non-occurrences), and reporting these in a real-time fashion. The second [Wang 2002, Lee 2012] is a statistical approach aimed at obtaining aggregate statistical features in the time or frequency domain, through appropriate feature extraction. Since the former approach can lead to processing delay, especially in real-time situations, in our work we adopted the statistical approach for quality processing.

The goal of this study was to design a quality processing system to identify signals of interest from noisy and nonstationary BCG signals. The quality process reduced the computational and/or communications load significantly because only useful data was transmitted and processed for vital sign extraction. Thereafter, interbeat intervals were estimated using Complete Ensemble Empirical Mode Decomposition with Adaptive Noise (CEEMDAN) algorithm. The following sections are summarized as follows. Section 5.2.1 presents the generic algorithm for quality processing. Section 5.2.2 presents a definition of data quality relevant to the needs of the application at hand. Section 5.2.3 presents the data collection protocol, a labeling tool used to label datasets manually, and the proposed approach.

¹“Opportunistic sensing is seen as a way to gather information about the physical world in the absence of a stable and permanent networking infrastructure” [Scholten 2011].

5.2.1 Quality Processing of Fiber Optic Sensor Data

As we pointed out in several parts of the thesis, ballistocardiography is a technique that measures the mechanical vibrations arising from the recoil of the body, caused by the ventricular ejection of blood from the heart into the arterial tree along with each heartbeat [Park 2018]. In this particular application, the sensing system consisted of a pressure mat and a transceiver which included a light source, a light detector, amplifiers, filters, an analog-to-digital converter, a microprocessor, and circuits for connecting the transceiver to a computer via Bluetooth. A low-pass filter at 250Hz was built into the transceiver to eliminate high-frequency noise. When a pressure is applied to the mat, the displacement between two microbenders changes, the light intensity of the clamped multimode fiber changes with the subject's body vibrations caused by respiration/heart beating. The light intensity in the microbending fiber is modulated by the body vibrations. This modulated signal is extracted as ballistocardiogram and respiratory signals. The microbending FOS

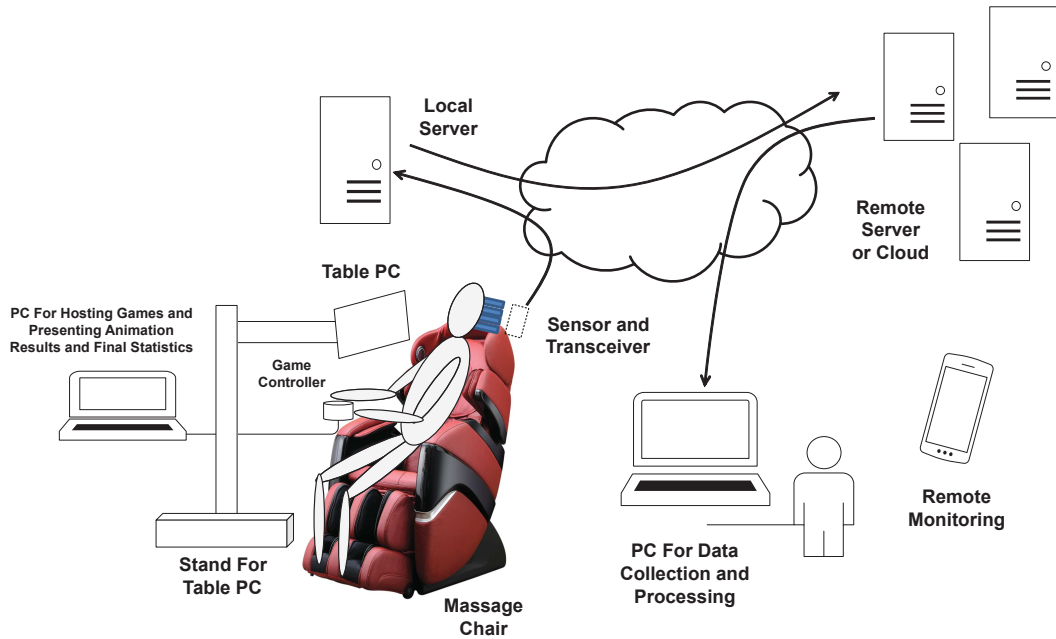


Figure 5.1: Opportunistic remote monitoring of vital signs.

pressure mat can be used to collect physiological data of people from ambient locations, i.e., mattresses, pillows, chairs, etc. In these situations, a major obstacle is to handle noise and motion artifacts since the quality of the sensed data is easily corrupted. If, however, some expected characteristics (or features) of the signals can be exploited, the sensor signals may be processed in such a way that the vital signs are recovered with higher accuracy. The basic idea is to detect the quality of the data and classify the data into good, noisy or no-data segments for further processing. The algorithm involves carrying out labeling of sensor data, in order to establish a reliable ground truth, which can then be used to segment decent

quality signals from real-time sensor data streams. This is a step towards improving the reliability of sensors used to monitor vital signs in diverse ambient settings. Figure 5.1 illustrates the manner in which the FOS pressure mat was deployed in wellness applications for the opportunistic monitoring of vital signs. The local server was optional and might be replaced with a direct connection to the remote server or cloud, with the appropriate 3G transceiver.

5.2.2 Application Specific Signal Data Quality

Sensor signal quality and data quality are important measures for medical devices and health monitoring. In morphological analysis, a missed detection is characterized by the absence of a particular waveform. The missing or erroneous waveform is corrected and the feature (e.g., heartbeat) is then detected from the augmented waveform. In statistical analysis, the individual waveforms are not analyzed, but the signal is processed, and feature detected (e.g., through peak detection) and thereafter the output statistic (e.g., HR) computed.

The statistical approach at data quality requires manual labeling of the rendering of the signal on a viewer with the help of a suitable tool. The waveforms are classified, sometimes with the help of logged information that supply details that may be useful for more accurate labeling. Since the fiber-optic sensor can be used in various settings for various applications, the statistical approach towards the study of quality is more meaningful, as it may be used with parametric or algorithmic changes and applied to various applications and indeed to various sensors as well. In this application, we considered the following definitions of quality:

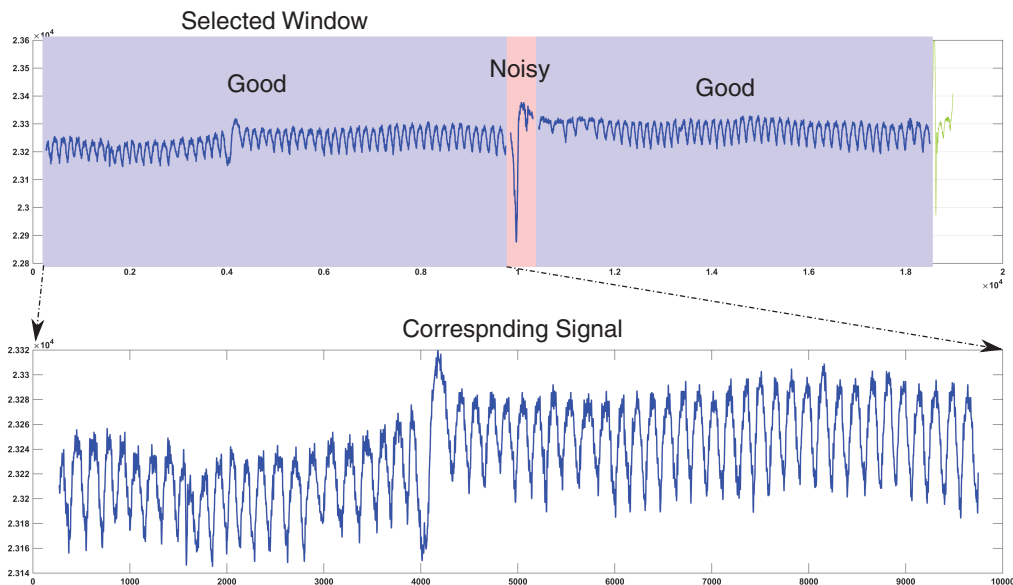


Figure 5.2: Screen capture of the labeling tool.

- **Informative signal:** It included a good quality signal and a noisy signal.

The former signal was a data stream from which features might be extracted by standard algorithms, without any further filtering or processing to remove noise or any conflicting artifacts. The latter signal was a data stream that contained the observed signal mixed with other artifacts and noise, such that more processing was needed before algorithms might be used to extract the vital signs.

- **Non-informative signal:** It was a data stream where retrieval of physiological properties was impossible.

Because noise was introduced through activities of various kinds, in the experimental stage we incorporated mechanisms to embed information into the data that indicate the occurrence of events. These labels gave major cues, which served as a foothold in the data, in order to analyze it further for quality processing. Note that even though our data was collected in the lab, it was unreasonable and impossible to label each event. This was the reason why we were required to undertake post-processing of the data through a manual labeling effort. From [Figure 5.2](#), it can be seen that there are certain periods when good data was expected (such as the rest periods), and certain other periods where the data was expected to be noisy (such as the massage period when the massage chair is in motion). There are also periods when due to non-contact there is no signal presented. This happens, for example, when the subject is answering the questionnaire or undergoing some mental tasks involving the use of the computer. Once the subject leans forward the contact between the pillow sensor and the subject's head is lost, and thus there is no signal.

5.2.3 Data Processing

5.2.3.1 Data Collection

The data was collected in a realistic setting from 50 human subjects sitting in a massage chair to assess their levels of stress at different moments. The data was collected in a sitting position to explore the capability of the optical-fiber mat for heart rate measurement from different positions of the body (e.g., below the head). This particular position was interesting as the optical-fiber mat could have been located in a pillow rather than below the bed mattress. Consent forms were sought from every human subject following the approval of the institutional review board. Participants completed stress-inducing exercises, proceeded by rest and relief therapy. During the process, subjects were instructed to complete well-suited survey questionnaires for gathering self-reported ground truth. Meanwhile, physiological parameters of subjects were recorded in real-time using a range of sensors. This included ballistocardiography, electroencephalography, galvanic skin response, and some other sensors to measure electrocardiography and respiratory efforts.

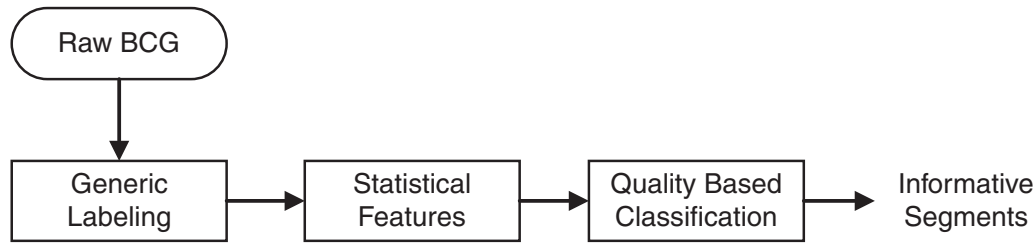


Figure 5.3: Flowchart of the quality processing system.

5.2.3.2 Classification

The flowchart of the quality processing system is shown in [Figure 5.3](#) and it can be illustrated as follows:

Preprocessing: The sensor data was manually labeled by a human observer into two classes such as 1) informative (58% of dataset) and 2) non-informative (42% of dataset), where a labeling tool was developed that enabled the user to quickly label data from MATLAB[®] based software. [Figure 5.2](#) shows a screen capture of the labeling tool. The labeled sensor data were randomly divided into two groups, i.e., Group1 and Group2. The former consisted of 2085 segments (1296 informative and 789 non-informative), whereas the latter included 1546 segments (813 informative and 733 non-informative). The length of each segment was 10 seconds/500 samples, where the data was sampled at a sampling frequency of 50Hz. The idea was to use Group1 as a training set while Group2 as a test set, and vice versa. Subsequently, each segment was band-pass filtered to extract the BCG component using a Butterworth band-pass filter with frequency limits of 1Hz and 12Hz. [Figure 5.4](#) shows two examples for informative and non-informative segments.

Feature Extraction: A set of 13 statistical features was extracted i.e., mean (\bar{x}), standard deviation (σ), minimum (min), maximum (max), skewness (S), kurtosis (K), range (R), interquartile range (IQR), mean absolute deviation (MAD), number of zero crossings, the variance of local maxima, the variance of local minima, mean of the signal envelope using the analytic signal. The analytic signal was obtained by taking the Hilbert transform of the signal and then the envelope was extracted by taking the magnitude of the analytic signal. [Table 5.1](#) gives mathematical equations for some features; given a set of samples $\{x_1, x_2, \dots, x_N\}$.

Training and Testing: Five classifiers were employed, i.e., random forest (RF), support vector machine (SVM), multilayer, feedforward neural network (NN), linear discriminant analysis (LDA), and decision tree (DT). Then, a training model was created for each classifier using the features of training set, where each set was 10-fold cross-validated to evaluate the predictive ability of the models. Finally, each segment

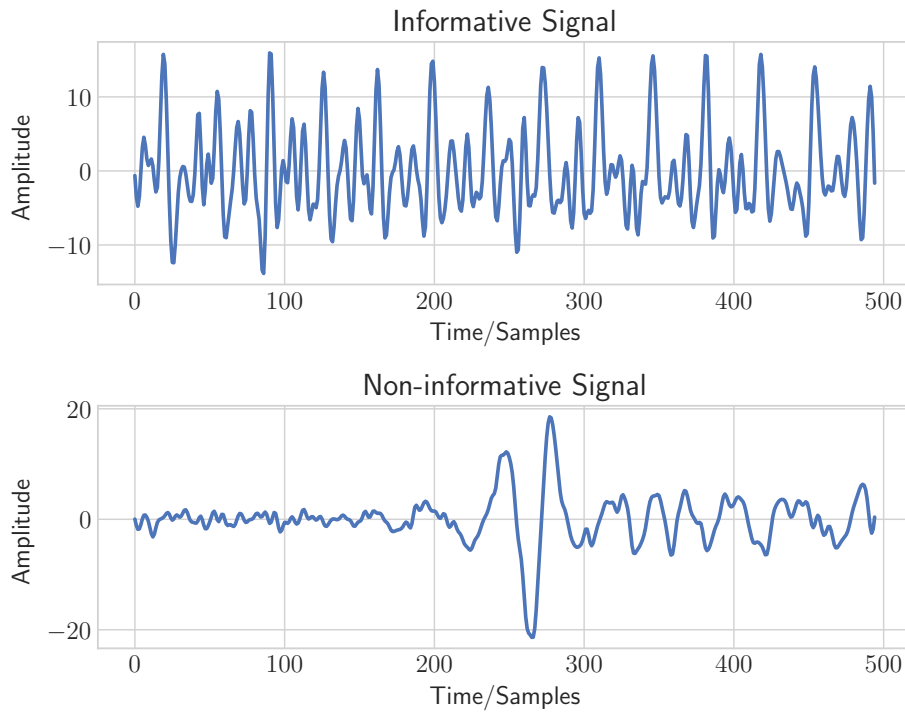


Figure 5.4: Two examples for informative and non-informative segments (sampling frequency: 50Hz).

in the test set was classified into one of the classes based on the features of the test set. Furthermore, an accuracy criterion was computed for appraising the performance of the classifiers and the results of the proposed approach in discriminating between informative and non-informative segments.

Heart Rate Estimation The conventional empirical mode decomposition (EMD) along with two modulation-based approaches were used in [Pinheiro 2010a] to suppress generated noise when a single channel EMFi sensor was placed in the backrest of a moving wheelchair. Although the EMD approach helps to remove generated noise in the BCG signal, it has two limitations i.e., end effects and mode mixing. Ensemble EMD (EEMD) was used in [Cao 2013, Ni 2017] to eliminate generated noise as well as to solve the mode mixing problem. Nevertheless, the EEMD still does not completely solve the mode mixing problem and requires high computational time. We proposed to use the CEEMDAN algorithm (Section 5.2.3.3) as a noise removal tool since it provides a complete reconstruction of the signal and it is proved to be robust towards motion artifacts originated due to body movements.

The 6th decomposition component (DC6) was chosen for HR measurement because each local maximum shows a match with a cardiac cycle [Sadek 2015]. Figure 5.5 shows an example of a BCG signal with its DC6. The local maxima of

Table 5.1: Features' mathematical equations.

Feature	Equation	Notes
<i>Mean</i>	$\bar{x} = \frac{1}{n-1} \sum_{i=1}^n x_i$	
<i>Variance</i>	$\sigma^2 = \frac{1}{n-1} \sum_{i=1}^n (x_i - \bar{x})^2$	It is a measure used to quantify the amount of variation of a set of data values.
<i>Standard Deviation</i>	$\sigma = \sqrt{\frac{1}{n-1} \sum_{i=1}^n (x_i - \bar{x})^2}$	It measures how far a set of numbers are spread out from their average value.
<i>Skewness</i>	$S = \frac{\frac{1}{n} \sum_{i=1}^n (x_i - \bar{x})^3}{\left(\sqrt{\frac{1}{n} \sum_{i=1}^n (x_i - \bar{x})^2}\right)^3}$	It is a measure of the asymmetry of the data around the sample mean. <ul style="list-style-type: none"> • Zero → symmetric distribution • Negative → spread out more to the left of the mean. • Positive → spread out more to the right of the mean.
<i>Kurtosis</i>	$K = \frac{\frac{1}{n} \sum_{i=1}^n (x_i - \bar{x})^4}{\left(\frac{1}{n} \sum_{i=1}^n (x_i - \bar{x})^2\right)^2}$	It is a measure of how outlier-prone a distribution is. <ul style="list-style-type: none"> • Three → symmetric distribution • > Three → more outlier-prone than the normal distribution. • < Three → less outlier-prone than the normal distribution.
<i>Range</i>	$R = \max - \min$	It is the difference between the highest and lowest values.
<i>Interquartile Range</i>	$IQR = Q_3 - Q_1$	It indicates how the central 50% of values within the dataset are diffused. <ul style="list-style-type: none"> • Q_1 → median of the n smallest entries. • Q_3 → median of the n largest entries.
<i>Mean Absolute Deviation</i>	$MAD = \frac{1}{n} \sum_{i=1}^n x_i - \bar{x} $	It is the average distance between each data value and the mean.

the DC6 were used for HR measurement, where the HR value at the time t_n , at which the n^{th} maximum occurred, was defined as follows:

$$HR_n = \frac{60}{t_n - t_{n-1}} \quad (5.1)$$

where t_n is the time at n^{th} local maxima and t_{n-1} is the time at $(n-1)^{th}$ local maxima in the DC6. In which, the HR was expressed as beats per minute (BPM).

5.2.3.3 Complete Ensemble EMD with Adaptive Noise

The Empirical Mode Decomposition (EMD) [Huang 1998] is an adaptive method, which can be used to break down a nonlinear and a nonstationary signal as a combination of amplitude and frequency modulated functions named intrinsic mode functions (IMFs) without leaving the time domain. IMF should fulfill two conditions:

- In the entire dataset, the number of extrema and the number of zero crossings must be equal or vary at most by one.
- At any time instant, the mean value of the upper and lower envelope is zero, i.e., the signal has zero mean.

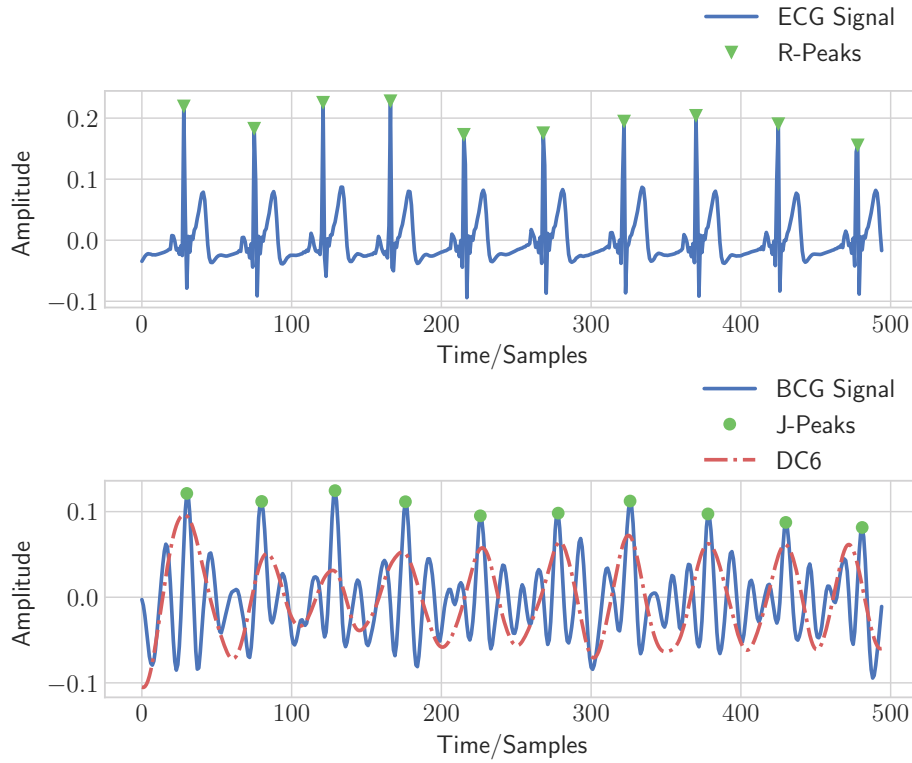


Figure 5.5: BCG signal with a reference ECG signal. ECG is shown in 1st row. However, BCG signal and its 6th decomposition component are shown in 2nd row (sampling frequency: 50Hz).

Even though EMD proved to be applicable in several areas of research, such as biomedical signal processing, it encounters some limitations as follows. First, end effects that destroy the IMFs at its endpoints. Second, mode mixing, which causes very similar oscillations to exist in different modes or oscillation of very dissimilar amplitudes to exist in a mode [Huang 2016]. In order to solve these problems, a new approach is introduced: Ensemble Empirical Mode Decomposition (EEMD) [Wu 2009a], the basic idea of the EEMD is to carry out the EMD over an ensemble of the signal besides white Gaussian noise (WGN). Adding WGN overcomes the mode mixing problem by processing the entire time-frequency space to make use of the dyadic filter bank behavior of the EMD. Nonetheless, a different number of modes may be generated. Apart from that, the CEEMDAN can provide a precise reconstruction of the original signal in addition to reducing the computational complexity [Torres 2011]. It further solves the boundary problems by mirrorizing extrema close to the edges [Rilling 2003]. Given a target signal x , assume $w^{(l)}$ is a WGN of zero mean and unit variance i.e., with $N(0, 1)$, ε is the noise standard deviation, and $E_k(\cdot)$ is an operator responsible for getting the k^{th} mode of a given signal by EMD. The algorithm for obtaining a k^{th} mode by EMD can be explained as follows [Huang 1998, Colominas 2014]:

1. Initialize $k = 0$ and detect all local extrema (i.e., all local maxima and local minima) of $r_0(t) = x(t)$.
2. Obtain the maximum & minimum envelopes of local extrema ($e_{max}(t), e_{min}(t)$) using a cubic spline interpolation.
3. Compute the mean of the envelopes $m(t) = (e_{max}(t) + e_{min}(t))/2$.
4. Extract the IMF candidate $d_{k+1}(t) = r_k(t) - m(t)$. This procedure is called *sifting process*.
5. Is d_{k+1} an IMF?
 - Yes. Save $d_{k+1}(t)$, compute the residue $r_{k+1}(t) = x(t) - \sum_{i=1}^k d_i(t)$, do $k = k + 1$, and treat r_k as input data in step 2.
 - No. Treat $d_{k+1}(t)$ as input data in step 2.
6. Iterate on the final residual $r_k(t)$ until a predefined stopping criterion is fulfilled.

According to Rilling *et al.* [Rilling 2003], the stopping criterion is based on two thresholds, i.e., θ_1 and θ_2 . These two thresholds aim at guaranteeing globally small fluctuations as well as considering locally large excursions. To achieve this goal, the ratio of the mean value of the envelope of iterated mode and the amplitude of this envelope is checked in each iteration:

$$\sigma(t) = \left| \frac{m(t)}{a(t)} \right| \quad (5.2)$$

where $m(t) = (e_{max}(t) + e_{min}(t))/2$ and $a(t) = (e_{max}(t) - e_{min}(t))/2$. The sifting process is iterated until $\sigma(t) < \theta_1$ for some prescribed fraction $(1 - \alpha)$ and $\sigma(t) < \theta_2$ for the remaining fraction. Typically, $\alpha \approx 0.05$, $\theta_1 \approx 0.05$ and $\theta_2 \approx 10 \cdot \theta_1$. Following the EMD algorithm, the CEEMDAN can be illustrated in following steps:

1. Each $x^{(l)} = x + \varepsilon_0 w^{(l)}$ is decomposed similar to EMD for $l = 1, \dots, L$ to obtain its first mode (\tilde{d}_1):

$$\tilde{d}_1 = \frac{1}{L} \sum_{l=1}^L d_1^{(l)} = \bar{d}_1. \quad (5.3)$$

2. For $k = 1$, compute the first residue (r_1):

$$r_1 = x - \tilde{d}_1. \quad (5.4)$$

3. Decompose $r_1 + \varepsilon_1 E_1(w^l)$, $l = 1, \dots, L$ until its first EMD mode, and then define the second mode:

$$\tilde{d}_2 = \frac{1}{L} \sum_{l=1}^L E_1(r_1 + \varepsilon_1 E_1(w^l)). \quad (5.5)$$

4. For $k = 2, \dots, K$, compute the k th residue:

$$r_k = r_{(k-1)} - \tilde{d}_k. \quad (5.6)$$

5. Decompose realizations $r_k + \varepsilon_k E_k(w^l)$, $l = 1, \dots, L$ until their first mode by EMD, and then determine the $(k + 1)$ th mode:

$$\tilde{d}_{k+1} = \frac{1}{L} \sum_{n=1}^N E_1(r_k + \varepsilon_k E_k(w^l)). \quad (5.7)$$

6. Go to step 4 for next k

Steps 4 – 6 are repeated until the obtained residue cannot be decomposed anymore by EMD (it contains less than three local extrema). Thus, the final residue fulfills:

$$r_k = x - \sum_{k=1}^K \tilde{d}_k. \quad (5.8)$$

where K is the total number of decomposition modes. As a result, the target signal can be represented as:

$$x = \sum_{k=1}^K \tilde{d}_k + r_k. \quad (5.9)$$

As it can be seen in [Figure 5.6](#), the BCG signal ([Figure 5.5](#)) was decomposed into nine components. However, only the 6th component, i.e., DC6 showed agreement with cardiac cycles. As a result, the local maxima of this component were employed for heart rate measurement. Moreover, it should be noted that the first two components, i.e., DC1 and DC2 represented the noise embedded in the signal. Up to now, we have explained our initial approach to process the fiber-optic data using a machine learning approach and therefore implementing the CEEMDAN algorithm to compute the heart rate.

The next two sections will discuss the automated signal quality algorithm ([Section 5.2.3.4](#)) and the multiresolution analysis of the Maximal overlap discrete wavelet transform ([Section 5.2.3.5](#)). The formal algorithm replaced the manual labeling required for training data, while the latter algorithm replaced the CEEMDAN algorithm due to its high computational cost.

5.2.3.4 Automated Signal Data Quality

In health and wellness application, the monitoring system was designed to send fiber-optic sensor data to a nearby computer via Bluetooth. However, the processing unit of the current system has a built-in Micro-SD card and a Wi-Fi signal transmission module for sending the data to a remote cloud server ([Section 4.2.1](#)).

Typically, every 5 minutes, a file was created and stored in the micro-SD card. After that, this file was sent to the cloud server for processing and extracting relevant information. In order to achieve automated signal data quality, three different states

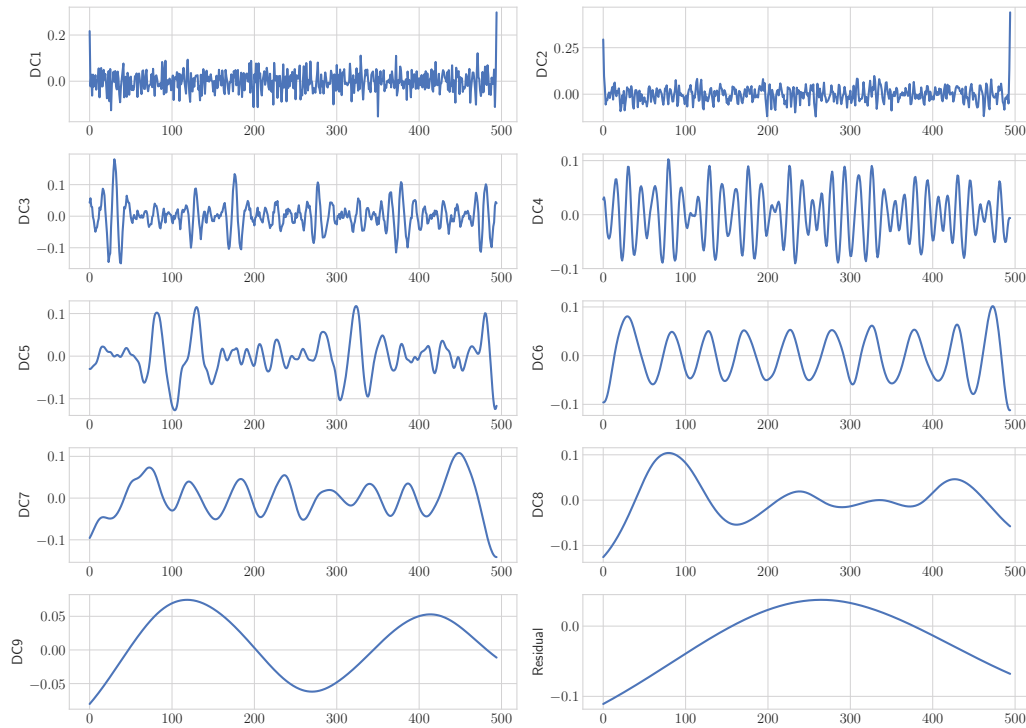


Figure 5.6: Intrinsic mode functions (DC1-DC9) of a typical BCG signal (Figure 5.5); the 6th component shows a match with cardiac cycles (sampling frequency: 50Hz).

were recognized for each 5-minutes recording using a sliding time-window (w_i) with a size of 500 samples (10 seconds) as follows. First, if the standard deviation (SD) of the time-window was greater than twice the mean absolute deviation (MAD) of all time-windows SD, the state was considered as a body movement (Figure 5.9). Second, if the SD of the time-window was lower than a fixed threshold of 15 mV, the state was regarded as no activity (unoccupied mat sensor) (Figure 5.10). Finally, in other cases, the state was identified as asleep (Figure 5.8), where apneas and vitals could be measured. This process was repeated for all the data-files on the Micro SD-Card, and the sleep data were then concatenated together to form a continuous time series, i.e., excluding body movements and unoccupied bed events. Algorithm 1 illustrates the sleep data processing of a resident's bed state.

Figure 5.7 gives an example of a signal data quality processing for a 20-minute fiber-optic data recording. The data was collected from a healthy young male subject and the optical fiber mat was placed underneath the mattress covering the upper half of the subject. In this example, folly color defines segments of body movements, aqua color defines segments of sleep and blond color defines segments of bed-exits. The two folly colored regions indicate the time when the subject entered and exited the bed. On the other hand, Figures 5.8 to 5.10 show one example for each bed state, i.e., sleep, body movement, and bed-exit.

Algorithm 1 Sleep Data Processing**Input:**

- 1: $W \leftarrow \{w_1, w_2, \dots, w_N\}$
- 2: $Tr \leftarrow 15$

Output:

- 3: state
- 4: **for** $i = 1, \dots, N$ **do**
- 5: $S(i) \leftarrow SD(w_i)$
- 6: **end for**
- 7: $M \leftarrow MAD(S)$
- 8: **for** $j = 1, \dots, N$ **do**
- 9: **if** $SD(w_j) > 2 * M$ **then**
- 10: state \leftarrow bed movement
- 11: **else if** $SD(w_j) < Tr$ **then**
- 12: state \leftarrow bed empty
- 13: **else**
- 14: state \leftarrow sleep
- 15: **end if**
- 16: **end for**

5.2.3.5 Maximal Overlap Discrete Wavelet Transform

In healthy subjects, ECG signal, which is considered as a reference to measure interbeat intervals has a uniform and repeated template known as PQRST complex, i.e., the pattern of electrical activity of the heart during one cardiac cycle (Figure 3.2). Thus, this property facilitates the measurement of the subject's heart rate. Unlike ECG signals, the BCG morphology varies between and within subjects, and the shape of the signal is highly dependent on the subject's positions, i.e., sleeping or sitting. In addition, the raw signal is noisy and nonstationary owing to body movement, induced respiratory efforts, and the characteristics of the sensing system itself, therefore, estimating interbeat intervals from BCG signals is a troublesome procedure.

In [Jin 2009] a translation-invariant adaptive discrete wavelet transform (DWT) was proposed to denoise BCG signals. Then, the heart rate was computed using a pseudo-period detection approach. In [Noh 2010] DWT was implemented to cancel related BCG artifacts and a template matching for interbeat intervals detection. The BCG data were collected from five healthy subjects in a sitting position using an electromechanical film sensor. In [Gilaberte 2010] continuous wavelet transform (CWT) was introduced for HR and respiratory rate measurements. Where, in each case, the scale which presented an agreement with the periodicity of the signal was selected. The proposed approach was applied to six healthy subjects standing on a bathroom scale equipped with multiple strain gauges. A similar approach was proposed in [Alvarado-Serrano 2016], where authors used CWT with splines

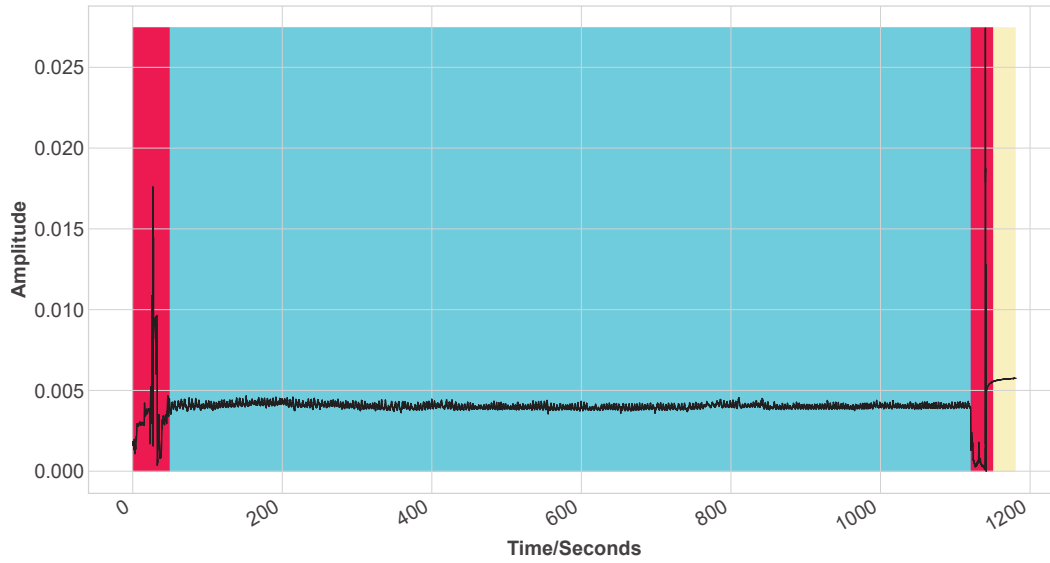


Figure 5.7: An example of a signal data quality processing (sampling frequency: 50Hz).

for optimal scale selection. However, this approach required a training phase for parameter initialization. The BCG data was acquired from seven seated healthy subjects via a piezoelectric sensor.

We implemented multiresolution analysis decomposition using MODWT. This is because the MODWT overcomes the time variant drawback of the classical DWT by up-sampling the filter coefficients [Percival 2006].

Generally speaking, the wavelet transform is a mechanism for converting a function or a signal into another form, which either makes particular features of the original signal more manageable to study or allows the original dataset to be interpreted more concisely. In order to implement a wavelet transform, we require a wavelet, i.e., a localized waveform [Addison 2002]. More specifically, Discrete Wavelet Transform (DWT), is a multiresolution analysis that can cut up an original signal into approximation (smooth) and detail components. The following equation can denote the DWT:

$$\psi_{j,k}(t) = \frac{1}{\sqrt{a_0^j}} \psi\left(\frac{t - k b_0 a_0^j}{a_0^j}\right), \quad (5.10)$$

where j and k are integer values used to control wavelet dilation and translation respectively; a_0 is a predetermined fixed dilation step parameter set at a value greater than 1 (commonly $a_0 = 2$); ψ is the mother wavelet; and b_0 is the location parameter which must be greater than zero (commonly $b_0 = 1$). Hence, Equation (5.10) can be written in a more compact form as following; provided that $a_0 = 2$ and $b_0 = 1$:

$$\psi_{j,k}(t) = 2^{-j/2} * \psi(2^{-j} t - k). \quad (5.11)$$

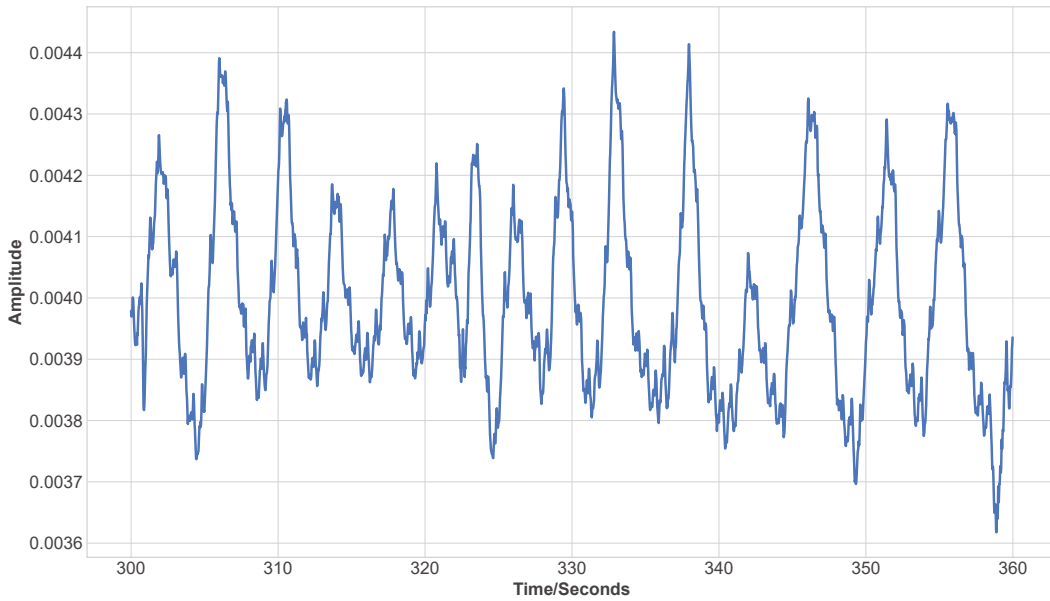


Figure 5.8: An example of a 60-second sleep signal (sampling frequency: 50Hz).

For a discrete signal $X = \{X_t, t = 0, 1, \dots, N - 1\}$, the DWT computes the wavelet coefficient for the discrete wavelet of dilation 2^j and translation $2^j k$ using the following equation:

$$W_X(j, k) = \sum_{t=0}^{N-1} X_t \psi_{j,k}(t), \quad (5.12)$$

where $W_X(j, k)$ is the wavelet coefficient and N is an integer power of two (a restrictive property). In practice, Mallat's algorithm [Mallat 1989] is used for implementation of DWT. The idea of the algorithm is to apply low-pass and high-pass filters instead of wavelets, and hence decompose the signal into details components and an approximation component. It should be noted that the decomposition level L should be determined in advance and it has to be less than or equal $\log_2(N)$ [Seo 2017]. Although DWT is a powerful tool for signal analysis, it has some limits. These limits include shift sensitivity, poor directionality, and lack of phase information [Fernandes 2003]. On the other hand, the Maximal Overlap Discrete Wavelet Transform (MODWT) introduced by Percival and Walden [Percival 2006] offers more advantages over the typical DWT, even though it does not provide an orthogonal decomposition. The properties that distinguish the MODWT from the DWT can be explained as follows:

- The MODWT is a translation-invariant process.
- The MODWT can manipulate any sample size n , which is not required to be divisible by 2.
- The smooth and detail coefficients of the MODWT are affiliated with zero-phase

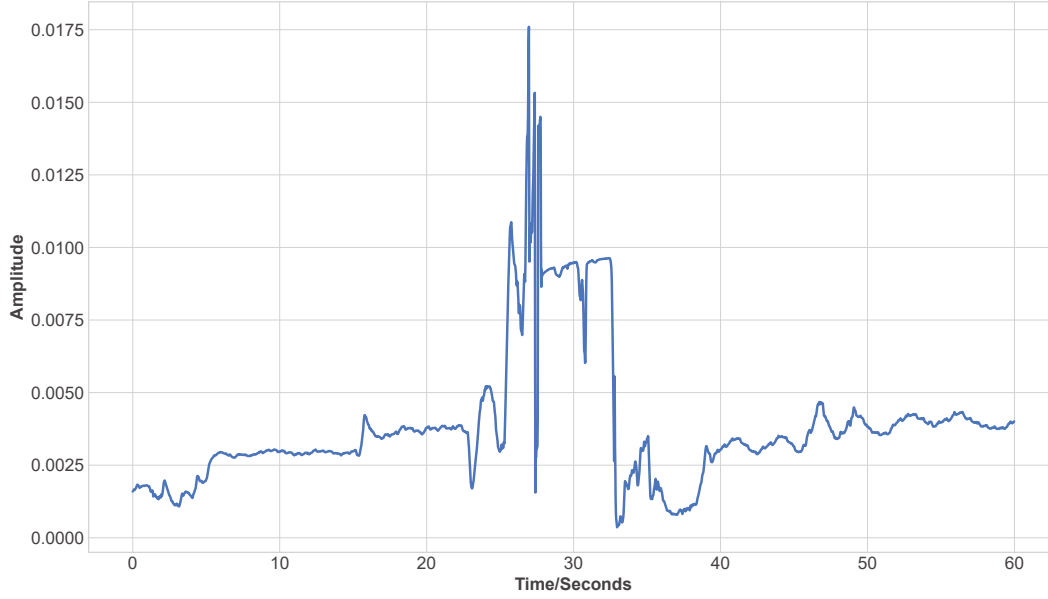


Figure 5.9: An example of a 60-second body movement signal (sampling frequency: 50Hz).

filters, and therefore making it easy to line up features in a multiresolution analysis with the original time series in a meaningful way. In other words, extracted features will be time-aligned with the original time-series.

Given a discrete time signal $X = \{X_t, t = 0, 1, \dots, N - 1\}$, the j^{th} level MODWT wavelet and scaling coefficients, i.e., $W_{k,t}$ and $V_{k,t}$ can be computed as indicated by Equation (5.13) and Equation (5.14), respectively.

$$W_{j,t} = \sum_{l=0}^{N-1} \tilde{h}_{j,l}^{\circ} X_{t-l \bmod N}, \quad (5.13)$$

$$V_{j,t} = \sum_{l=0}^{N-1} \tilde{g}_{j,l}^{\circ} X_{t-l \bmod N}, \quad (5.14)$$

where $j = 1, 2, \dots, L$; $W_{j,t}$ is the t^{th} element of the j^{th} level MODWT wavelet coefficient; $V_{j,t}$ is the t^{th} element of the j^{th} level MODWT scaling coefficient; $\tilde{h}_{j,l}^{\circ}$ and $\tilde{g}_{j,l}^{\circ}$ are the j^{th} level MODWT high- and low-pass filters, i.e., wavelet and scaling filters produced by periodizing (i.e., adding zeros) $\tilde{h}_{j,l}$ and $\tilde{g}_{j,l}$ to length N , respectively; $\tilde{h}_{j,l}$ and $\tilde{g}_{j,l}$ are the j^{th} level MODWT high-pass filter ($\tilde{h}_{j,l} = h_{j,l}/2^{j/2}$) and low-pass filter ($\tilde{g}_{j,l} = g_{j,l}/2^{j/2}$); $h_{j,l}$ and $g_{j,l}$ are the j^{th} level DWT high- and low-pass filters; and L is the highest decomposition level.

On the other hand, the multiresolution analysis decomposes an original signal X into a low-pass filtered approximation (smooth) component and high-pass filtered detail components [Percival 2006]. Typically, the multiresolution analysis of the MODWT can be formulated as provided by Equations (5.15) to (5.17):

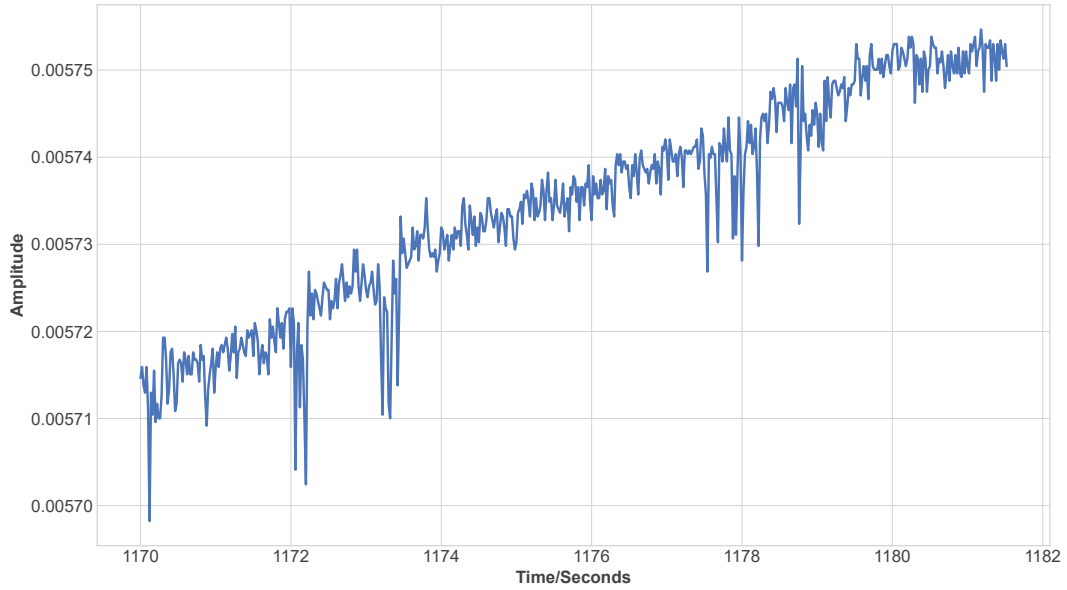


Figure 5.10: An example of a 60-second bed-exit signal (sampling frequency: 50Hz).

$$X = \sum_{j=1}^{J_0} D_j + S_{J_0}, \quad J_0 \geq 1 \quad (5.15)$$

$$D_{j,t} = \sum_{l=0}^{N-1} \tilde{h}_{j,l}^{\circ} W_{j, t+l \bmod n}, \quad (5.16)$$

$$S_{j,t} = \sum_{l=0}^{N-1} \tilde{g}_{j,l}^{\circ} V_{j, t+l \bmod n}, \quad (5.17)$$

where D_j is the detail components and $S_{j,t}$ is the smooth component. Figure 5.11 gives an example of a three-level MODWT. After explaining automated signal data quality algorithm and MODWT approach, the following steps can be used to measure the heart rate (Figure 5.12).

1. BCG Signal Extraction: First, motion artifacts were excluded using Algorithm 1. Second, the BCG signal was retrieved by performing a Butterworth band-pass filter with frequency limits between 1Hz and 10Hz.
2. Decomposition: A sliding time-window of a length (10 seconds/500 samples) was used to measure the heart rate for BCG and ECG signals. Therefore, for each 10-second of the BCG signal, a multiresolution analysis based on MODWT was employed to decompose the signal into approximation and detail coefficients.
3. Suitable Level Selection: The 4th level smooth coefficient was preferred for HR computation because the periodicity of the maxima showed an agreement with the heartbeats as presented in Figure 5.13.

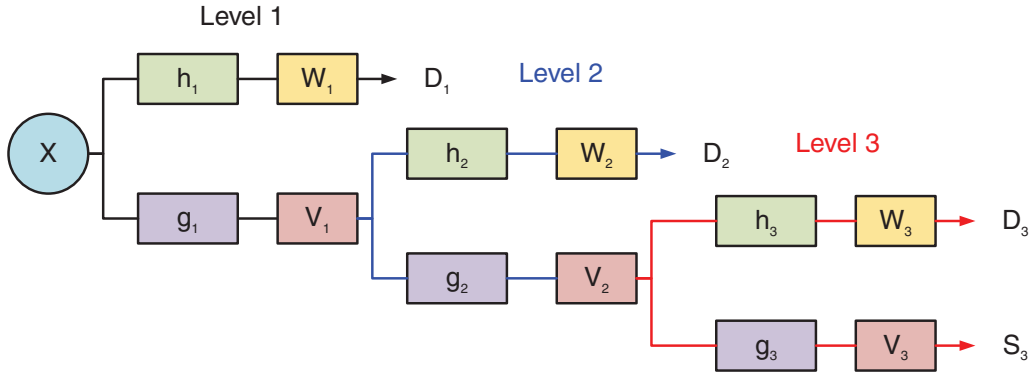


Figure 5.11: Example for three-level MODWT; $h_{\{\cdot\}}$ is a high-pass filter, $g_{\{\cdot\}}$ is a low-pass filter, $W_{\{\cdot\}}$ is a wavelet coefficient, and $V_{\{\cdot\}}$ is a scaling coefficients.

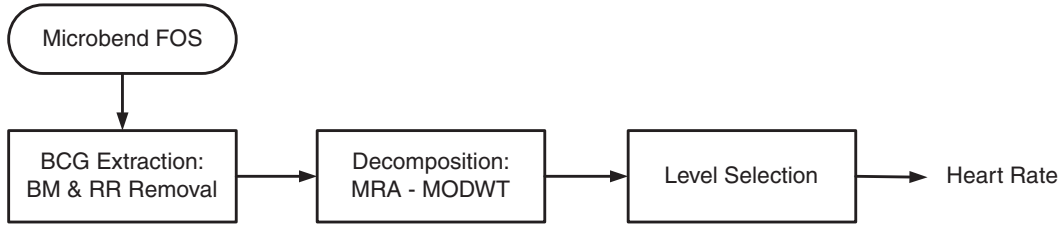


Figure 5.12: The flowchart of the proposed heart rate estimation method; BM: Body Movement, RR: Respiratory Rate, and MRA: Multiresolution Analysis.

To this end, we have addressed how ballistocardiogram signals were acquired during health and wellness application. Other than that, we have explained the proposed methodology to analyze and interpret ballistocardiogram signals in order to measure interbeat intervals. In the subsequent section (Section 5.3), we discuss our clinical validation approach.

5.2.3.6 Cepstral Transform

The cepstrum is defined as the inverse discrete Fourier transform (DFT) of the log-magnitude of the DFT of a signal, i.e., spectrum [Oppenheim 2004]. The cepstrum c of a signal x can be denoted as follows:

$$c[n] = \mathcal{F}^{-1}\{\log |\mathcal{F}\{x[n]\}|\}, \quad (5.18)$$

where \mathcal{F} is the DFT and \mathcal{F}^{-1} is the inverse DFT. Since ballistocardiogram signal is nonlinear and nonstationary, the DFT was implemented by applying a window or a.k.a, “windowing”. The windowing process consists of multiplying a portion of a signal by a finite-length window with an amplitude that varies smoothly and gradually toward zero at the edges. By doing this, the effect of the leakage that occurs during an FFT of the signal is reduced. Leakage consists of spectral information

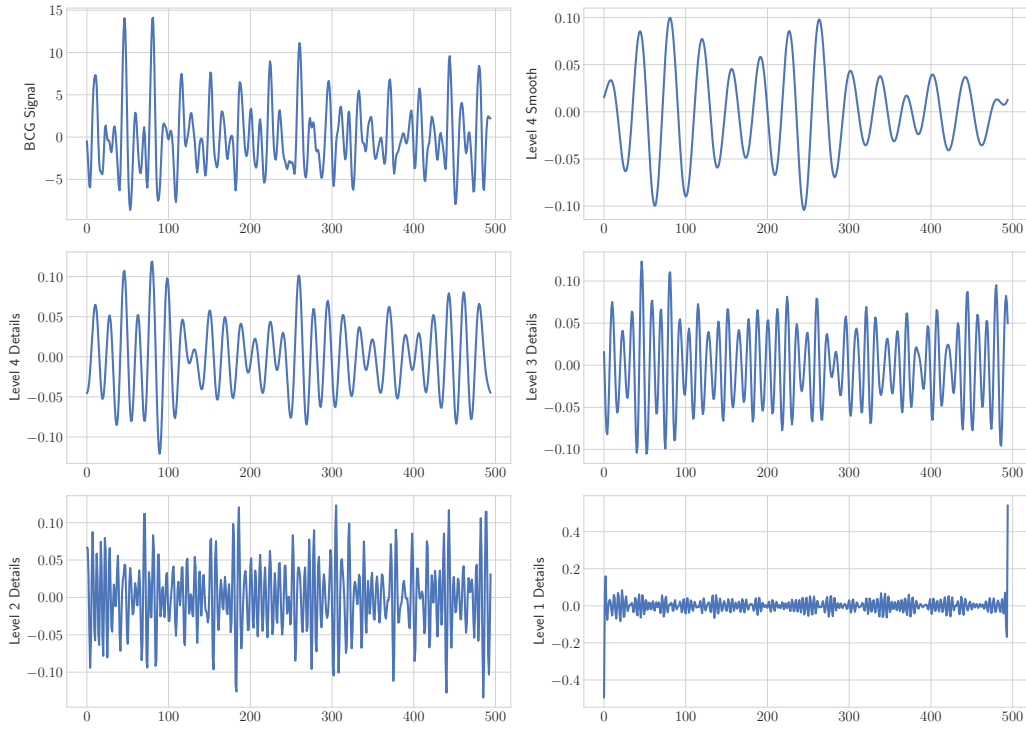


Figure 5.13: Symlet-8 MODWT multiresolution decomposition of a BCG signal (sampling frequency: 50Hz).

from an FFT showing up at the wrong frequencies. For a windowed portion of ballistocardiogram signal $y[n]$, the cepstrum is computed as follows:

$$c[n] = \sum_{n=0}^{N-1} \log \left(\left| \sum_{n=0}^{N-1} x[n] e^{-j \frac{2\pi}{N} kn} \right| \right) e^{j \frac{2\pi}{N} kn}, \quad (5.19)$$

where n is the time index; k is the frequency index; and N is the number of samples (N must be of power two, e.g., 256, 512, 1024, ...). For ballistocardiogram heartbeat signal, the spectrum consists of the peaks at the harmonic frequencies of the fundamental heartbeat frequency. This periodicity in the spectrum is presented as a peak value in the spectrum located at the corresponding ballistocardiogram interbeat interval lag-time value [Kortelainen 2007, Kortelainen 2012, Brüser 2015]. In our case, the lag-time range is from 0.4 second (= 2.5Hz) to 1.5 seconds (= 0.67Hz), i.e., the normal human heartbeat duration [Zhu 2014]. Figure 5.14 shows the cepstrum of a 30-second ballistocardiogram signal, in which the Fourier transform is computed by applying a Hanning window.

5.2.3.7 Autocorrelation

The autocorrelation function (ACF) measures the correlation between y_t and y_{t+k} , where $k = 0, \dots, K$. The formula for the autocorrelation for lag k is given by

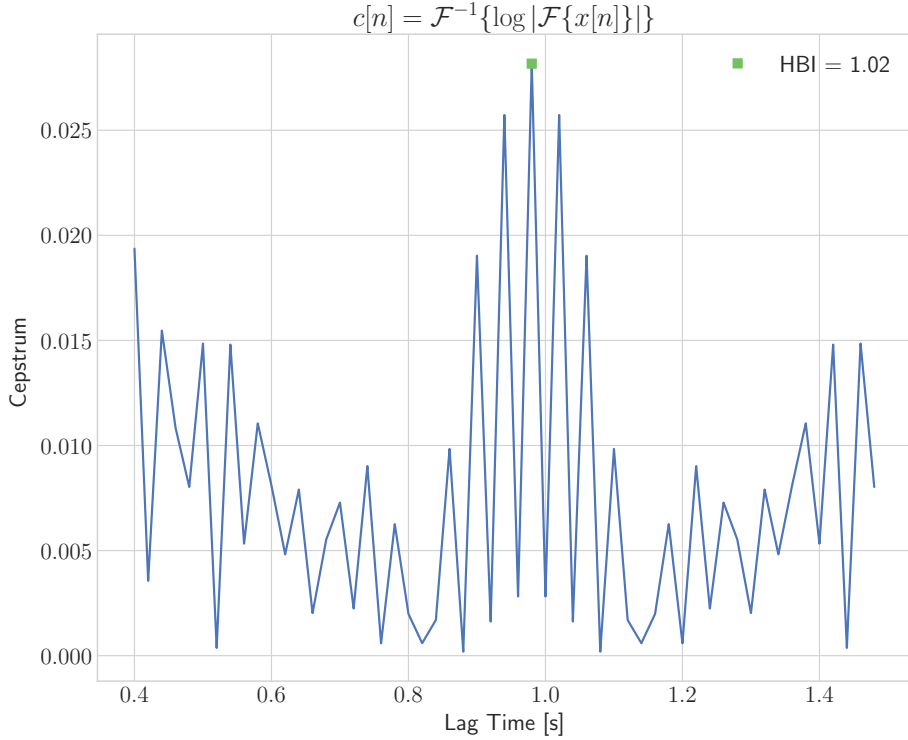


Figure 5.14: The cepstrum of a 30-second ballistocardiogram signal; the heart beat interval (HBI) is 1.02 seconds.

Equations (5.20) and (5.21):

$$r_k = \frac{c_k}{c_0}, \quad (5.20)$$

$$c_k = \frac{1}{T} \sum_{t=1}^{T-k} (y_t - \bar{y})(y_{t+k} - \bar{y}), \quad (5.21)$$

where c_0 is the sample variance of the time series, and T is the total number of samples in the window for the ACF calculation. As mentioned above, the lag-time range is from 0.4 second (= 2.5Hz) to 1.5 seconds (= 0.67Hz). Figure 5.14 shows the autocorrelation of a 30-second ballistocardiogram signal. The ACF is symmetric around lag zero, thus the function is normally plotted one-sidedly for positive lag.

5.3 Clinical Application

In this application, we aimed at validating our system for noninvasive monitoring of vital signs (heart rate, respiratory rate, and body movements) during sleep as well as monitoring of sleep apnea. As a beginning, sleep is one of the most important elements every human needs similar to oxygen, water, and food. Nevertheless, most

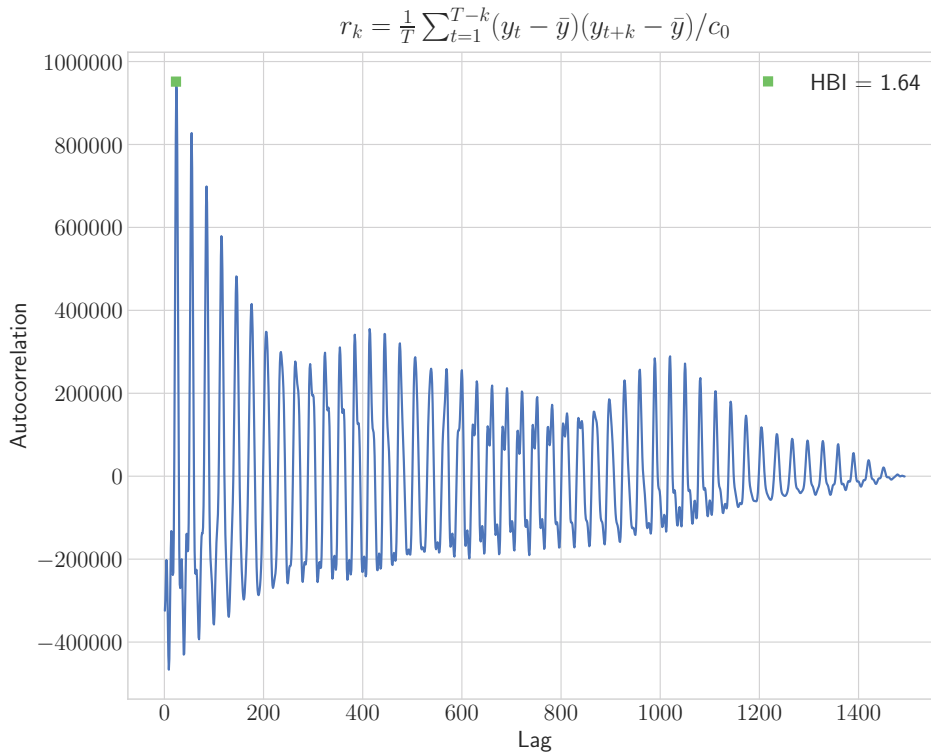


Figure 5.15: The autocorrelation of a 30-second ballistocardiogram signal; the heart beat interval (HBI) is 1.64 seconds.

people do not realize the importance of getting enough quality sleep. As stated by the *U.S. National Sleep Foundation (NSF)*, millions of people do not have sufficient sleep, and many may experience a lack of sleep.

To give an example, an individual might have the condition of sleep-disordered breathing (SDB). The SDB or a.k.a., obstructive sleep apnea syndrome (OSAS) is the most common sleep-related breathing disorders. The estimated prevalence of moderate-to-severe OSAS is reported to be 6 to 17% in the general population, being as high as 49% in the elderly [Senaratna 2017]. The OSAS is described by recurrent events, usually longer than 10 seconds of a complete (apnea) or partial (hypopnea) closure of the airflow throughout sleep (Figure 5.16). These episodes are typically joined with blood oxygen desaturation and arousals from sleep. OSAS can negatively affect the patient's cognitive function, mood, and quality of life. Besides, patients affected with OSAS are at a considerable risk of developing cardiovascular morbidity, and mortality [Peppard 2013, Kimoff 2016, Senaratna 2017].

In-lab polysomnography (PSG) is currently the most reliable approach to assess OSAS severity. The PSG test involves multiple physiological sensors attached to the body to record several body functions during sleep, i.e., brain wave activi-

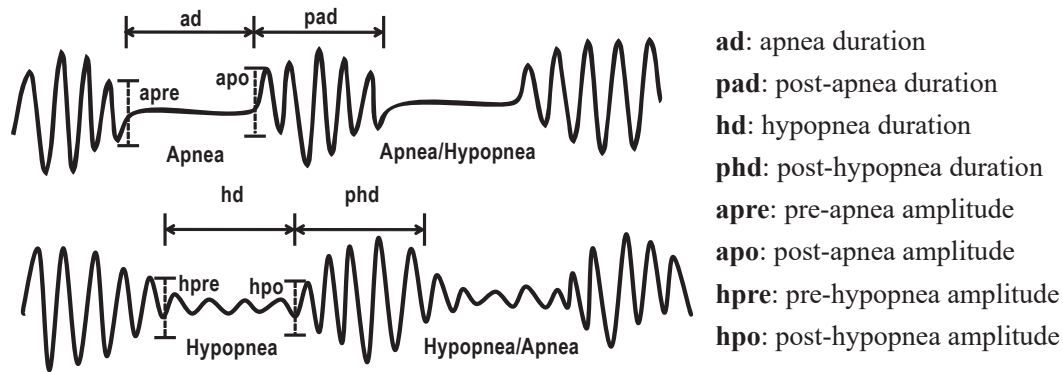


Figure 5.16: Drawing representing event and inter-event duration, as well as pre-and post-event amplitude (with upward deflection of flow during inspiration). Image adapted from [Jaimcharyatam 2013].

ties, breathing patterns, heartbeats, blood oxygen levels, body movements, etc [Wang 2017, Erdenebayar 2017, Lin 2017b]. Despite the apparent feasibility of the PSG to provide real-time and accurate information about OSAS; it introduces some limitations, i.e., complexity, invasiveness, time-consuming, excessive cost, high maintenance, and lack of privacy. As a result, there is an increasing demand from healthcare communities to look for novel unobtrusive methods that are inexpensive, non-disruptive, and more widely applied than the standard full polysomnography to assess and diagnose sleep disorders [Koenig 2008].

Recent alternatives such as ballistocardiography (BCG) can provide unobtrusive monitoring of physiological signals without the necessity of any wearable sensors connected to the patient's body. By way of illustration, a noninvasive analysis of physiological signals (NAPSTM) system was developed by the Medical Automation Research Center at the University of Virginia, which can measure physiological and environmental characteristics in a noninvasive manner [Koenig 2008]. The system used two resilient force coupling pads placed under the bed sheet of a standard hospital bed to detect the minute forces produced during cardiac contraction and relaxation. Moreover, the system could detect body movements from the respiratory effort and postural changes. Additionally, it could detect environmental changes such as room temperature or light levels. The system was tested and validated on 40 healthy subjects in an overnight study. The system provided satisfactory results compared to the reference electrocardiogram, pulse oximetry, and respiratory inductance plethysmography [Mack 2002, Mack 2003, Mack 2009].

Few approaches in existing literature are dedicated to unobtrusive OSAS detection. For example, Mack *et al.* [Mack 2006] advised to use the NAPSTM system for unconstrained apnea and arousal detection, the proposed system was validated using data from forty subjects. Hwang *et al.* [Hwang 2014] proposed to use a polyvinylidene-fluoride film sensor placed on top of the mattress for apneic events' detection in a dataset with thirty-two subjects. Beattie *et al.* [Beattie 2013] reported

the use of load cells located below the supports of bed to detect apneic events for forty-five subjects, where the apneic detection is done manually by an expert. Finally, Waltisberg *et al.* [Waltisberg 2017] introduced a sensor with integrated strain gauges installed below the bed mattress to detect apneic and limb movement events for nine subjects. An ongoing study between Personal Health Analytics Company Zansors² and researchers at the University of Michigan, could bring to market the first-ever low-priced, US Food and Drug Administration (FDA)–approved over-the-counter sleep apnea sensor for in-home use next year. The small, wireless wearable patch detects sleep breathing patterns using microphone and accelerometer data. The rechargeable battery-powered device transmits the data to the patient’s smart-phone via Bluetooth. It will be distributed for about \$70 to \$150. The company aims at targeting 2018 for market availability [Jennifer 2017].



Figure 5.17: Sleep apnea sensor proposed by Zansors, LLC. Image adapted from [Jennifer 2017]

PSG was used to assess the performance of aforementioned methods to identify apneic events, and it is worth mentioning that a fair comparison between different methods is difficult to make because the BCG’s morphology is highly dependent on the type of the sensor and its location.

The objective of this study was to present preliminary results of a noninvasive vital sign (i.e., heart and respiratory rate) monitoring system for sleep apnea patients using a microbend fiber-optic sensor (MFOS). In addition, we assessed the capacity of the proposed system for noninvasive OSAS detection as compared to the most commonly used portable monitoring device (ApneaLink, ResMed, San Diego, California, USA). In the subsequent sections, we discuss the data collection protocol and the principles of the deployed sensors in Section 5.3.1. Afterward, we explain the algorithms used to analyze the sleep data in Section 5.3.2.

²<https://www.zansors.com/>

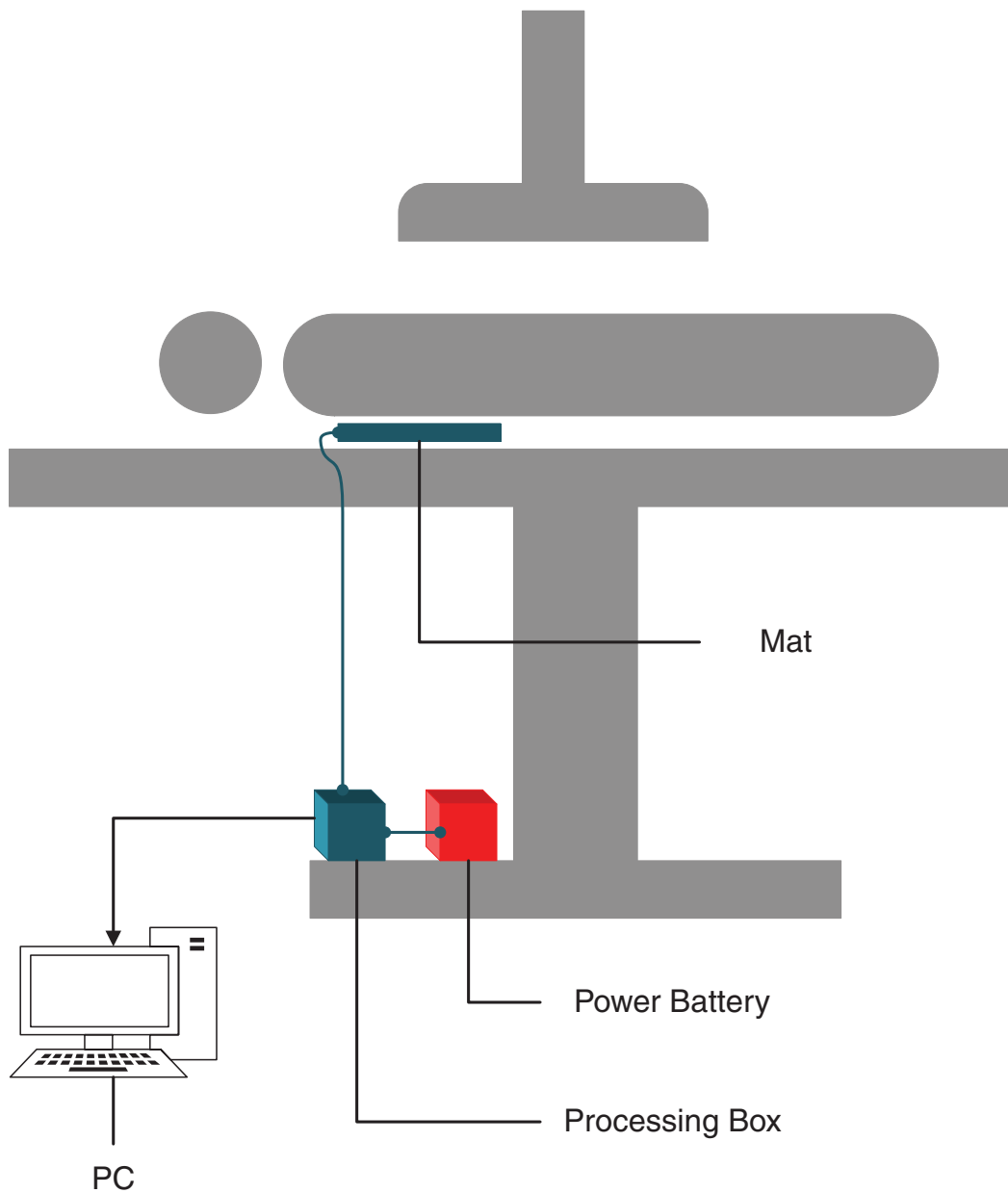


Figure 5.18: The positioning of the optical fiber mat on the operating room table.

5.3.1 Experimental Setup and Data Collection

The primary objective of the current study was to examine the accuracy of a single mat integrated with MFOS for unobtrusive vital signs monitoring such as heart and respiratory rates, while the secondary purpose was to examine its performance for unobtrusive detection of apneic events against a home sleep apnea device, i.e., ApneaLink. The National Healthcare Group (NHG) Domain Specific Review Board

(NHG DSRB Ref: 2016/00553) has approved the study and informed consent forms were obtained from the patients before data collection. All the procedures were implemented in agreement with the guidelines and regulations of the NHG DSRB. After informed consent, we recruited twelve patients suspected to have OSAS scheduled to undergo drug-induced sleep endoscopy in the operating theatre of Khoo Teck Puat Hospital. Only ten patients completed the study with complete data. Table 5.2 shows patients' demographic information and sleep apnea severity.

Table 5.2: Patients' demographic information.

Patient No.	Gender	Severity	AHI [†]	BMI [‡] (kg m ⁻²)	Age (years)
1	Male	mild	11	26.72	40
2	Female	mild	5	28.75	37
3	Male	mild	8	25.39	35
4	Male	mild	10	30	42
5	Male	severe	51	32.86	46
6	Male	severe	77	29.38	56
7	Male	severe	25	28.65	49
8	Male	severe	72	26.81	35
9	Male	severe	51	26.03	42
10	Male	severe	67	34.74	32
Overall*				28.65 ± 3.17	41.40 ± 7.34

[†] AHI: Apnea-hypopnea index

[‡] BMI: Body mass index

* Overall values are described as mean ± standard deviation.

Data was continuously collected during and after a drug-induced sleep endoscopy procedure. Patients were placed in a supine position on the operating table under propofol-induced moderate to deep sedation under processed electroencephalogram bispectral index monitoring guidance for about 30 minutes. Then they were transferred to a recovery room for about 90 minutes. For each patient, we collected sleep data using our proposed sensor and the ApneaLink device.

The fundamental principle of the proposed sensor was discussed in Section 4.2.1. In this clinical deployment, the mat processing unit operated on battery power, with a sampling frequency of 50Hz. It had a 16-bit ADC (internal memory storage is 4 GB) which enabled continuous recording when the patients were transferred from the operating room to the recovery room.

Figure 5.18 and Figure 5.19 show how the optical fiber mat was positioned on the operating room table approximately below the patient's chest and stomach. The second measurement device was a portable device, which measured airflow via a nasal pressure cannula, respiratory effort through a belt placed around the chest, heart rate and pulse oximetry using finger pulse sensor and pulse oximeter with sampling frequencies of 100, 10, 1 and 1Hz respectively. It was battery powered

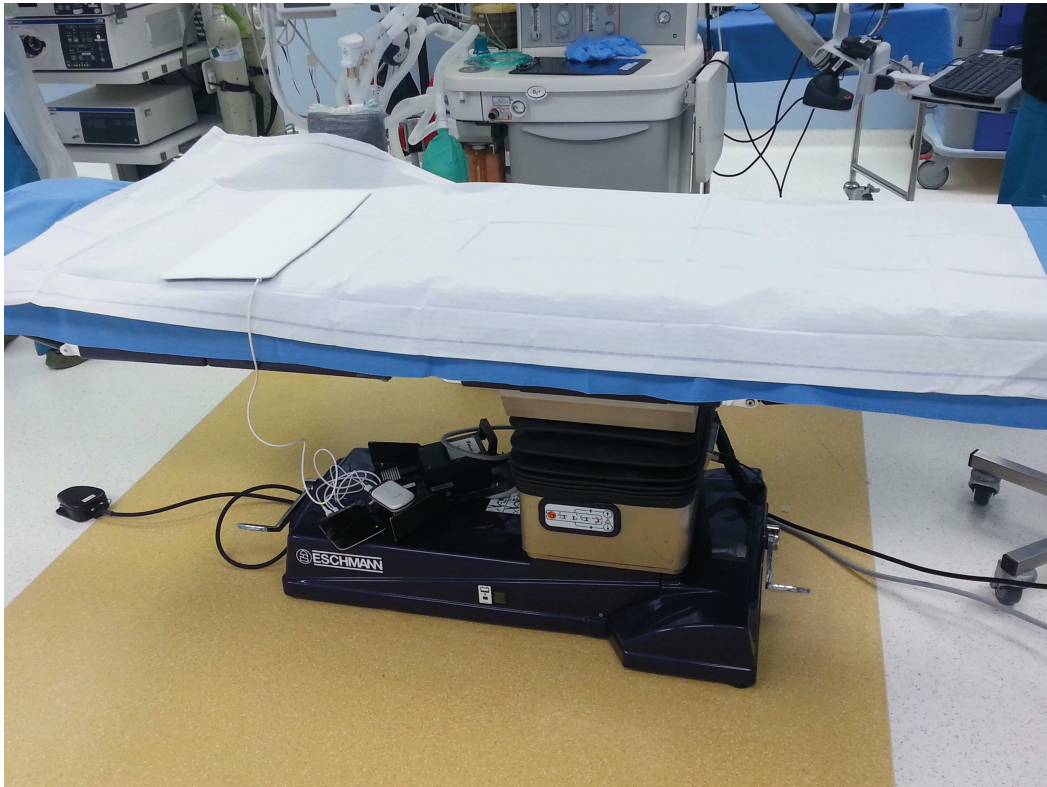
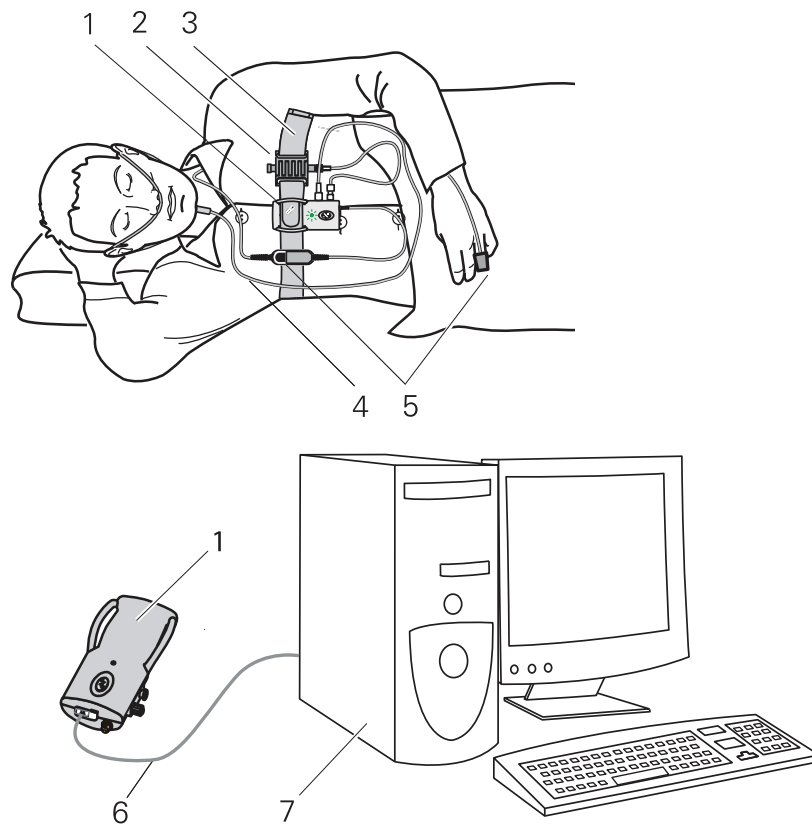


Figure 5.19: Real deployment of the MFOS mat in the operating theatre of Khoo Teck Puat Hospital.

by 16-bit ADC and 15MB internal storage. The apnea-hypopnea index (AHI), i.e., the mean number of all apnea classes (unclassified, central, mixed, obstructive) and hypopneas per hour in the evaluation period was used in the analysis for our study, while the default parameters of the ApneaLink device for apneas and hypopneas were used. The device is highly sensitive and specific in estimating AHI against the in-lab PSG. “An apnea was identified as a decrease in airflow by 80% of baseline for at least 10 seconds. The ApneaLink default maximum apnea duration was set at 80 seconds. A hypopnea was identified as a decrease in airflow by 50% of baseline for at least 10 seconds. The ApneaLink default maximum hypopnea duration was set at 100 seconds” [Erman 2007, Chen 2009a, Ng 2009, Crowley 2013, Chan 2014, Araújo 2018]. The ApneaLink results were also manually scored by a medical expert to avoid any short evaluation period. In addition, they were stored in EDF format, while keeping the patient’s data anonymized for further analysis with the proposed method. Figure 5.20 shows the system components and operation of the ApneaLink device.

5.3.2 Data Processing

The raw data was stored in 5-minute chunks on a Micro SD-Card embedded in the processing unit. Then all data-files were sent to a personal computer for data



- 1- ApneaLink/ApneaLink Plus device recorder
- 2- Effort sensor (ApneaLink Plus only)
- 3- Belt (Single or multi-use)
- 4- ApneaLink nasal cannula
- 5- Pulse oximeter with finger pulse sensor
- 6- USB cable
- 7- Computer with ApneaLink/ApneaLink Plus software installed

Figure 5.20: System components and operation of ApneaLink device (ApneaLink, ResMed, San Diego, California, USA).

processing. In general, three signals can be extracted from the raw data including body movement, heartbeat, and respiration. One of the biggest challenges of unobtrusive sensing is the body movement. Although it plays a vital role in sleep stage estimation [Watanabe 2004, Kortelainen 2010, Shin 2010, Lin 2017a], it has an unfavorable impact on the quality of physiological signals. As a result, the first step in our analysis was to identify and remove the body movement as explained in Algorithm 1. After that, BCG and respiratory signals were extracted from the bandpass filtered data. At last, apneic and non-apneic events were detected based on the respiratory signal. Figure 5.21 presents the overall flowchart of the suggested

system. To reach our goal, three different states were recognized for each 5-minutes

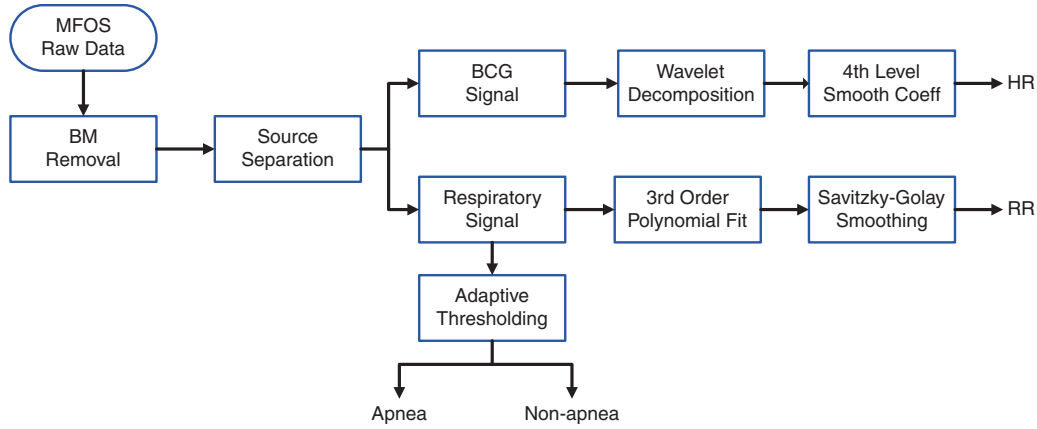


Figure 5.21: Overall system flowchart; BM: Body Movement, HR: Heart Rate, and RR: Respiratory Rate.

recording, i.e., body movements, no activity, and sleep as provided by Algorithm 1. The BCG (2nd row of Figure 5.24) and respiratory (3rd row of Figure 5.24) signals were extracted from the sleep data (1st row of Figure 5.24) using a Chebyshev type I bandpass filter. The lower and upper cutoff frequencies of the filters were (a lower pass-band frequency of 2.5Hz, an upper pass-band frequency of 5Hz, and a pass-band ripple frequency 0.5dB) and (a lower pass-band frequency of 0.01Hz, an upper pass-band frequency of 0.4Hz, and a pass-band ripple frequency 0.5dB) respectively.

The maximal overlap discrete wavelet transform with the multiresolution analysis Section 5.2.3.5 was implemented for the heart rate (HR) estimation [Sadek 2017a]. The BCG signal was cut up into approximation and detail information by passing through low-pass and high-pass filters, respectively without subsampling the filter coefficients. The wavelet bi-orthogonal 3.9 (bior3.9) basis function with level 4 was adopted for the decomposition process. The 4th level smooth coefficient (second row of Figure 5.24) was selected to measure the HR because the periodicity of the maxima showed an agreement with heart cycles. On the other hand, three steps were applied to the respiratory signal to measure the respiratory rate (RR). First, second, and third, the nonlinear trend was eliminated by subtracting a 3rd order polynomial fit, the detrended signal was filtered using a Savitzky-Golay smoothing filter (window length of 11 and polynomial order of 3), and a simple peak detector was utilized to detect the respiratory peaks. The local maxima of the respiratory signal were used for RR measurement, where the RR value at the time t_n , at which the n^{th} maximum occurred, was defined as follows:

$$RR_n = \frac{60}{t_n - t_{n-1}} \quad (5.22)$$

where t_n is the time at n^{th} local maxima and t_{n-1} is the time at $(n-1)^{th}$ local

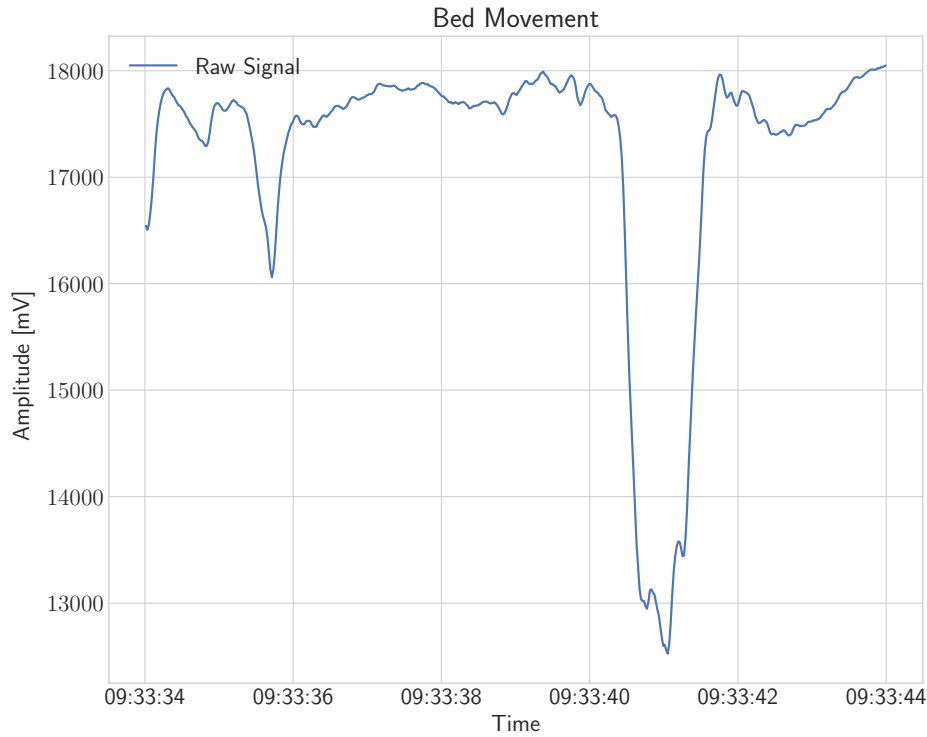


Figure 5.22: An example of a 10-second body movement signal for patient No. 4.

maxima in the respiratory signal. In which, the RR is expressed as breaths per minute (BPM).

The sleep apnea was identified using an adaptive threshold method based on the SD of the respiratory signal. For each patient, the respiratory signal was divided into 30 seconds' consecutive epochs, i.e., $W_i^{30} = \{W_1^{30}, W_2^{30}, \dots, W_N^{30}\}$. Then, every 30-second period was further divided into three 10 seconds' periods, i.e., $W_j^{30} = \{w_1^{10}, w_2^{10}, w_3^{10}\}$. For every 30-second epoch, if the SD of a 10-second epoch (W_k^{10}) was less than 30% of the maximum SD of the three 10-second epochs, the current epoch was considered as an apneic event. Otherwise, it was considered as a non-apneic event [Sadek 2018a]. The threshold was selected based on the mean performance evaluation of all patients for apneic event detection. We selected Cohen's Kappa coefficient as a mean performance [Hwang 2014] because it is thought to be a robust tool to evaluate the agreement between two raters.

In the previous two sections (Sections 5.2 and 5.3), we have demonstrated how our system was validated in health and wellness environment as well as the clinical environment. In the next section (Section 5.4), we explain how we implemented our sleep monitoring system in real-life environments.

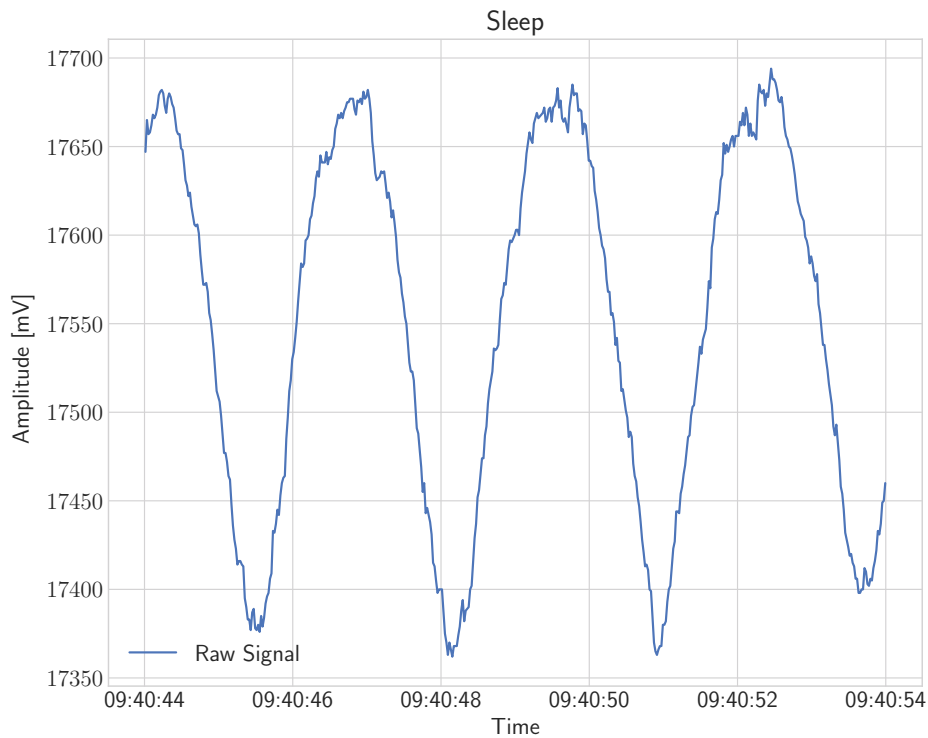


Figure 5.23: An example of a 10-second sleep signal for patient No. 4.

5.4 Real-life Deployment

We have successfully deployed our sleep monitoring system in thirteen homes with mainly senior residents for more than six months. Nevertheless, in this research, we concentrated on a one-month deployment with three senior residents as follows. The proposed system was deployed for 30 days in a home-based living situation and sleep data was collected from 3 senior female residents (68, 69 and 65 years old) in real-time using our MFOS sleep mat. To make the residents feel more comfortable, the optical fiber mat was hidden beneath the bed mattress so that they can sleep as normal while being monitored closely. One of the residents did not like to sleep in the bed, whereas she preferred sleeping on the floor. Thus, we placed the mat under the sleeping rug. The sleep data was stored in 5-minute chunks on a Micro-SD card installed in the processing unit, then it was sent to a cloud-based server for a deeper processing to extract the quantity of sleep in addition to heart and respiratory rates.

In our study, we determined the residents' sleep quality based on the duration of sleep (total sleep time), sleep interruptions (bed movements, bed exit), vital signs (heart rate, respiratory rate, and body movements). [Figure 5.25](#) summarizes a deployment of the presented system in user's home. In the ensuing sections, we explain the data collection protocol [Section 5.4.1](#). Thereafter, we discuss the

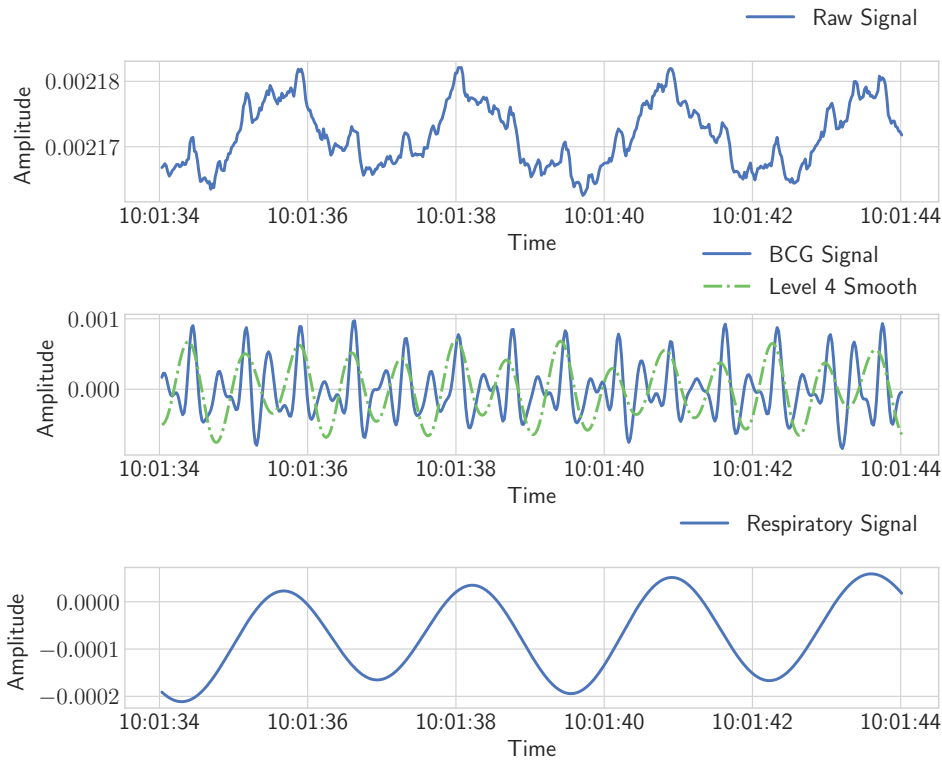


Figure 5.24: The first, second, and third rows represent a typical 10-second time-window of the raw signal, the BCG signal along with the 4th wavelet smooth coefficient, and the respiratory signal respectively; amplitude values were normalized between -1 and 1.

algorithms used to analyze the sleep data in Section 5.4.2.

5.4.1 Data Collection

The proposed solution was deployed in real conditions for 30 days in order to validate our approach. During the deployment in participants' homes, our system recorded data, and they were post-processed and evaluated. The objective of this validation was to study the reliability of the sleep monitoring and the performance of the entire system in a distant real deployment. At the same time, this deployment allowed us to validate the inter-connectivity of different sensors, the communication between the gateway and the server, and presentation of results in real time.

The sleep signals were continuously acquired from three HDB³ flats with elderly female residents, where the MFOS sleep mat shown in Figure 4.1 was placed under

³ <http://www.hdb.gov.sg> Housing & Development Board is a Singaporean governmental organization responsible for public housing, on their website, HDB claims: "HDB flats are home to over 80% of Singapore's resident population"

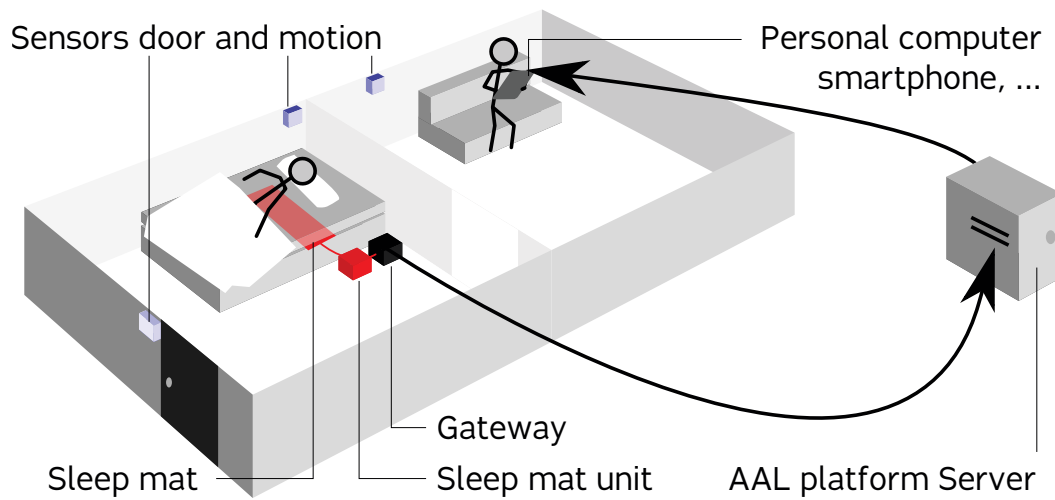


Figure 5.25: Overview of our unobtrusive monitoring in a living space.

the bed mattress. However, one of the residents prefers to sleep on the floor thus the sleep mat was placed under the sleeping rug (*bamboo sleeping mat*). Prior to data collection, written informed consent was thought from all residents involved in the study. In addition, a survey was obtained from the residents to summarize their living situation, sleeping and waking-up time, and napping time. We used the survey (Table 5.3) as a reference to validate the capability of the proposed system to detect different sleep patterns. Figure 5.26 (a), (b), (c) show the sleep mat deployment in the three HDB apartments.

5.4.2 Data Processing

In our real-life deployment, vital signs and sleep parameters, i.e., waking-up time, sleeping time, sleep interruptions, and total sleep time were computed based on Section 5.3.2. However, we implemented a moving time window (w_i) of 30-second length to get information about sleep, movement, and bed-empty events. Moreover, it should be mentioned that during the deployment, the residents were living as normal without any constraints, i.e., they could sleep on the bed at any time they prefer. Figure 5.27 shows a representation of a participant's night from our real-life deployment. As mentioned previously in Chapter 4, the sleep monitoring system was being deployed along with other sensors such as motion and contact sensors, and therefore we can predict the activities of daily living of the residents and to provide rich services in the right context through appropriate channels. Typically, motion sensors are installed in the lounge, living room, kitchen, and bathroom. Whereas, contact sensors can be attached to main door, fridges, and kitchen drawers.

Table 5.3: Home situation and sleep habits of each resident.

	Home Situation	Sleeping Time	Waking-up Time	Napping Time
Res1	Alone	23 : 00 – 00 : 00	07:00 Sometimes at 05 : 30	1 – 2 times 13 : 00 – 15 : 00 30 – 60 min
Res2	Family	21 : 00 – 23 : 00	07 : 00 Wednesday at 04 : 00	N/A
Res3	Family	18 : 30 – 19 : 30 Sometimes at 22 : 00	02 : 30	2 – 3 times 13 : 00 – 15 : 00 30 min

- According to the residents, the reported time is approximate.
- Residents do not report chronic diseases or disabilities.
- Resident No. 1 sleeps on the floor, resident No. 2 sleeps in a double bed. However, she always sleeps on one side of the bed, and resident No. 3 sleeps in a single bed.

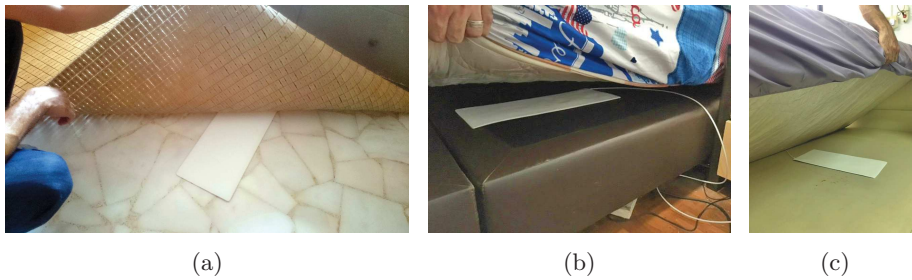


Figure 5.26: Sleep mat integration at the three HDB apartments; (a) 1st home with mat under sleeping rug, (b) 2nd home with mat under bed mattress, (c) 3rd home with mat under bed mattress.

5.5 Conclusion

This chapter discusses the two different applications we have implemented to evaluate our non-obstructive vital signs monitoring system. The first application aimed at measuring heart rate in a sitting position using data collected from 50 individuals during a massage session. This application simulated real-life deployment because of the movement of the chair, as well as the movement of the body. These movements had a strong impact on the quality of the signal, and therefore the proposed quality data processing can be evaluated properly. Other than that, the second application aimed at validating the proposed system for unobtrusive vital signs monitoring as well as unobtrusive sleep apnea detection. In this application, the data was collected from 10 patients in a clinical setting during a drug-induced sleep endoscopy. In conclusion, the data quality processing algorithm, which is based on the signal's

variance removes non-informative signals, i.e., motion artifacts and no-activity segments. Subsequently, the multiresolution analysis of the MODWT can be applied to detect heart cycles. Furthermore, the respiratory cycles can also be detected after removing the nonlinear trend in the band-pass filtered signal. Then, the local peaks of the respiratory signal can be utilized to measure the respiratory rate. Additionally, the system has been evaluated for unobtrusive monitoring of sleep-disordered breathing, in particular, obstructive sleep apnea. At last, we have described our real-life deployment and how the sleep data was collected for several nights from three senior residents in a home-based situation. The next section will discuss in detail the results achieved in each of aforementioned applications.

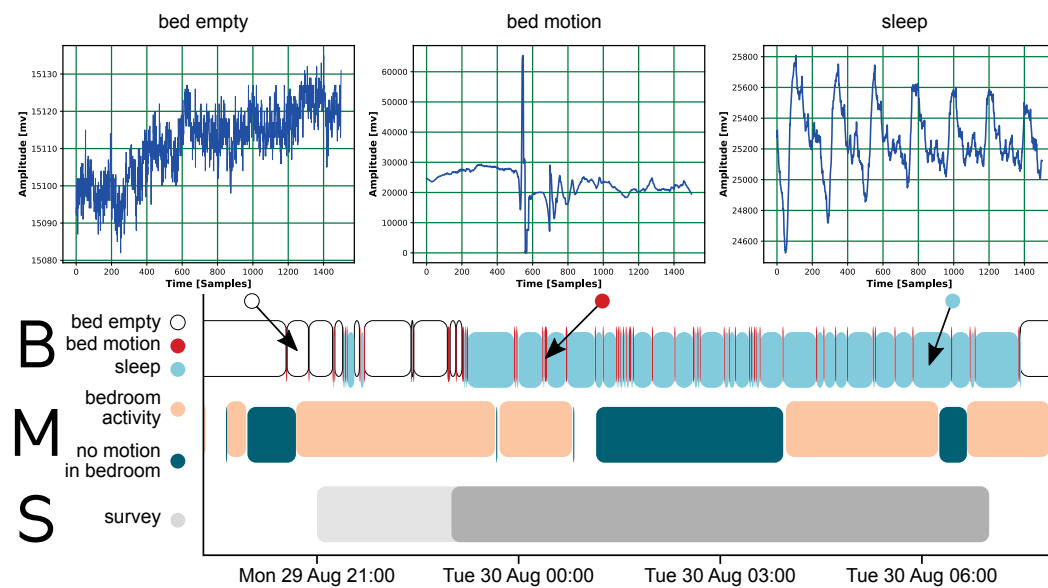


Figure 5.27: Representation of a participant's night from our real-life deployment. Three typical signal shapes are labeled according to recognized conditions: *bed empty*, *bed motion*, *sleep*. Gantt diagram: Row “B” is the result of the signal processing from the bed sensor. Row “M” shows a very inaccurate detection using motion sensors (blank space indicates activity detection in other rooms out of scope). Row “S” indicates the participant's answer in the survey [Table 5.3](#) about their waking and sleeping habits.

Results and Discussion

Contents

6.1	Introduction	97
6.2	Results of Health and Wellness Application	97
6.2.1	Wavelet Analysis Versus CEEMDAN Algorithm	102
6.3	Results of Clinical Application	105
6.3.1	Heart and Respiratory Rate Estimation	105
6.3.2	Sleep Apnea Event Detection	107
6.4	Results of Real-life Deployment	111
6.5	Conclusion	117

6.1 Introduction

This chapter discusses thoroughly the results of our two validation procedures, i.e., health and wellness application (Section 5.2) besides clinical application (Section 5.3). In the former, we explain how the heart rate estimation is enhanced by implementing the classification process. In addition, we provide a comparative study of various methods to measure the heart rate. These methods include Complete Ensemble EMD with Adaptive Noise (CEEMDAN) algorithm, the multiresolution analysis of the MODWT, fast Fourier transform (FFT), cepstrum, and autocorrelation approach. In the latter, we present the suitability of the proposed sleep monitoring system for unobtrusive vital signs monitoring in a clinical setting. The chapter also provides in detail the results of our real-life deployment (Section 5.4) in three users' homes in one month's time.

6.2 Results of Health and Wellness Application

As we deliberated before in Section 5.2.3.2, the goal was to use a cross-dataset testing in which Group1 was to be used as a training set while Group2 as a test set and vice versa. Therefore, the selected classifier should be able to correctly classify the data of Group2 based on Group1 and the other way around. Following the 10-fold cross-validation of each group, the optimal parameters of the classifiers were identified, and the mean accuracy of each classifier was determined. In general, the cross-validation is an approach to assess predictive models by subdividing the

initial sample into a training set to train the model, and a test set to assess it. More precisely, in 10-fold cross-validation, the initial sample is randomly subdivided into 10 equal size sub-samples. Of the 10 sub-samples, a single sub-sample is maintained as the validation data for testing the model, and the remaining 9 sub-samples are implemented as training data. The cross-validation process is thus repeated 10 times, i.e., the folds, with each of the 10 sub-samples applied exactly once as the validation data. The 10 results from the folds can thus be averaged to provide an individual estimation. The added-value of this approach is that all measurements are employed for both training and validation, and each measurement is adopted for validation exactly once.

Table 6.1 presents the mean accuracy of the 10-fold cross validation for each classifier. For random forest classifier (RF), the optimal number of trees or a.k.a., ntree was 50 trees. For support vector machine (SVM), the radial basis function kernel (RBF) provided better results than other kernel functions. For feedforward neural network (NN), the number of hidden layers was 50 layers.

Table 6.1: 10-fold cross validation mean accuracy for Group1 and Group2, (RF: ntree = 50, SVM: RBF kernel, NN: 50 hidden neuron).

	RF	SVM	NN	LDA	DT
Group1	98.13%	93.38%	91.61%	89.26%	97.51%
Group2	92.30%	90.49%	85.89%	79.37%	89.39%

In both groups mentioned above, random forest classifier showed superior performance over the other classifiers with a mean accuracy of 98.13% and 92.30% for Group1 and Group2 respectively. Using the same classifier, comparable results were achieved when Group2 was tested versus Group1 and the other way around with an accuracy of 90.75% and 97.99% for Experiment1 and Experiment2 accordingly as presented in Table 6.2.

Table 6.3 shows the confusion matrix of random forest for Experiment2. Moreover, it can be included that the percentage of recovered informative data was 57.37%, which can be calculated as follows. Percentage = $(1270 + 813)/(2085 + 1546)$. Decision tree and support vector machine classifiers attained relatively similar results to the random forest with accuracy results of (88.10% & 97.41%) and (84.54% & 97.46%) for Experiment1 and Experiment2, respectively.

Table 6.2: Accuracy results for testing Group2 Vs. Group1 (Experiment1) and testing Group1 Vs. Group2 (Experiment2).

	RF	SVM	NN	LDA	DT
Experiment1	90.75%	84.54%	82.34%	73.29%	88.1%
Experiment2	97.99%	97.46%	87.10%	90.26%	97.41%

Table 6.3: Confusion Matrix of random forest classifier for testing Group1 Vs. Group2 (Experiment2).

		Actual	
		Informative	Non-Informative
Predicted	Informative	1270	26
	Non-Informative	18	771

On the other hand, the CEEMDAN algorithm (Section 5.2.3.3) was applied to BCG signals following a noise standard deviation of 0.35, an ensemble size of 100, and a maximum number of iterations of 30 to obtain interbeat intervals. Referring to the amplitude of the added noise, Wu and Huang [Wu 2009b] recommended to apply small amplitude values for data influenced by high-frequency signals, and likewise. In addition, a smaller ensemble size can be employed. This is because the CEEMDAN adds a specific noise at each stage and produces a complete decomposition with no reconstruction error [Colominas 2012]. Furthermore, a balance between the amplitude of the added noise and the ensemble size should be considered. This is due to the fact that, if the added noise amplitude is too small, therefore it may not produce the change of extrema that the EMD depends on. Nevertheless, by increasing the ensemble size, the effect of the added white noise will always be able to be reduced to a minimally small level [Wu 2009b]. For ECG and BCG segments, the heart rate was estimated in beats per minute (BPM). Additionally, the mean absolute error (MAE) was implemented to evaluate the performance of the CEEMDAN algorithm for heart rate estimation with respect to the reference ECG. The MAE (Equation (6.1)), as the name suggests is the mean of the absolute errors, in which the absolute error is the absolute value of the difference between the forecasted value and the actual value.

$$\text{MAE} = \frac{\sum_{i=1}^n |R_i - M_i|}{n}, \quad (6.1)$$

where M , R , and n refer to measured data, reference data, and number of samples.

Table 6.4: The MAE for Group1 and Group2 before and after classification regarding the average beats per minute.

	MAE (before)	MAE (after)
Group1	11.16	7.26
Group2	15.24	9.68
Average	13.2	8.47

In order to estimate the effectiveness of the quality processing system, the HR was estimated before and after applying the classification process. From Table 6.4,

it can be noted that, the MAE was largely reduced from (G1: 11.16 and G2: 15.24) to (G1: 7.26 and G2: 9.68) after the classification process. As a result, the quality processing system can effectively increase robustness of the system for vital signs monitoring. [Figure 6.1](#) shows the Bland-Altman plot between the reference

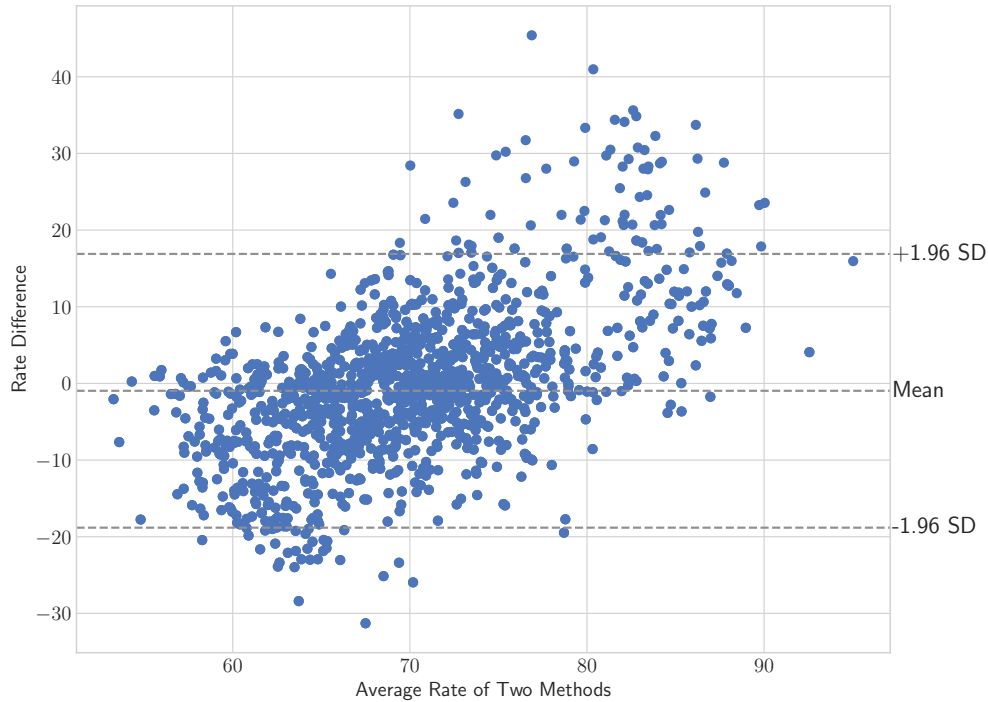


Figure 6.1: Bland-Altman plot between the reference ECG-derived heartbeat intervals to associated BCG-derived heartbeat intervals for Group1.

ECG-derived heartbeat intervals to associated BCG-derived heartbeat intervals for Group1. The limit of agreement was $[-18.82, 16.89]$ beats/minute (standard deviation $\sigma = 9.11$ beats/minute). [Figure 6.2](#) shows the Bland-Altman plot between the reference ECG-derived heartbeat intervals to associated BCG-derived heartbeat intervals for Group2. The limit of agreement was $[-25.2, 18.99]$ beats/minute (standard deviation $\sigma = 11.27$ beats/minute). There were a few reasons, which might have increased measurement deviation between the reference ECG and the proposed device as follows. During the massage session, ECG electrodes might not have been attached correctly to the subject's body. As a result, incorrect synchronization between both signals has occurred [[Hoog Antink 2018](#)]. Although the microbend fiber-optic sensor can detect the heart rate from various locations such as under the head; under the chest; under chest and abdomen; and under

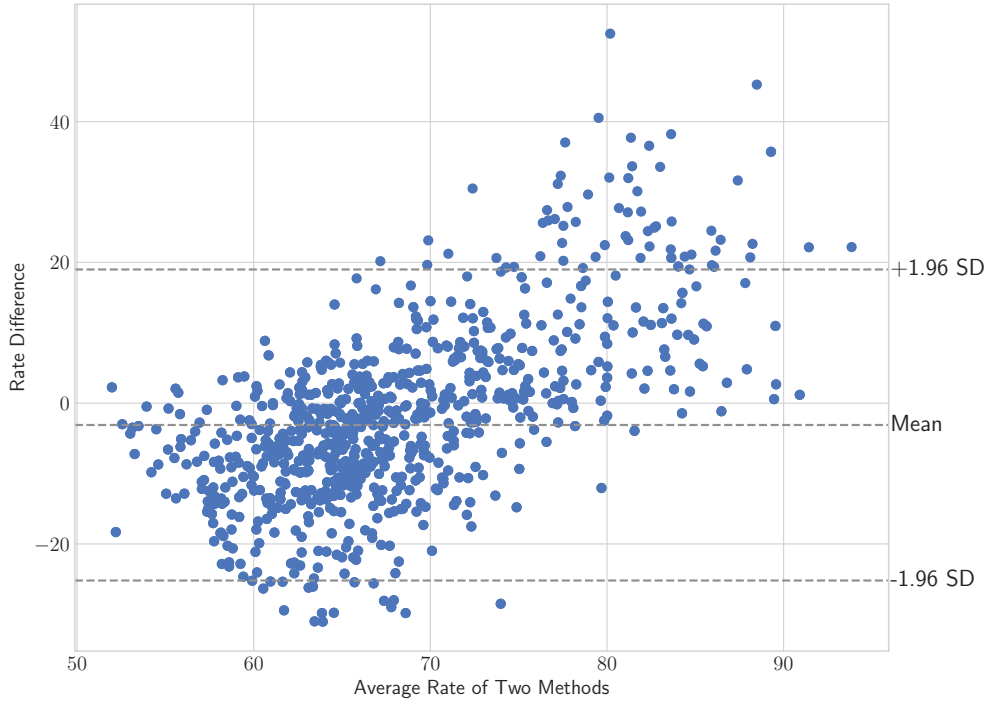


Figure 6.2: Bland-Altman plot between the reference ECG-derived heartbeat intervals to associated BCG-derived heartbeat intervals for Group2.

hips, the most accurate location for unobtrusive heart rate measurement is under the chest and abdomen [Sadek 2015]. Another reason is that the BCG signal does not display consistent J-peaks, and therefore cardiac peaks might not have been detected correctly. In other words, the BCG signal is not uniform within and across subjects [Sadek 2017a].

Since our ultimate goal is to implement the proposed device under real-life conditions, sensor data should be processed in a small-time period (or near real-time). As a result, the CEEMDAN algorithm was not a suitable choice for our data processing. The aforementioned algorithm is faster than the ensemble EMD. Nevertheless, it is still a time-consuming process. Besides, the manual labeling of training data should be replaced by an automated data quality processing. In what follows, we explain the results of implementing the automated data quality processing as well as the wavelet analysis (Section 5.2.3.5) to the same datasets.

6.2.1 Wavelet Analysis Versus CEEMDAN Algorithm

As we mentioned in [Section 5.2.3.4](#), the variance of the data was utilized to classify every 10-second time window into body movement, unoccupied, or sleep signal. For body movement signals, the magnitude of the pressure force was large enough to destroy any vital information. In other words, retrieval of any vital information was impossible. For unoccupied signals, the amplitude of the signal was always lower than a predetermined value, i.e., there was no any pressure force applied to the optical sensor mat. At last, for sleep signals, there was a uniform pressure applied to the optical sensor mat, i.e., the force applied to the mat is originated from the cardiac circulation as well as the movement of other body organs. Subsequently, for each subject, we first applied the automated data quality processing to exclude body movements and unoccupied events. Afterward, we implemented the wavelet analysis to detect the heart rate.

Table 6.5: The mean and standard deviation (SD) of the MAE for MODWT and CEEMDAN regarding the average beats per minute across all 50 subjects.

	CEEMDAN	db1	sym2	coif1	bior3.9	rbio3.1
Mean	9.4	12.64	14.11	14.17	10.12	10.13
SD	6.16	6.36	7.4	7.42	4.69	4.79

In order to achieve satisfactory results, several different families of wavelets have been evaluated such as Daubechies, Symlet, Coiflets, Biorthogonal, and Reverse Biorthogonal. Since every wavelet family has different numbers of vanishing moments, for our analysis we selected the vanishing moment yielding the lowest mean absolute error. We used Daubechies-1 (db1), Symlet-2 (sym2), Coiflets-1 (coif1), Biorthogonal-3.1 (bior3.9), and Reverse Biorthogonal-3.1 (rbio3.1) bases with 4-level decomposition. For each wavelet, the 4th level smooth coefficient was selected for heart rate measurement. This was because the periodicity of the local maxima presented an agreement with cardiac cycles.

As we can see in [Table 6.5](#), the Biorthogonal-3.9 basis function produced the lowest MAE (10.12 ± 4.69) among other wavelet basis functions. The Reverse Biorthogonal-3.1 achieved proportional results to Biorthogonal-3.9 basis function (10.13 ± 4.79). The Daubechies-1, Symlet-2, and Coiflets-1 achieved higher error rates such as 12.64 ± 6.36 , 14.11 ± 7.4 , and 14.17 ± 7.42 , respectively. [Figure 6.3](#) shows the box plots of the average MAE for CEEMDAN algorithm and wavelet methods regarding the average beats per minute across all 50 subjects. We can also see that, the CEEMDAN algorithm achieved slightly better results (9.4 ± 6.16) than the best wavelet, i.e., Biorthogonal-3.9. However, this algorithm is time consuming compared with wavelet transform ([Section 4.2.2](#)). To explain, the run-time of a 10-second signal was approximately 20 seconds and 0.04 seconds for CEEMDAN and wavelet transform, receptively. This happened when the algorithm was tested on a Windows-based laptop computer with Intel Core i5-4200U, 2.4GHz CPU clock

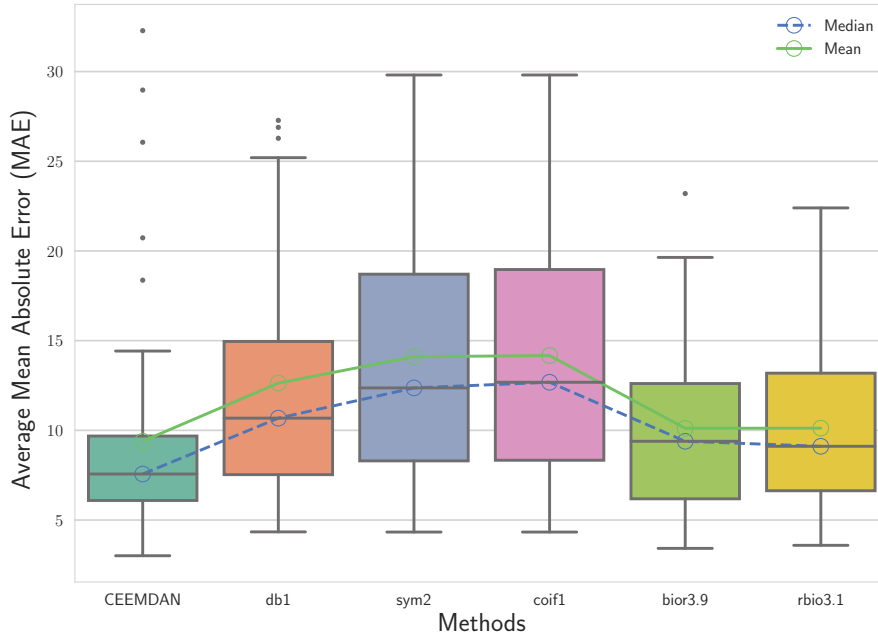


Figure 6.3: Box plots of the average MAE for CEEMDAN algorithm and wavelet methods regarding the average beats per minute across all 50 subjects.

and 6GB of RAM. As a result, the wavelet analysis was more suitable for our real-time applications. In many situations, the MODWT was able to handle the motion artifacts originated during the massage session. As shown in Figure 6.4, the algorithm managed to detect all the corresponding J-Peaks in the noisy BCG signal.

So far, we have shown the superiority of the wavelet analysis over the CEEMDAN algorithm considering real-time data processing. Next, we compared the best wavelet, i.e., Biorthogonal-3.9 with FFT, cepstrum, and autocorrelation methods. In these three methods, the heart rate was computed using a sliding time-window of a length 10-seconds (i.e., 500 samples) with 50% overlap between consecutive windows. After detecting the heartbeat interval (HBI) in each window, the heart rate was computed such as $HR = 60 * HBI$. As we can see from Table 6.6 and Figure 6.5,

Table 6.6: The mean and standard deviation (SD) of the MAE for best wavelet, FFT, cepstrum, and autocorrelation methods considering the average beats per minute across all 50 subjects.

	FFT	Cepstrum	Autocorrelation	bior3.9
Average	29.99	58.36	76.54	10.12
SD	12.21	8.08	22.58	4.69

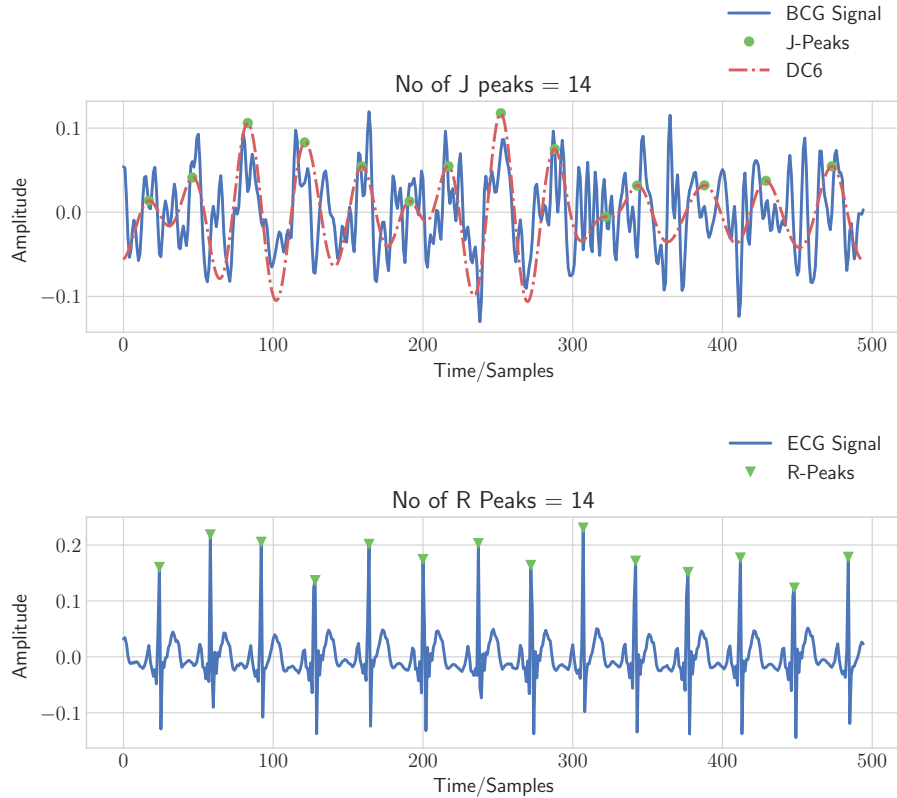


Figure 6.4: BCG signal with the 4th level smooth coefficient during a massage session (sampling frequency: 50Hz).

there is a major difference between the reference ECG and the proposed device when we implemented the frequency analysis and autocorrelation function for heart rate estimation. The error of the average beats per minutes obtained by FFT, cepstrum, and autocorrelation was 29.99 ± 12.21 , 58.36 ± 8.08 , and 76.54 ± 22.58 , respectively. We can also see that the best wavelet (Biorthogonal-3.9) performed much better results (10.12 ± 4.69) than others. Hence, we can conclude that the wavelet analysis is better suited than the Fourier analysis for analyzing the optical fiber data. This happened because wavelets are localized in both the time and frequency. Furthermore, the adaptive time-frequency resolution of wavelet signal processing allowed us to perform multiresolution analysis on ballistocardiogram signals. On the other hand, the frequency analysis did not provide better results due to the nonstationary characteristics of ballistocardiogram signals, whose spectral content varies over time. For the rest of this chapter, we will employ the wavelet analysis using Biorthogonal-3.9 as a basis function to compute the heart rate. The next section will provide and discuss the results of our clinical validation study.

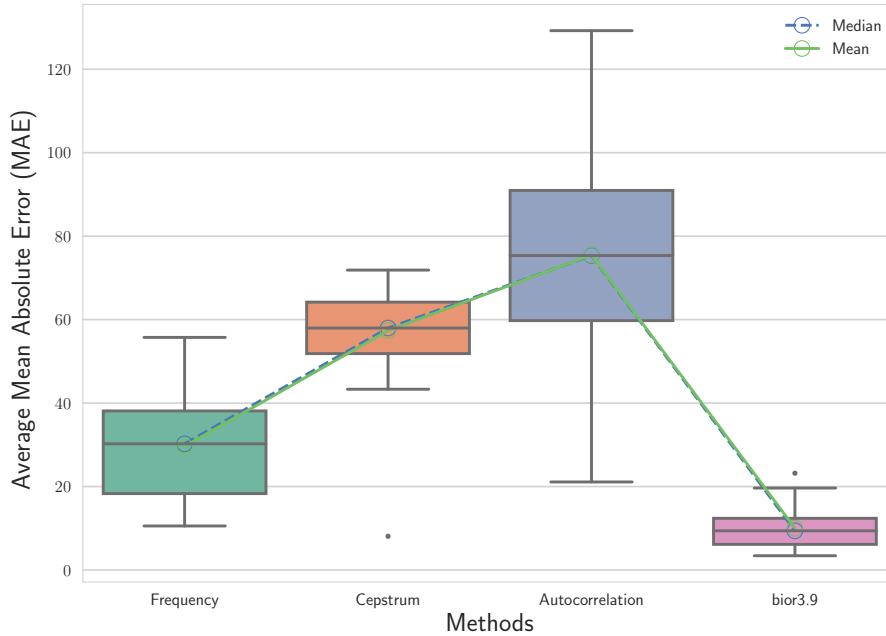


Figure 6.5: Box plots of the average MAE for best wavelet, FFT, cepstrum, and autocorrelation methods regarding the average beats per minute across all 50 subjects.

6.3 Results of Clinical Application

In this section, we explain the effectiveness of the optical fiber mat for unobtrusive vital signs monitoring, i.e., heart rate and breathing rate as well as for unobtrusive monitoring of sleep apnea during a drug-induced sleep endoscopy study.

6.3.1 Heart and Respiratory Rate Estimation

The reference HR and RR were obtained from the ApneaLink finger pulse sensor and chest belt, respectively. The mean HR was estimated in beat per minute (beats/minute) using a 10-second time window, whereas the mean RR was computed in breath per minute (breaths/minute) using a 10-second time window. To measure the performance of the introduced algorithms for HR and RR estimation, we used the mean absolute error (MAE). The Bland-Altman plot [Bland 1990], as well as the Pearson correlation coefficient, were also used to check the agreement between the reference and estimated values. The MAE for the mean beats per minute and the mean breaths per minute of all ten patients is listed in Table 6.7 and Table 6.8 respectively. Averaged across the ten patients, the MAE error was 0.55 ± 0.59 beats/minute and 0.38 ± 0.32 breaths/minute for the mean HR and mean RR

Table 6.7: The mean absolute error of all 10 patients for the average beats per minute computed during the entire study.

Patient #	Mean HR (beats/minute)		
	ApneaLink	MFOS Mat	Absolute Error
1	70.67	70.87	0.2
2	81.43	81.5	0.07
3	79.35	79.6	0.25
4	77.32	77.83	0.51
5	70.22	72.34	2.12
6	72.52	72.41	0.11
7	66.72	67.4	0.68
8	72.84	72.49	0.35
9	71.09	71.6	0.51
10	90.57	89.95	0.62
Overall*			0.55 ± 0.59

* Overall values are described as mean ± standard deviation.

Table 6.8: The mean absolute error of all 10 patients for the average breaths per minute computed during the entire study.

Patient #	Mean RR (breaths/minute)		
	ApneaLink	MFOS Mat	Absolute Error
1	15.05	14.85	0.2
2	19.47	19.63	0.16
3	16.66	17.59	0.93
4	17.38	17.96	0.58
5	18.98	19.06	0.08
6	19	18.57	0.43
7	20.42	20.21	0.21
8	19.52	20.38	0.86
9	17.44	17.72	0.28
10	20.02	20.07	0.05
Overall*			0.38 ± 0.32

* Overall values are described as mean ± standard deviation.

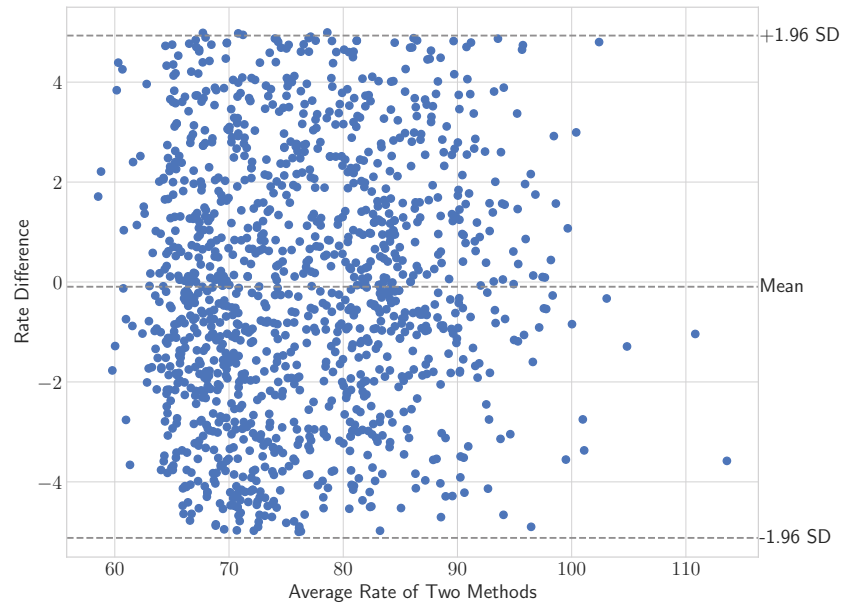
respectively. [Figure 6.6\(a\)](#) and [Figure 6.6\(b\)](#) show the Bland-Altman plot and the Pearson correlation plot of the HR between the two methods. The limit of agreement was $[-5.12, 4.92]$ beats/minute (standard deviation $\sigma = 3.07$ beats/minute). The Pearson correlation coefficient was 0.96.

In the same manner, [Figure 6.7\(a\)](#) and [Figure 6.7\(b\)](#) give the Bland-Altman plot and the Pearson correlation plot of the RR between the two methods. The limit of agreement was $[-5.13, 4.98]$ breaths/minute (standard deviation $\sigma = 2.56$ breaths/minute). The Pearson correlation coefficient was 0.78. In conclusion, the system achieved very close results to the ApneaLink device (finger pulse sensor and respiratory belt). The average error was very small for both vital signs as shown in the overall results of [Table 6.7](#) and [Table 6.8](#). Furthermore, the agreement between the reference ApneaLink and the sleeping mat was assessed using the Bland-Altman plot and the Pearson correlation coefficient, which revealed a very good agreement for both vital signs.

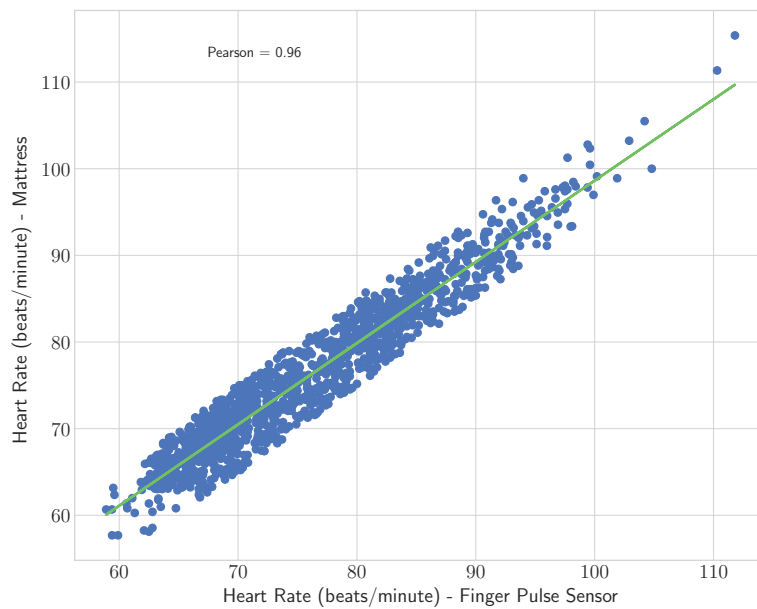
Broadly speaking, the estimation of the respiratory rate for normal subjects was easier than the heart rate. This is because the amplitude of the dominant J-peak (equivalent to the R-peak of the electrocardiogram signal) of the BCG signal was not uniform throughout the entire signal. However, for sleep apnea patients, the estimation of respiratory rate was very challenging. This is because, for sleep apnea patients, the morphology of the respiratory signal varies quite a lot during time due to the absence or decrease of breathing that makes the respiratory rate difficult to compute. As shown in [Figure 6.8](#), all the J-peaks of the BCG signal (1st row) can be easily detected. However, the respiratory cycles (inhalations and exhalations) are difficult to detect from the signal (2nd row). Thereafter, sometimes the respiratory peaks may not be detected correctly. It also can be noted that the Pearson correlation coefficient was 0.96 ([Figure 6.6\(b\)](#)) for heart rate estimation, while the value was 0.79 ([Figure 6.7\(b\)](#)) for respiratory rate estimation.

6.3.2 Sleep Apnea Event Detection

We correlated the AHI provided by the ApneaLink device (flow signal) with the AHI obtained from the optical fiber mat. The AHI derived from both systems was depending on the total time of the study. The severity of the apnea was graded based on the AHI value, i.e., mild ($5 \leq \text{AHI} < 15$), moderate ($15 \leq \text{AHI} < 30$), severe ($\text{AHI} \geq 30$). The sensitivity and specificity were employed to appraise the performance of the sleeping mat against the ApneaLink device. In this research, the sensitivity represented the proportion of correctly identified apnea events, whereas the specificity represented the proportion of correctly identified non-apnea events. The results of the sleep apnea detection algorithm are presented in [Table 6.9](#). The statistical values were computed based on the severity of the apnea at 30% threshold value. The sensitivity and specificity were $24.24 \pm 12.81\%$, $85.88 \pm 6.01\%$ for sleep apnea detection. The source code of the proposed methodology, in Python, is available at [[Sadek 2018b](#)]. In summation, the reference ApneaLink device measures the sleep apnea using the flow signal through a nasal cannula, which may not be

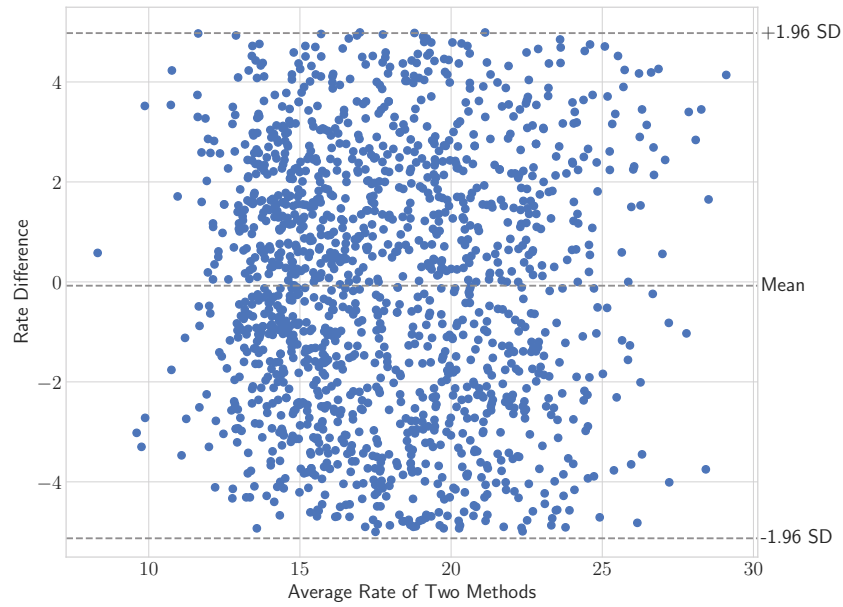


(a)

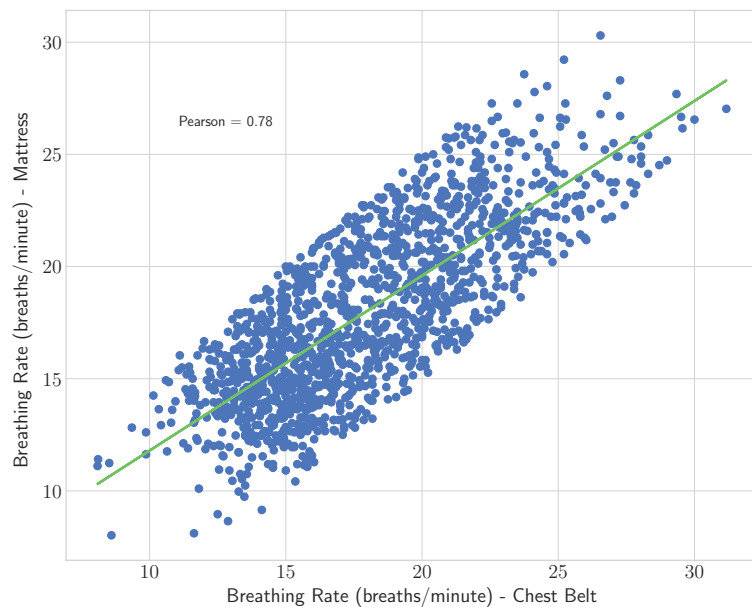


(b)

Figure 6.6: (a) Bland-Altman plot and (b) Pearson correlation plot of all patients regarding the HR measurement.



(a)



(b)

Figure 6.7: (a) Bland-Altman plot and (b) Pearson correlation plot of all patients regarding the RR measurement.

Table 6.9: Sensitivity and specificity of sleep apnea detection

Patient No.	AHI		Statistics (%)	
	ApneaLink	MFOS Mat	Sensitivity	Specificity
1	11	42	34.76	93.79
2	5	32	12.79	92.72
3	8	8	11.63	95.25
4	10	90	24.37	77.13
5	51	15	24.37	85.14
6	77	10	14.29	89.29
7	25	30	24.24	81.83
8	72	46	21.36	82.08
9	51	98	57.20	80.32
10	67	64	17.45	81.19
Overall*			24.24 ± 12.81	85.88 ± 6.01

* Overall values are described as mean ± standard deviation.

an appropriate choice for some groups of people. On the contrary, the proposed optical fiber mat can be integrated into different ambient assisted living locations such as beds, cushions, chairs, etc. In order to appraise the capacity of the mat for sleep apnea detection, we grouped the patient based on the AHI severity, as listed in Table 5.2. In general, the system provided very low sensitivity and relatively high specificity as shown in overall results of Table 6.9.

The measured sensitivity was very low compared to the measured specificity because of a number of reasons that can be explained as follows. First, motion artifacts originated due to the body movements were extremely high, which is a normal behavior for sleep apnea patients. Second, for hypopnea events, the amplitude of the respiratory signal was very similar to the normal events. Third, for central apnea events, there were no any respiratory efforts, which was very difficult for the mat to detect. In addition to above-mentioned reasons, there were other limitations, which have to be considered for the nonintrusive apnea detection. To start with, the small sample size, i.e., 10 patients and the short sleep time might have a negative effect on the measured statistics. Moreover, even though ApneaLink is a reasonable test in clinical settings, it still has lower sensitivity than a PSG. For more accurate results, the analysis should be performed in a natural sleep state with the PSG as a gold standard comparison. In which, we can infer that the microbend fiber-optic sensor in the current study was not sensitive enough to discriminate between shallow breathing and no breathing.

In order to overcome the shortcomings of the current study, we are now in the process of recruiting new patients for overnight PSG study. Up to now, we have

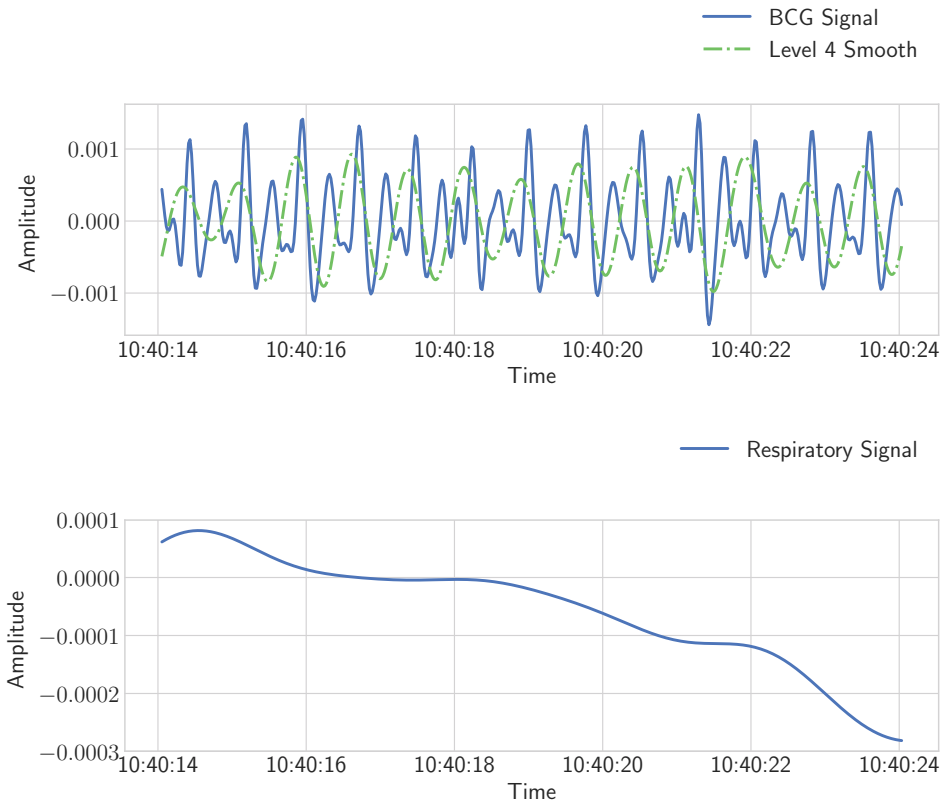


Figure 6.8: The first and second rows represent a 10-second time window of the BCG signal and the respiratory signal for patient No. 4.

shown the efficacy of the proposed system for unobtrusive nocturnal monitoring of vital signs, in which we validated our system in two different scenarios. Next, we introduce and discuss the results of our real-life deployment.

6.4 Results of Real-life Deployment

As we discussed in [Section 5.4.1](#), prior to data collection, written informed consent was obtained from all residents involved in the study. In addition, a survey was collected from the residents to summarize their living situation, sleeping and waking-up time, and nap time. We used the survey ([Table 5.3](#)) as a reference to validate the capability of the proposed system to detect the different sleep patterns of the three residents. We constructed a modified Bland-Altman plot for the sleep parameters in order to measure how the proposed approach matches with the users' survey. The idea was to define three limits, i.e., a mean, an upper limit of agreement (LOA), and a lower limit of agreement (LOA) as follows.

1. The first limit was the mean of the measurement of interest, for example, waking-up time, sleeping time, and total time of sleep.

2. The second limit was computed as follows:

$$\text{mean}[\text{measurement}] + 2 \times \text{SD}[\text{measurement}]. \quad (6.2)$$

3. The third limit was computed as follows:

$$\text{mean}[\text{measurement}] - 2 \times \text{SD}[\text{measurement}]. \quad (6.3)$$

By doing that, we can search for systematic bias or mean and also identify any possible outliers outside the two limits of agreements. To go into detail, as we can see in Figure 6.9, on most occasions, resident No. 2 wakes up around 07 : 15 with an upper LOA of 09 : 45 and a lower LOA of 04 : 52. However, on Wednesday the resident wakes up around 04 : 30. These results agree with the user’s survey because she usually wakes up around 07 : 00. Nevertheless, on Wednesday she wakes up around 04 : 00.

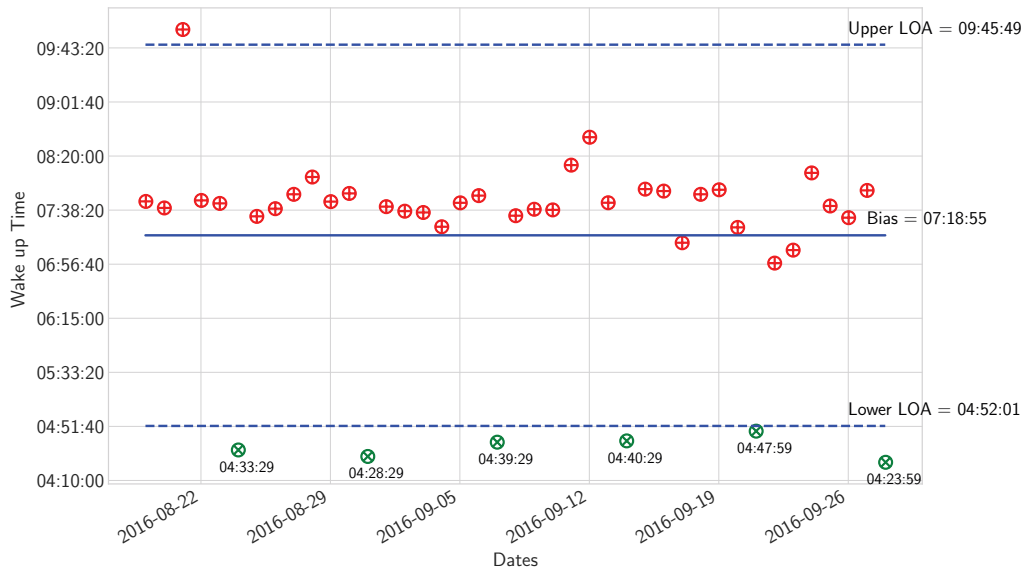


Figure 6.9: Bland-Altman plot of waking-up time for resident No. 2; green *bigotimes* symbols represent Wednesday.

Another example representing the time of sleep for resident No. 3 is shown in Figure 6.10 . It may be noted that most of the time the resident sleeps around 18 : 30. On two occasions, the resident went to bed before 14 : 30. This situation might occur when the resident stays on the bed for the entire day instead of sitting in a chair to watch television. We can also notice that on two other occasions the resident went to bed after 22 : 00 which agrees with user’s survey.

On the other hand, the resident reported having a nap two to three times between 13 : 00 and 15 : 00. This also agrees with our results presented in Table 6.10, in which the average time of starting the nap is 13 : 34 : 14 and the average time of ending the nap is 15 : 09 : 59. In addition, the average napping duration is about one and half hour. The waking-up time for this particular user was very surprising

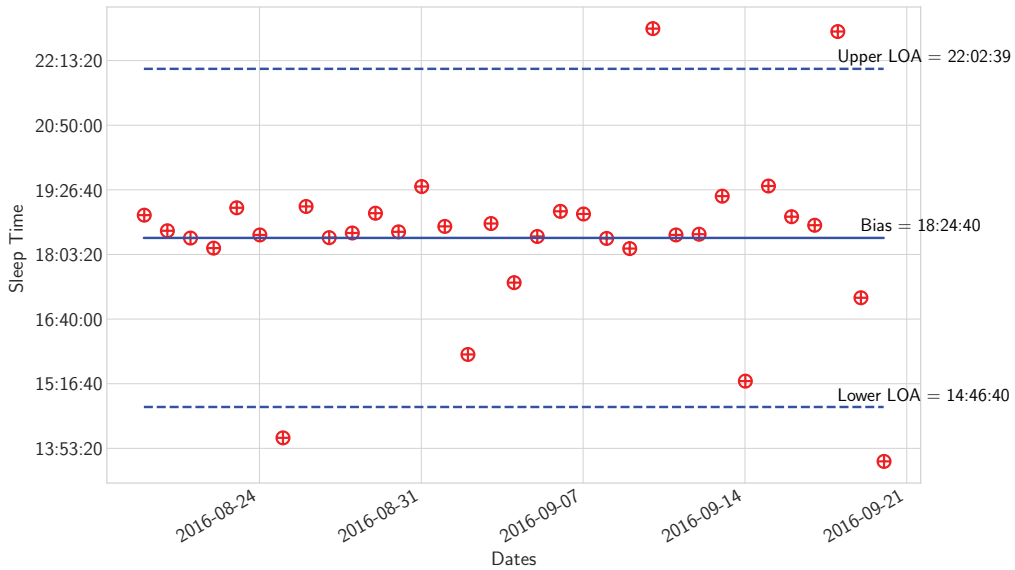


Figure 6.10: Bland-Altman plot of sleep time for resident No. 3 over deployment time.

to us. This was because according to our sleep monitoring system, the resident used to wake up around 03 : 30, which is very early in the morning (Figure 6.11). However, when we double checked with the resident, she confirmed the outcome as she used to practice some religious traditions at this specific time.

Table 6.10: Starting and ending of napping time for resident No. 3.

Days	Start Napping	Last Napping	Difference
8/19/2016	13 : 16 : 29	15 : 42 : 29	2 : 26 : 00
8/22/2016	13 : 52 : 29	15 : 47 : 59	1 : 55 : 30
8/27/2016	12 : 37 : 59	14 : 49 : 29	2 : 11 : 30
8/29/2016	13 : 09 : 29	14 : 40 : 29	1 : 31 : 00
9/5/2016	13 : 40 : 59	14 : 30 : 59	0 : 50 : 00
9/7/2016	14 : 47 : 59	15 : 28 : 29	0 : 40 : 30
Mean	13 : 34 : 14	15 : 09 : 59	1 : 35 : 45

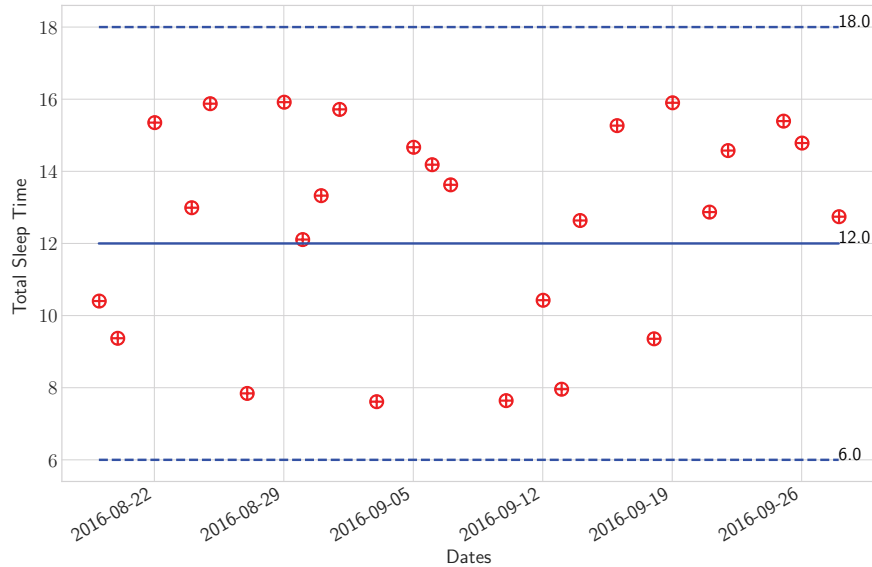


Figure 6.12: Bland-Altman plot of total sleep time for the 2nd resident over deployment time.

two limits of agreements that might indicate a normal behavior for this particular resident. Since trends in vital signs are key factors to determine critical conditions for an individual [Churpek 2016], if we notice any large deviation in either heart or respiratory rate we immediately inform the residents and their caregivers to consult with a doctor.

As the three residents were not adapted to use the Internet, relatives and caregivers were given access to a user-friendly web framework Figure 4.4 within the UbiSMART to follow the sleep patterns of the residents. The framework allows the caregivers to track the sleep parameters of the residents for days, weeks, etc. To give some examples, Figure 6.13 shows the distribution of the mean heart rate for resident No. 3 during the deployment time.

The data in Figure 6.13 indicates that the mean heart rate for that resident was almost uniformly distributed throughout the entire time. Likewise, Figure 6.14 presents the distribution of the breathing rate for resident No. 2. The data in Figure 6.14 also indicates almost a uniform distribution. In both examples, the moving average is calculated using a time-window of three days.

During the deployment, we have encountered some technical issues due to a slow or unstable Internet connection. However, thanks to the Micro-SD card embedded in the processing unit, the sleep files can be retrieved again. In the worst-case scenario, the sleep files can be recovered off-line from the Micro-SD card. Fortunately, this situation did not happen during the deployment time. In addition, one of the

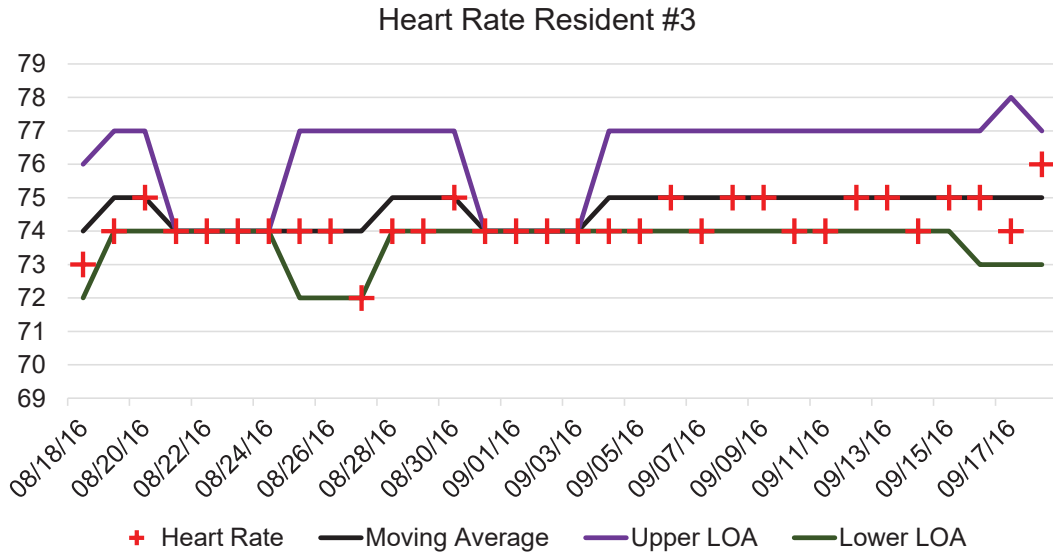


Figure 6.13: Bland-Altman plot of heart rate representation of resident No. 3 over deployment time.

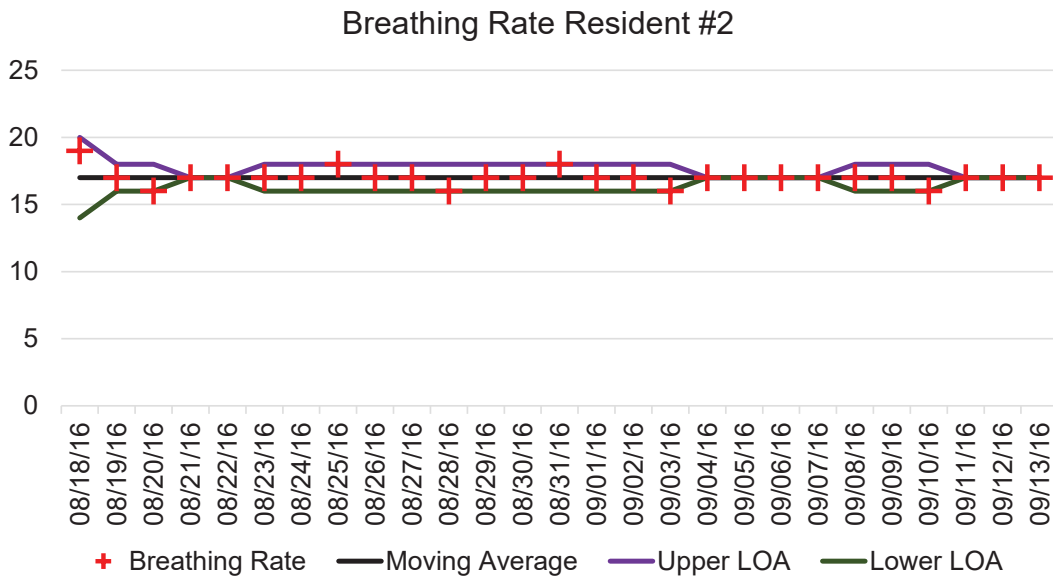


Figure 6.14: Bland-Altman plot of breathing rate representation of resident No. 2 over deployment time.

residents complained that the bed become warmer because of the presence of the mat underneath the bed mattress.

Technically speaking, this situation cannot happen as we are using fiber-optic technology. When we approached the resident, and discussed with the caregiver, we found out that this feeling occurred as the resident was a little bit afraid of the new system. After explaining again, the safety of the system to the resident, she became more comfortable and she did not complain again about the mat.

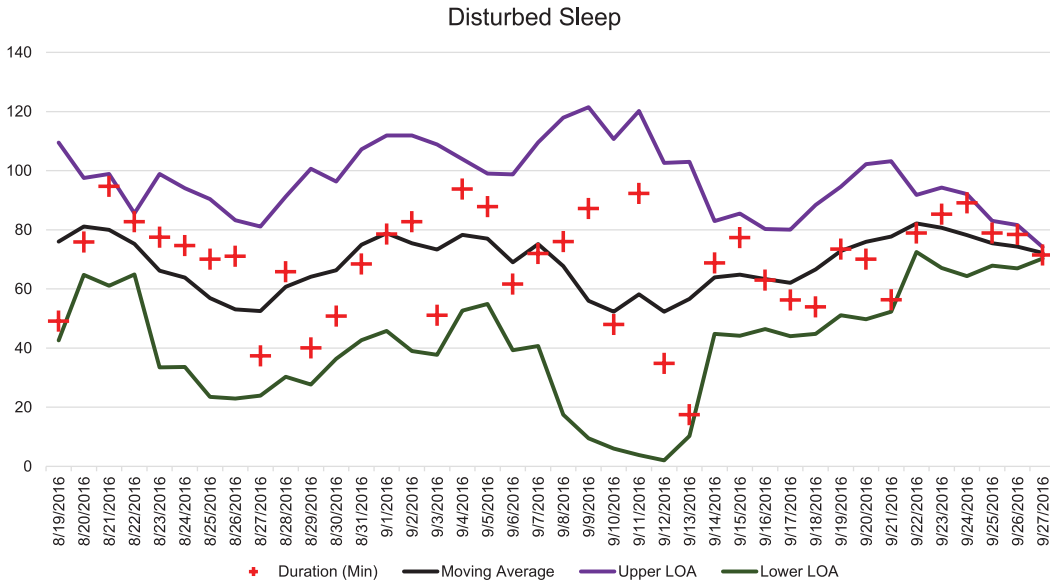


Figure 6.15: Sleep disturbance distribution for resident No. 2 over deployment time; the moving average is computed using a time-window of three days.

To summarize, the proposed sleep monitoring system does not require any close contact with the human body. This feature was very suitable for the residents because they did not agree to put on any wearable devices. Although wearable devices like smart-watches can provide more accurate and continuous monitoring of different body functions, they might be more suitable for young people. This is not always true, it depends on the level of education and the ability to learn and accept modern technologies. Based on the total time of sleep, frequent body movements, bed exit activities, vital signs, i.e., heart rate and respiratory rate, we can infer the sleep quality of the residents.

6.5 Conclusion

In this chapter, we have reported the results of our health and wellness validation as well as clinical validation. Various approaches have been implemented to detect interbeat intervals for noisy and nonstationary ballistocardiogram signals. The wavelet analysis among other methods was able to provide satisfactory results in reasonable running time. In consideration of the foregoing, the frequency-domain approaches do not yield satisfactory results due to the characteristics of ballistocardiogram signals. In other words, the interbeat intervals are not uniform within the time. Further, interbeat interval measures are very susceptible to surrounding noise. Therefore, locating the fundamental heartbeat frequency is very challenging, which results in imprecise heartbeats. Considering the clinical validation, the proposed nonintrusive sleep monitoring system provided very reasonable results compared

with a home sleep testing device, i.e., ResMed's ApneaLink despite the large body movements originated during apnea events. Nonetheless, nonintrusive sleep apnea detection is a very challenging task because the same signs and symptoms of sleep apnea might also occur in healthy people. With respect to real-life deployment, the proposed system presented very good results for identifying various sleep parameters such as waking-up time, sleeping time, the total time of sleep, and physiological signs, i.e., heartbeat and respiration. Moreover, the residents were very interested in the system because they feel more safe and comfortable. In the future, we are aiming at extending the indoor monitoring to an outdoor monitoring using beacons placed near to areas of interest such as food courts, sports facilities, bus stops, senior activity centers where the elderly used to go. The next section will conclude the thesis and outlines directions for future research.

Conclusion and Future Directions

Contents

7.1 Conclusion	119
7.2 Future Directions	121

In this last chapter, we present conclusions about our proposed work. Furthermore, we describe possible research directions to continue the work described in this thesis.

7.1 Conclusion

In this thesis, we have presented a unique nonintrusive vital sign monitoring system using a mat embedded with microbend fiber-optic sensors. The fundamental principle of the proposed system is to record the mechanical vibrations of the body caused by cardiac activity as well as the chest and abdominal movements.

The heartbeat intervals, i.e., the millisecond interval between two consecutive heartbeats can be computed from the vibrational activity of the heart whereas the breathing rate can compute from the movements of the chest and abdomen.

The microbend fiber-optic sensor is a very suitable choice for nonintrusive monitoring of vital signs, i.e., heart rate and breathing as it is highly sensitive to pressure variations produced by the ballistic forces of the heart and it does not require close contact with the body. Furthermore, it is relatively small, lightweight, and affordable. In other words, we only need to locate the optical fiber mat underneath the subject's mattress, therefore, we can measure his/her vital signs.

The proposed system can also be used to monitor the sleep quality of the subjects as the system can provide information about physiological signals such as heart rate, breathing rate, and body movements. Based on this information, various sleep parameters can be measured, namely waking-up time, sleeping time, the total time of sleep, and sleep interruptions.

Since the optical fiber mat can be located underneath the subject mattress, the acquired signal is very susceptible to motion artifacts. Hence, extracting heartbeat intervals is a very challenging task. In existing literature, different methods have been employed to detect heart and breathing rate non-intrusively. Nevertheless,

most of these methods have been deployed in a controlled laboratory environment. As a result, they might not be applicable for real-life environments such as users' homes.

In this research, we have proposed to use the multiresolution analysis of the maximal overlap discrete wavelet transform to measure heart rate. To begin with, an automated signal data quality algorithm based on the signal variance has been implemented to eliminate unwanted body movements that might destroy the vital information in the signal. Afterward, a band-pass filter with specific frequency limits equivalent to human heart rate was applied to the clean signal to extract cardiac signal or as known as ballistocardiogram. Next, the wavelet analysis was employed to analyze the cardiac signal into detail and smooth components. Additionally, the smooth component was selected for heart rate estimation since their local maxima show an agreement with cardiac cycles. At last, interbeat intervals were computed by finding the distance between successive local peaks of the smooth component.

On the other hand, the respiratory rate, representing the chest and abdominal movements, was computed by applying a band-pass filter with specific frequency limits equivalent to human breathing rate. Thereafter, the nonlinear trend was eliminated by subtracting a 3rd order polynomial fit, the detrended signal was filtered using a Savitzky-Golay smoothing filter (window length of 11 and polynomial order of 3), and a peak detector was applied to detect the respiratory peaks.

The proposed system has been validated in a health and wellness environment as well as a clinical environment. In the first, the data was acquired from 50 subjects sitting in a massages chair where the sensor was embedded in the headrest of the chair. The electrocardiogram sensor was used as a reference to assess the quality of the system for heart rate estimation. In the second, the data was collected in a clinical setting from a small cohort of subjects during a drug-induced sleep endoscopy study. The system was evaluated against a commercially available home-based sleep apnea monitoring device known as ApneaLink. In both applications, the proposed system achieved promising results compared with the reference devices. We also evaluated the capability of the proposed sensor for unobtrusive monitoring of sleep apnea during the clinical study. However, the system achieved lower sensitivity compared with airflow sensor of the ApneaLink device.

Considering heart rate estimation, the wavelet analysis has shown superior results compared with fast Fourier transform, cepstrum, and autocorrelation function. The empirical mode decomposition has been also implemented. Although it provided slightly better results than the wavelet analysis, it is a time-consuming process, therefore, it is not applicable for real-time analysis.

Following satisfactory results obtained during the two phases of validation, the system has been deployed in thirteen homes with mainly senior residents for more than six months. In this research, we analyzed the sleep data collected from three senior female residents during a one-month period. The proposed system has shown very good agreement with a user's survey collected before the study. Moreover, the sleep monitoring system has been integrated within an existing Ambient Assisted Living (AAL) platform, better known as UbiSMART. As a result, relatives and

caregivers could track the residents' sleep quality using a user-friendly interface within the UbiSMART. Likewise, the residents were very interested in the system because they feel more safe and comfortable. Along with the sleep monitoring system, the UbiSMART system collected other activities of daily living using motion and contact sensors. Combining of all sensory data can have a positive impact to enhance the quality of life and social well-being of the seniors.

7.2 Future Directions

In the future work, new directions might be included to improve the proposed system as follows.

In order to provide continuous vital sign monitoring, a multimodal sensing approach should be implemented. In other words, wearable devices such as smart-watches and smart-phones should be employed to enable continuous monitoring of vital activities. Thanks to the accelerometer, the wearable devices can monitor and record real-time information about one's physiological condition and motion activities. The outcome of our proposed sensor and other wearable devices can be fused together to yield more robust and accurate information about the health status of individuals. In addition, wearable devices can also be used as a reference to segment unwanted body movements during sleep which might have a negative effect on the signal quality.

Considering nonintrusive monitoring of sleep apnea, we can also use another sensor such as finger pulse oximeter to get more accurate information about obstructive apnea events. Our ultimate goal is to reduce as much as possible the number of sensors/electrodes need to be attached to the human body. However, in case of apnea detection, the polysomnography is still the gold-standard approach to determine the apnea severity for individuals. This is because several electrodes are used to detect several physiological signals. Our proposed device might have provided lower sensitivity for sleep apnea detection. However, it can provide long-term data monitoring which is not possible in a hospital environment.

We are also preparing a second phase for sleep apnea detection and the sleep monitoring system will be deployed during an overnight polysomnography study. This means that we can have more informative data that will help improve our current results.

Bibliography

- [Acampora 2013] G. Acampora, D.J. Cook, P. Rashidi and A.V. Vasilakos. *A Survey on Ambient Intelligence in Healthcare*. Proceedings of the IEEE, vol. 101, no. 12, pages 2470–2494, Dec 2013. (Cited on page 64.)
- [Addison 2002] P.S. Addison. The illustrated wavelet transform handbook: Introductory theory and applications in science, engineering, medicine and finance. Taylor & Francis, 2002. (Cited on page 76.)
- [Alametsä 2004] Jarmo Alametsä, Alpo Värri, Mikko Koivuluoma and Laurentiu Barna. *The potential of EMFi sensors in heart activity monitoring*. In 2nd OpenECG Workshop Integration of the ECG into the EHR and Interoperability of ECG Device Systems, Berlin, Germany, 2004. (Cited on page 37.)
- [Alametsä 2018] Jarmo Alametsä and Jari Viik. Twelve years follow-up of ballistocardiography, pages 1117–1120. Springer Singapore, Singapore, 2018. (Cited on page 40.)
- [Alihanka 1981] J. Alihanka, K. Vaahtoranta and I. Saarikivi. *A new method for long-term monitoring of the ballistocardiogram, heart rate, and respiration*. American Journal of Physiology - Regulatory, Integrative and Comparative Physiology, vol. 240, no. 5, pages R384–R392, 1981. (Cited on pages 27 and 28.)
- [Aloulou 2012] Hamdi Aloulou, Mounir Mokhtari, Thibaut Tiberghien, Jit Biswas and Lin Jin Hong Kenneth. A semantic plug&play based framework for ambient assisted living, pages 165–172. Springer Berlin Heidelberg, Berlin, Heidelberg, 2012. (Cited on page 61.)
- [Aloulou 2016] Hamdi Aloulou, Bessam Abdulrazak, Romain Endelin, João Bentes, Thibaut Tiberghien and Joaquim Bellmund. Simplifying installation and maintenance of ambient intelligent solutions toward large scale deployment, pages 121–132. Springer International Publishing, Cham, 2016. (Cited on page 60.)
- [Alvarado-Serrano 2016] Carlos Alvarado-Serrano, Pablo Samuel Luna-Lozano and Ramon Pallàs-Areny. *An algorithm for beat-to-beat heart rate detection from the BCG based on the continuous spline wavelet transform*. Biomedical Signal Processing and Control, vol. 27, no. Supplement C, pages 96 – 102, 2016. (Cited on pages 35, 36 and 75.)
- [Araújo 2018] Inês Araújo, Filipa Marques, Sandra André, Manuel Araújo, Sara Marques, Rita Ferreira, Patrícia Moniz, Margarida Proença, Pedro Borrego

- and Cândida Fonseca. *Diagnosis of sleep apnea in patients with stable chronic heart failure using a portable sleep test diagnostic device*. *Sleep and Breathing*, Jan 2018. (Cited on page 88.)
- [Aubert 2008] X. L. Aubert and A. Brauers. *Estimation of vital signs in bed from a single unobtrusive mechanical sensor: Algorithms and real-life evaluation*. In 2008 30th Annual International Conference of the IEEE Engineering in Medicine and Biology Society, pages 4744–4747, Aug 2008. (Cited on pages 37 and 41.)
- [Basner 2012] Robert C Basner. *Case studies in polysomnography interpretation*. Cambridge University Press, 2012. (Cited on pages xv and 17.)
- [Battle 2009] C.U. Battle. *Essentials of public health biology: A guide for the study of pathophysiology*. *Essential public health*. Jones & Bartlett Learning, 2009. (Cited on pages 13 and 14.)
- [Beattie 2013] Zachary T. Beattie, Tamara L. Hayes, Christian Guilleminault and Chad C. Hagen. *Accurate scoring of the apnea-hypopnea index using a simple non-contact breathing sensor*. *Journal of Sleep Research*, vol. 22, no. 3, pages 356–362, 2013. (Cited on page 84.)
- [Bellmunt 2015] Joaquim Bellmunt, Thibaut Tiberghien, Mounir Mokhtari, Hamdi Aloulou and Romain Endelin. *Technical challenges towards an aal large scale deployment*, pages 3–14. Springer International Publishing, Cham, 2015. (Cited on page 60.)
- [Bellmunt 2016] Joaquim Bellmunt, Mounir Mokhtari, Bessam Abdulzarak and Hamdi Aloulou. *Agile Framework for Rapid Deployment in Ambient Assisted Living Environments*. In Proceedings of the 18th International Conference on Information Integration and Web-based Applications and Services, iiWAS '16, pages 410–413, New York, NY, USA, 2016. ACM. (Cited on page 61.)
- [Berthold 1995] J. W. Berthold. *Historical review of microbend fiber-optic sensors*. *Journal of Lightwave Technology*, vol. 13, no. 7, pages 1193–1199, Jul 1995. (Cited on page 50.)
- [Bland 1990] J.M. Bland and D.G. Altman. *A note on the use of the intraclass correlation coefficient in the evaluation of agreement between two methods of measurement*. *Computers in Biology and Medicine*, vol. 20, no. 5, pages 337 – 340, 1990. (Cited on page 105.)
- [Brink 2006] Mark Brink, Christopher H. Müller and Christoph Schierz. *Contact-free measurement of heart rate, respiration rate, and body movements during sleep*. *Behavior Research Methods*, vol. 38, no. 3, pages 511–521, Aug 2006. (Cited on pages 42 and 46.)

- [Bruser 2011] C. Bruser, K. Stadlthanner, S. de Waele and S. Leonhardt. *Adaptive Beat-to-Beat Heart Rate Estimation in Ballistocardiograms*. IEEE Transactions on Information Technology in Biomedicine, vol. 15, no. 5, pages 778–786, Sept 2011. (Cited on pages 44 and 46.)
- [Brüser 2013] C Brüser, S Winter and S Leonhardt. *Robust inter-beat interval estimation in cardiac vibration signals*. Physiological Measurement, vol. 34, no. 2, page 123, 2013. (Cited on pages 39 and 41.)
- [Brüser 2015] C. Brüser, J. M. Kortelainen, S. Winter, M. Tenhunen, J. Pärkkä and S. Leonhardt. *Improvement of Force-Sensor-Based Heart Rate Estimation Using Multichannel Data Fusion*. IEEE Journal of Biomedical and Health Informatics, vol. 19, no. 1, pages 227–235, Jan 2015. (Cited on pages 34, 36 and 81.)
- [Cao 2013] Xinrong Cao, Hong Guo and Jintian Tang. *Heart Rate Extraction of Ballistocardiogram Based on Hilbert-Huang Transformation*. In Mian Long, editor, World Congress on Medical Physics and Biomedical Engineering May 26-31, 2012, Beijing, China, volume 39 of *IFMBE Proceedings*, pages 619–622. Springer Berlin Heidelberg, 2013. (Cited on page 69.)
- [Chan 2014] Matthew T V Chan, Chew-Yin Wang, Edwin Seet, Stanley Tam, Hou-Yee Lai, Stuart Walker, Timothy G Short, Richard Halliwell and Frances Chung. *Postoperative vascular complications in unrecognised Obstructive Sleep apnoea (POSA) study protocol: an observational cohort study in moderate-to-high risk patients undergoing non-cardiac surgery*. BMJ Open, vol. 4, no. 1, 2014. (Cited on page 88.)
- [Chee 2005] Yongjoon Chee, Jooman Han, Jaewoong Youn and Kwangsuk Park. *Air mattress sensor system with balancing tube for unconstrained measurement of respiration and heart beat movements*. Physiological Measurement, vol. 26, no. 4, page 413, 2005. (Cited on pages 40 and 43.)
- [Chen 2009a] Hui Chen, Alan A. Lowe, Yuxing Bai, Peter Hamilton, John A. Fleetham and Fernanda R. Almeida. *Evaluation of a portable recording device (ApneaLinkTM) for case selection of obstructive sleep apnea*. Sleep and Breathing, vol. 13, no. 3, pages 213–219, Aug 2009. (Cited on page 88.)
- [Chen 2009b] W. Chen, X. Zhu and T. Nemoto. *A new sensory device and optimal position for monitoring hr/rr during sleep*, pages 126–129. Springer Berlin Heidelberg, Berlin, Heidelberg, 2009. (Cited on pages 33 and 36.)
- [Chen 2009c] Zhihao Chen, Ju Teng Teo and Xiufeng Yang. *In-bed fibre optic breathing and movement sensor for non-intrusive monitoring*. In Proc.SPIE, volume 7173, pages 7173 – 7173 – 6, 2009. (Cited on pages 50 and 54.)

- [Chen 2012] Zhihao Chen, Ju Teng Teo, Soon Huat Ng and Xiufeng Yang. *Portable fiber optic ballistocardiogram sensor for home use*. In Proc.SPIE, volume 8218, pages 8218 – 8218 – 7, 2012. (Cited on pages 50, 54, 58 and 59.)
- [Chen 2013] Z. Chen, X. Yang, J. T. Teo and S. H. Ng. *Noninvasive monitoring of blood pressure using optical Ballistocardiography and Photoplethysmograph approaches*. In 2013 35th Annual International Conference of the IEEE Engineering in Medicine and Biology Society (EMBC), pages 2425–2428, July 2013. (Cited on pages 50 and 54.)
- [Chen 2014a] Z. Chen, J. T. Teo, S. H. Ng, X. Yang, B. Zhou, Y. Zhang, H. P. Loo, H. Zhang and M. Thong. *Monitoring respiration and cardiac activity during sleep using microbend fiber sensor: A clinical study and new algorithm*. In 2014 36th Annual International Conference of the IEEE Engineering in Medicine and Biology Society, pages 5377–5380, Aug 2014. (Cited on pages 51 and 54.)
- [Chen 2014b] Zhihao Chen, Doreen Lau, Ju Teng Teo, Soon Huat Ng, Xiufeng Yang and Pin Lin Kei. *Simultaneous measurement of breathing rate and heart rate using a microbend multimode fiber optic sensor*. Journal of Biomedical Optics, vol. 19, pages 19 – 19 – 11, 2014. (Cited on pages 51, 54, 58 and 59.)
- [Chethana 2017] K Chethana, AS Guru Prasad, SN Omkar and S Asokan. *Fiber bragg grating sensor based device for simultaneous measurement of respiratory and cardiac activities*. Journal of biophotonics, vol. 10, no. 2, pages 278–285, 2017. (Cited on pages 52 and 54.)
- [Choe 2017] Sun-Taag Choe and We-Duke Cho. *Simplified real-time heartbeat detection in ballistocardiography using a dispersion-maximum method*. Biomedical Research, vol. 28, no. 9, 2017. (Cited on pages 35 and 36.)
- [Chow 2000] Patrick Chow, Gangadharan Nagendra, John Abisheganaden and Y T Wang. *Respiratory monitoring using an air-mattress system*. Physiological Measurement, vol. 21, no. 3, page 345, 2000. (Cited on page 40.)
- [Churpek 2016] Matthew M. Churpek, Richa Adhikari and Dana P. Edelson. *The value of vital sign trends for detecting clinical deterioration on the wards*. Resuscitation, vol. 102, pages 1 – 5, 2016. (Cited on page 115.)
- [Colominas 2012] Marcelo A Colominas, Gastón Schlotthauer, MARÍA E TORRES and Patrick Flandrin. *Noise-assisted EMD methods in action*. Advances in Adaptive Data Analysis, vol. 4, no. 04, page 1250025, 2012. (Cited on page 99.)
- [Colominas 2014] Marcelo A. Colominas, Gastón Schlotthauer and María E. Torres. *Improved complete ensemble EMD: A suitable tool for biomedical signal processing*. Biomedical Signal Processing and Control, vol. 14, no. Supplement C, pages 19 – 29, 2014. (Cited on page 71.)

- [Cooke 2011] Jana R Cooke and Sonia Ancoli-Israel. *Normal and abnormal sleep in the elderly*. Handbook of clinical neurology/edited by PJ Vinken and GW Bruyn, vol. 98, page 653, 2011. (Cited on page 27.)
- [Crowley 2013] Kate E Crowley, SM Rajaratnam, Steven A Shea, Lawrence J Epstein, Charles A Czeisler, Steven W Lockley *et al.* *Evaluation of a single-channel nasal pressure device to assess obstructive sleep apnea risk in laboratory and home environments*. J Clin Sleep Med, vol. 9, no. 2, pages 109–116, 2013. (Cited on page 88.)
- [Davidovich 2016] M. L. Y. Davidovich, R. Karasik, A. Tal and Z. Shinar. *Sleep apnea screening with a contact-free under-the-mattress sensor*. In 2016 Computing in Cardiology Conference (CinC), pages 849–852, Sept 2016. (Cited on page 24.)
- [de Zambotti 2017] Massimiliano de Zambotti, Leonardo Rosas, Ian M. Colrain and Fiona C. Baker. *The Sleep of the Ring: Comparison of the \bar{O} URA Sleep Tracker Against Polysomnography*. Behavioral Sleep Medicine, vol. 0, no. 0, pages 1–15, 2017. PMID: 28323455. (Cited on page 20.)
- [Deepu 2012] C. J. Deepu, Z. Chen, J. T. Teo, S. H. Ng, X. Yang and Y. Lian. *A smart cushion for real-time heart rate monitoring*. In 2012 IEEE Biomedical Circuits and Systems Conference (BioCAS), pages 53–56, Nov 2012. (Cited on pages 50 and 54.)
- [Di Rienzo 2017] Marco Di Rienzo, Emanuele Vaini and Prospero Lombardi. *An algorithm for the beat-to-beat assessment of cardiac mechanics during sleep on Earth and in microgravity from the seismocardiogram*. Scientific Reports, vol. 7, no. 1, page 15634, 2017. (Cited on page 30.)
- [Díaz 2017] Camilo AR Díaz, Cátia Leitão, Carlos A Marques, M Fátima Domingues, Nélia Alberto, Maria José Pontes, Anselmo Frizzera, Moisés Ribeiro, Paulo SB André and Paulo FC Antunes. *Low-Cost Interrogation Technique for Dynamic Measurements with FBG-Based Devices*. Sensors, vol. 17, no. 10, page 2414, 2017. (Cited on page 50.)
- [Dimitrov 2016] Dimiter V Dimitrov. *Medical internet of things and big data in healthcare*. Healthcare informatics research, vol. 22, no. 3, pages 156–163, 2016. (Cited on page 5.)
- [Dziuda 2013a] Ł. Dziuda, M. Krej and F. W. Skibniewski. *Fiber Bragg Grating Strain Sensor Incorporated to Monitor Patient Vital Signs During MRI*. IEEE Sensors Journal, vol. 13, no. 12, pages 4986–4991, Dec 2013. (Cited on pages 51 and 54.)
- [Dziuda 2013b] Łukasz Dziuda, Franciszek W. Skibniewski, Mariusz Krej and Paulina M. Baran. *Fiber Bragg grating-based sensor for monitoring respiration and heart activity during magnetic resonance imaging examinations*.

- Journal of Biomedical Optics, vol. 18, pages 18 – 18 – 15, 2013. (Cited on pages 51 and 54.)
- [Dziuda 2014] Łukasz Dziuda and Franciszek W. Skibniewski. *A new approach to ballistocardiographic measurements using fibre Bragg grating-based sensors*. Biocybernetics and Biomedical Engineering, vol. 34, no. 2, pages 101 – 116, 2014. (Cited on pages 51 and 54.)
- [Dziuda 2015] Łukasz Dziuda. *Fiber-optic sensors for monitoring patient physiological parameters: a review of applicable technologies and relevance to use during magnetic resonance imaging procedures*. Journal of Biomedical Optics, vol. 20, pages 20 – 20 – 23, 2015. (Cited on page 51.)
- [Eblen-Zajjur 2003] Antonio Eblen-Zajjur. *A simple ballistocardiographic system for a medical cardiovascular physiology course*. Advances in Physiology Education, vol. 27, no. 4, pages 224–229, 2003. (Cited on pages xv and 28.)
- [Erdenebayar 2017] Urtnasan Erdenebayar, Jong-Uk Park, Pilsoo Jeong and Kyoung-Joung Lee. *Obstructive Sleep Apnea Screening Using a Piezo-Electric Sensor*. Journal of Korean medical science, vol. 32, no. 6, pages 893–899, 2017. (Cited on page 84.)
- [Erman 2007] Milton K Erman, Deirdre Stewart, Daniel Einhorn, Nancy Gordon and Eileen Casal. *Validation of the ApneaLink for the screening of sleep apnea: a novel and simple single-channel recording device*. J Clin Sleep Med, vol. 3, no. 4, pages 387–392, 2007. (Cited on page 88.)
- [Fajkus 2017a] Marcel Fajkus, Jan Nedoma, Radek Martinek, Vladimir Vasinek, Homer Nazeran and Petr Siska. *A non-invasive multichannel hybrid fiber-optic sensor system for vital sign monitoring*. Sensors, vol. 17, no. 1, page 111, 2017. (Cited on pages 52 and 54.)
- [Fajkus 2017b] Marcel Fajkus, Jan Nedoma, Radek Martinek and Wojciech Walendziuk. *Comparison of the FBG sensor encapsulated into PDMS and FBG sensor glued on the plexiglass pad for respiratory and heart rate monitoring*. In Photonics Applications in Astronomy, Communications, Industry, and High Energy Physics Experiments 2017, volume 10445, page 104450B. International Society for Optics and Photonics, 2017. (Cited on page 52.)
- [feng Hu 2016] Hai feng Hu, Si jia Sun, Ri qing Lv and Yong Zhao. *Design and experiment of an optical fiber micro bend sensor for respiration monitoring*. Sensors and Actuators A: Physical, vol. 251, no. Supplement C, pages 126 – 133, 2016. (Cited on page 50.)
- [Fernandes 2003] F. C. A. Fernandes, R. L. C. van Spaendonck and C. S. Burrus. *A new framework for complex wavelet transforms*. IEEE Transactions on Signal Processing, vol. 51, no. 7, pages 1825–1837, July 2003. (Cited on page 77.)

- [Gilaberte 2010] S. Gilaberte, J. Gómez-Clapers, R. Casanella and R. Pallas-Areny. *Heart and respiratory rate detection on a bathroom scale based on the ballistocardiogram and the continuous wavelet transform*. In 2010 Annual International Conference of the IEEE Engineering in Medicine and Biology, pages 2557–2560, Aug 2010. (Cited on page 75.)
- [Giovangrandi 2011] L. Giovangrandi, O. T. Inan, R. M. Wiard, M. Etemadi and G. T. A. Kovacs. *Ballistocardiography – A method worth revisiting*. In 2011 Annual International Conference of the IEEE Engineering in Medicine and Biology Society, pages 4279–4282, Aug 2011. (Cited on page 29.)
- [Guerrero 2013] G. Guerrero, J. M. Kortelainen, E. Palacios, A. M. Bianchi, G. Tachino, M. Tenhunen, M. O. Méndez and M. van Gils. *Detection of sleep-disordered breathing with Pressure Bed Sensor*. In 2013 35th Annual International Conference of the IEEE Engineering in Medicine and Biology Society (EMBC), pages 1342–1345, July 2013. (Cited on pages 34 and 36.)
- [Heise 2010] D. Heise and M. Skubic. *Monitoring pulse and respiration with a non-invasive hydraulic bed sensor*. In 2010 Annual International Conference of the IEEE Engineering in Medicine and Biology, pages 2119–2123, Aug 2010. (Cited on pages 47, 48 and 49.)
- [Heise 2011] D. Heise, L. Rosales, M. Skubic and M. J. Devaney. *Refinement and evaluation of a hydraulic bed sensor*. In 2011 Annual International Conference of the IEEE Engineering in Medicine and Biology Society, pages 4356–4360, Aug 2011. (Cited on pages 47 and 49.)
- [Heise 2013] D. Heise, L. Rosales, M. Sheahan, B. Y. Su and M. Skubic. *Non-invasive measurement of heartbeat with a hydraulic bed sensor Progress, challenges, and opportunities*. In 2013 IEEE International Instrumentation and Measurement Technology Conference (I2MTC), pages 397–402, May 2013. (Cited on page 48.)
- [Hoog Antink 2018] Christoph Hoog Antink, Florian Schulz, Steffen Leonhardt and Marian Walter. *Motion Artifact Quantification and Sensor Fusion for Unobtrusive Health Monitoring*. *Sensors*, vol. 18, no. 1, 2018. (Cited on page 100.)
- [Huang 1998] Norden E Huang, Zheng Shen, Steven R Long, Manli C Wu, Hsing H Shih, Quanan Zheng, Nai-Chyuan Yen, Chi Chao Tung and Henry H Liu. *The empirical mode decomposition and the Hilbert spectrum for nonlinear and non-stationary time series analysis*. *Proceedings of the Royal Society of London A: Mathematical, Physical and Engineering Sciences*, vol. 454, no. 1971, pages 903–995, 1998. (Cited on pages 70 and 71.)
- [Huang 2016] Norden E. Huang, Kun Hu, Albert C. C. Yang, Hsing-Chih Chang, Deng Jia, Wei-Kuang Liang, Jia Rong Yeh, Chu-Lan Kao, Chi-Hung Juan,

- Chung Kang Peng, Johanna H. Meijer, Yung-Hung Wang, Steven R. Long and Zhauhua Wu. *On Holo-Hilbert spectral analysis: a full informational spectral representation for nonlinear and non-stationary data*. Philosophical Transactions of the Royal Society of London A: Mathematical, Physical and Engineering Sciences, vol. 374, no. 2065, 2016. (Cited on page 71.)
- [Hwang 2014] S. H. Hwang, H. J. Lee, H. N. Yoon, D. W. Jung, Y. J. G. Lee, Y. J. Lee, D. U. Jeong and K. S. Park. *Unconstrained Sleep Apnea Monitoring Using Polyvinylidene Fluoride Film-Based Sensor*. IEEE Transactions on Biomedical Engineering, vol. 61, no. 7, pages 2125–2134, July 2014. (Cited on pages 84 and 91.)
- [Inan 2009] O T Inan, M Etemadi, R M Wiard, L Giovangrandi and G T A Kovacs. *Robust ballistocardiogram acquisition for home monitoring*. Physiological Measurement, vol. 30, no. 2, page 169, 2009. (Cited on pages 42 and 46.)
- [Inan 2010a] O. T. Inan, M. Etemadi, B. Widrow and G. T. A. Kovacs. *Adaptive Cancellation of Floor Vibrations in Standing Ballistocardiogram Measurements Using a Seismic Sensor as a Noise Reference*. IEEE Transactions on Biomedical Engineering, vol. 57, no. 3, pages 722–727, March 2010. (Cited on page 44.)
- [Inan 2010b] O. T. Inan, G. T. A. Kovacs and L. Giovangrandi. *Evaluating the Lower-Body Electromyogram Signal Acquired From the Feet As a Noise Reference for Standing Ballistocardiogram Measurements*. IEEE Transactions on Information Technology in Biomedicine, vol. 14, no. 5, pages 1188–1196, Sept 2010. (Cited on page 44.)
- [Inan 2015] O. T. Inan, P. F. Migeotte, K. S. Park, M. Etemadi, K. Tavakolian, R. Casanella, J. Zanetti, J. Tank, I. Funtova, G. K. Prisk and M. Di Rienzo. *Ballistocardiography and Seismocardiography: A Review of Recent Advances*. IEEE Journal of Biomedical and Health Informatics, vol. 19, no. 4, pages 1414–1427, July 2015. (Cited on pages 6 and 28.)
- [Inan 2018] Omer T. Inan, Maziyar Baran Pouyan, Abdul Q. Javaid, Sean Dowling, Mozziyar Etemadi, Alexis Dorier, J. Alex Heller, A. Ozan Bicen, Shuvo Roy, Teresa De Marco and Liviu Klein. *Novel Wearable Seismocardiography and Machine Learning Algorithms Can Assess Clinical Status of Heart Failure Patients*. Circulation: Heart Failure, vol. 11, no. 1, 2018. (Cited on page 30.)
- [Islam 2015] S. M. R. Islam, D. Kwak, M. H. Kabir, M. Hossain and K. S. Kwak. *The Internet of Things for Health Care: A Comprehensive Survey*. IEEE Access, vol. 3, pages 678–708, 2015. (Cited on page 5.)
- [Jaimcharyatam 2013] Nattapong Jaimcharyatam, Raed A Dweik, Roop Kaw and Loutfi S Aboussouan. *Polysomnographic determinants of nocturnal hypercapnia in patients with sleep apnea*. Journal of clinical sleep medicine: JCSM:

- official publication of the American Academy of Sleep Medicine, vol. 9, no. 3, page 209, 2013. (Cited on pages [xvi](#) and [84](#).)
- [Jennifer 2017] Abbasi Jennifer. *In-home, over-the-counter sleep apnea sensor on the horizon*. JAMA, vol. 317, no. 22, page 2271, 2017. (Cited on pages [xvi](#) and [85](#).)
- [Jeon 2015] LEE Jeon and Joseph Finkelstein. *Consumer sleep tracking devices: a critical review*. Digital Healthcare Empowering Europeans: Proceedings of MIE2015, vol. 210, page 458, 2015. (Cited on pages [19](#) and [21](#).)
- [Jiao 2016] C. Jiao, P. Lyons, A. Zare, L. Rosales and M. Skubic. *Heart beat characterization from ballistocardiogram signals using extended functions of multiple instances*. In 2016 38th Annual International Conference of the IEEE Engineering in Medicine and Biology Society (EMBC), pages 756–760, Aug 2016. (Cited on pages [48](#) and [49](#).)
- [Jin 2009] J. Jin, X. Wang, S. Li and Y. Wu. *A Novel Heart Rate Detection Algorithm in Ballistocardiogram Based on Wavelet Transform*. In Knowledge Discovery and Data Mining, 2009. WKDD 2009. Second International Workshop on, pages 76–79, Jan 2009. (Cited on page [75](#).)
- [Junnila 2005] S. Junnilla, A. Akhbardeh, A. Varri and T. Koivistoinen. *An EMFi-film sensor based ballistocardiographic chair: performance and cycle extraction method*. In IEEE Workshop on Signal Processing Systems Design and Implementation, 2005., pages 373–377, Nov 2005. (Cited on page [37](#).)
- [Junnila 2006] S. Junnilla, A. Akhbardeh, L. C. Barna, I. Defee and A. Varri. *A Wireless Ballistocardiographic Chair*. In 2006 International Conference of the IEEE Engineering in Medicine and Biology Society, pages 5932–5935, Aug 2006. (Cited on page [37](#).)
- [Kapadia 2009] A. Kapadia, D. Kotz and N. Triandopoulos. *Opportunistic sensing: Security challenges for the new paradigm*. In 2009 First International Communication Systems and Networks and Workshops, pages 1–10, Jan 2009. (Cited on page [64](#).)
- [Kapur 2017] Vishesh K Kapur, Dennis H Auckley, Susmita Chowdhuri, David C Kuhlmann, Reena Mehra, Kannan Ramar and Christopher G Harrod. *Clinical practice guideline for diagnostic testing for adult obstructive sleep apnea: an American Academy of Sleep Medicine clinical practice guideline*. J Clin Sleep Med, vol. 13, no. 3, pages 479–504, 2017. (Cited on page [5](#).)
- [Karki 2008] S. Karki and J. Lekkala. *Film-type transducer materials PVDF and EMFi in the measurement of heart and respiration rates*. In 2008 30th Annual International Conference of the IEEE Engineering in Medicine and Biology Society, pages 530–533, Aug 2008. (Cited on pages [38](#) and [41](#).)

- [Kärki 2009] S. Kärki and J. Lekkala. *A new method to measure heart rate with EMFi and PVDF materials*. Journal of Medical Engineering & Technology, vol. 33, no. 7, pages 551–558, 2009. (Cited on pages 38 and 41.)
- [Katz 2016] Y. Katz, R. Karasik and Z. Shinar. *Contact-free piezo electric sensor used for real-time analysis of inter beat interval series*. In 2016 Computing in Cardiology Conference (CinC), pages 769–772, Sept 2016. (Cited on pages 34 and 36.)
- [Kelly 2012] Jessica M Kelly, Robert E Strecker and Matt T Bianchi. *Recent developments in home sleep-monitoring devices*. ISRN neurology, vol. 2012, 2012. (Cited on pages 19, 20 and 21.)
- [Kimoff 2016] R. John Kimoff. *88 - Obstructive Sleep Apnea*. In V. Courtney Broaddus, Robert J. Mason, Joel D. Ernst, Talmadge E. King, Stephen C. Lazarus, John F. Murray, Jay A. Nadel, Arthur S. Slutsky and Michael B. Gotway, editors, Murray and Nadel’s Textbook of Respiratory Medicine (Sixth Edition), pages 1552 – 1568.e9. W.B. Saunders, Philadelphia, 2016. (Cited on pages 5 and 83.)
- [Koenig 2008] Steven M. Koenig, David Mack and Majd Alwan. *Sleep and sleep assessment technologies*, pages 77–120. Humana Press, Totowa, NJ, 2008. (Cited on pages 2, 15, 18 and 84.)
- [Koivistoinen 2004] T. Koivistoinen, S. Junnila, A. Varri and T. Koobi. *A new method for measuring the ballistocardiogram using EMFi sensors in a normal chair*. In The 26th Annual International Conference of the IEEE Engineering in Medicine and Biology Society, volume 1, pages 2026–2029, Sept 2004. (Cited on page 37.)
- [Kolla 2016] Bhanu Prakash Kolla, Subir Mansukhani and Meghna P. Mansukhani. *Consumer sleep tracking devices: a review of mechanisms, validity and utility*. Expert Review of Medical Devices, vol. 13, no. 5, pages 497–506, 2016. PMID: 27043070. (Cited on pages 19, 20, 21 and 22.)
- [Korhonen 2003] I. Korhonen, J. Parkka and M. Van Gils. *Health monitoring in the home of the future*. IEEE Engineering in Medicine and Biology Magazine, vol. 22, no. 3, pages 66–73, May 2003. (Cited on page 4.)
- [Kortelainen 2007] J. M. Kortelainen and J. Virkkala. *FFT averaging of multichannel BCG signals from bed mattress sensor to improve estimation of heart beat interval*. In 2007 29th Annual International Conference of the IEEE Engineering in Medicine and Biology Society, pages 6685–6688, Aug 2007. (Cited on pages 37, 41 and 81.)
- [Kortelainen 2010] J. M. Kortelainen, M. O. Mendez, A. M. Bianchi, M. Matteucci and S. Cerutti. *Sleep Staging Based on Signals Acquired Through Bed Sensor*.

- IEEE Transactions on Information Technology in Biomedicine, vol. 14, no. 3, pages 776–785, May 2010. (Cited on page 89.)
- [Kortelainen 2012] J. M. Kortelainen, M. van Gils and J. Pärkkä. *Multichannel bed pressure sensor for sleep monitoring*. In 2012 Computing in Cardiology, pages 313–316, Sept 2012. (Cited on pages 33, 34, 36 and 81.)
- [Kouroupetroglou 2014] C. Kouroupetroglou. Enhancing the human experience through assistive technologies and e-accessibility. *Advances in Medical Technologies and Clinical Practice*. IGI Global, 2014. (Cited on page 22.)
- [Krej 2015] M. Krej, Ł. Dziuda and F. W. Skibniewski. *A Method of Detecting Heartbeat Locations in the Ballistocardiographic Signal From the Fiber-Optic Vital Signs Sensor*. IEEE Journal of Biomedical and Health Informatics, vol. 19, no. 4, pages 1443–1450, July 2015. (Cited on pages 51 and 54.)
- [Kurihara 2012] Y. Kurihara and K. Watanabe. *Development of Unconstrained Heartbeat and Respiration Measurement System With Pneumatic Flow*. IEEE Transactions on Biomedical Circuits and Systems, vol. 6, no. 6, pages 596–604, Dec 2012. (Cited on pages 40 and 43.)
- [Lagakos 1987] Nicholas Lagakos, J. H. Cole and J. A. Bucaro. *Microbend fiber-optic sensor*. Appl. Opt., vol. 26, no. 11, pages 2171–2180, Jun 1987. (Cited on page 50.)
- [Lau 2013] D. Lau, Z. Chen, J. T. Teo, S. H. Ng, H. Rumpel, Y. Lian, H. Yang and P. L. Kei. *Intensity-Modulated Microbend Fiber Optic Sensor for Respiratory Monitoring and Gating During MRI*. IEEE Transactions on Biomedical Engineering, vol. 60, no. 9, pages 2655–2662, Sept 2013. (Cited on pages 50, 54, 58 and 59.)
- [Lee 2012] S.I. Lee, C. Ling, A. Nahapetian and M. Sarrafzadeh. *A mechanism for data quality estimation of on-body cardiac sensor networks*. In Consumer Communications and Networking Conference (CCNC), 2012 IEEE, pages 194–198, Jan 2012. (Cited on page 64.)
- [Lee 2016] Won Kyu Lee, Heenam Yoon, Chungmin Han, Kwang Min Joo and Kwang Suk Park. *Physiological signal monitoring bed for infants based on load-cell sensors*. Sensors, vol. 16, no. 3, page 409, 2016. (Cited on pages 45 and 46.)
- [Lin 2017a] F. Lin, Y. Zhuang, C. Song, A. Wang, Y. Li, C. Gu, C. Li and W. Xu. *SleepSense: A Noncontact and Cost-Effective Sleep Monitoring System*. IEEE Transactions on Biomedical Circuits and Systems, vol. 11, no. 1, pages 189–202, Feb 2017. (Cited on page 89.)
- [Lin 2017b] Y. Y. Lin, H. T. Wu, C. A. Hsu, P. C. Huang, Y. H. Huang and Y. L. Lo. *Sleep Apnea Detection Based on Thoracic and Abdominal Movement*

- Signals of Wearable Piezoelectric Bands*. IEEE Journal of Biomedical and Health Informatics, vol. 21, no. 6, pages 1533–1545, Nov 2017. (Cited on page 84.)
- [Liu 2016] Lili Liu, Eleni Stroulia, Ioanis Nikolaidis, Antonio Miguel-Cruz and Adriana Rios Rincon. *Smart homes and home health monitoring technologies for older adults: A systematic review*. International Journal of Medical Informatics, vol. 91, no. Supplement C, pages 44 – 59, 2016. (Cited on page 4.)
- [Liu 2017a] Mengxing Liu, Feng Jiang, He Jiang, Shuming Ye and Hang Chen. *Low-power, noninvasive measurement system for wearable ballistocardiography in sitting and standing positions*. Computers in Industry, vol. 91, no. Supplement C, pages 24 – 32, 2017. (Cited on pages 35 and 36.)
- [Liu 2017b] Yuhao Liu, Matt Pharr and Giovanni Antonio Salvatore. *Lab-on-Skin: A Review of Flexible and Stretchable Electronics for Wearable Health Monitoring*. ACS Nano, vol. 11, no. 10, pages 9614–9635, 2017. PMID: 28901746. (Cited on page 18.)
- [Luo 1999] Fei Luo, Jingyuan Liu, Naibing Ma and T.F. Morse. *A fiber optic microbend sensor for distributed sensing application in the structural strain monitoring*. Sensors and Actuators A: Physical, vol. 75, no. 1, pages 41 – 44, 1999. (Cited on page 50.)
- [Lydon 2015] K. Lydon, B. Y. Su, L. Rosales, M. Enayati, K. C. Ho, M. Rantz and M. Skubic. *Robust heartbeat detection from in-home ballistocardiogram signals of older adults using a bed sensor*. In 2015 37th Annual International Conference of the IEEE Engineering in Medicine and Biology Society (EMBC), pages 7175–7179, Aug 2015. (Cited on pages 48 and 49.)
- [Mack 2002] David C. Mack, Steve W. Kell, Majd Alwan, Beverly Turner and Robin A. Felder. *Non-Invasive Analysis of Physiological Signals (NAPS): A Low-Cost, Passive Monitor for Sleep Quality and Related Applications*. In Carillion Biomedical Institute Steps to Success Conference, Roanoke, VA: Carillion Biomedical Institute, October 2002. (Cited on page 84.)
- [Mack 2003] D Mack, S Kell, Majd Alwan, Beverly Turner and R Felder. *Non-invasive analysis of physiological signals (naps): A vibration sensor that passively detects heart and respiration rates as part of a sensor suite for medical monitoring*. In Summer Bioengineering Conference, pages 25–29, 2003. (Cited on page 84.)
- [Mack 2006] D. C. Mack, M. Alwan, B. Turner, P. Suratt and R. A. Felder. *A Passive and Portable System for Monitoring Heart Rate and Detecting Sleep Apnea and Arousals: Preliminary Validation*. In 1st Transdisciplinary Conference

- on Distributed Diagnosis and Home Healthcare, 2006. D2H2., pages 51–54, April 2006. (Cited on page 84.)
- [Mack 2009] D. C. Mack, J. T. Patrie, P. M. Suratt, R. A. Felder and M. Alwan. *Development and Preliminary Validation of Heart Rate and Breathing Rate Detection Using a Passive, Ballistocardiography-Based Sleep Monitoring System*. IEEE Transactions on Information Technology in Biomedicine, vol. 13, no. 1, pages 111–120, Jan 2009. (Cited on page 84.)
- [Mallat 1989] S. G. Mallat. *A theory for multiresolution signal decomposition: the wavelet representation*. IEEE Transactions on Pattern Analysis and Machine Intelligence, vol. 11, no. 7, pages 674–693, Jul 1989. (Cited on page 77.)
- [Martín-Yebra 2015] A. Martín-Yebra, F. Landreani, C. Casellato, E. Pavan, C. Frigo, P. F. Migeotte and E. G. Caiani. *Studying heart rate variability from ballistocardiography acquired by force platform: Comparison with conventional ECG*. In 2015 Computing in Cardiology Conference (CinC), pages 929–932, Sept 2015. (Cited on pages 34 and 36.)
- [Mihailidis 2011] Alex Mihailidis, Jennifer Boger, Jesse Hoey and Tizneem Jiancaro. *Zero effort technologies: Considerations, challenges, and use in health, wellness, and rehabilitation*. Synthesis Lectures on Assistive, Rehabilitative, and Health-Preserving Technologies, vol. 1, no. 2, pages 1–94, 2011. (Cited on page 1.)
- [Moghadas 2010] Amin A. Moghadas and Mehdi Shadaram. *Fiber Bragg Grating Sensor for Fault Detection in Radial and Network Transmission Lines*. Sensors, vol. 10, no. 10, pages 9407–9423, 2010. (Cited on page 50.)
- [Nedoma 2017] Jan Nedoma, Marcel Fajkus, Radek Martinek, Stanislav Kepak, Jakub Cubik, Stanislav Zabka and Vladimír Vasinek. *Comparison of BCG, PCG and ECG signals in application of heart rate monitoring of the human body*. In Telecommunications and Signal Processing (TSP), 2017 40th International Conference on, pages 420–424. IEEE, 2017. (Cited on pages 52 and 54.)
- [Ng 2009] SSS Ng, T-O Chan, K-W To, J Ngai, A Tung, FWS Ko and DSC Hui. *Validation of a portable recording device (ApneaLink) for identifying patients with suspected obstructive sleep apnoea syndrome*. Internal medicine journal, vol. 39, no. 11, pages 757–762, 2009. (Cited on page 88.)
- [Ni 2017] Hongbo Ni, Mingjie He, Guoxing Xu, Yalong Song and Xingshe Zhou. *Extracting heartbeat intervals using self-adaptive method based on ballistocardiography(bcg)*, pages 37–47. Springer International Publishing, Cham, 2017. (Cited on page 69.)

- [Niewolny 2013] David Niewolny. *How the Internet of Things Is Revolutionizing Healthcare*. Healthcare Segment Manager, Freescale Semiconductor, October 2013. (Cited on pages 2 and 5.)
- [Niizeki 2005] K. Niizeki, I. Nishidate, K. Uchida and M. Kuwahara. *Unconstrained cardiorespiratory and body movement monitoring system for home care*. Medical and Biological Engineering and Computing, vol. 43, no. 6, pages 716–724, Nov 2005. (Cited on pages 31 and 36.)
- [Noh 2010] Yun-Hong Noh, Soo-Young Ye and Do-Un Jeong. *Development of the BCG feature extraction methods for unconstrained heart monitoring*. In Computer Sciences and Convergence Information Technology (ICCIT), 2010 5th International Conference on, pages 923–928, Nov 2010. (Cited on page 75.)
- [Nukaya 2012] S. Nukaya, T. Shino, Y. Kurihara, K. Watanabe and H. Tanaka. *Noninvasive Bed Sensing of Human Biosignals Via Piezoceramic Devices Sandwiched Between the Floor and Bed*. IEEE Sensors Journal, vol. 12, no. 3, pages 431–438, March 2012. (Cited on page 45.)
- [Ong 2016] Adrian A. Ong and M. Boyd Gillespie. *Overview of smartphone applications for sleep analysis*. World Journal of Otorhinolaryngology-Head and Neck Surgery, vol. 2, no. 1, pages 45 – 49, 2016. (Cited on pages 19, 20 and 21.)
- [Oppenheim 2004] A. V. Oppenheim and R. W. Schaffer. *From frequency to quefrency: a history of the cepstrum*. IEEE Signal Processing Magazine, vol. 21, no. 5, pages 95–106, Sept 2004. (Cited on page 80.)
- [Paalasmaa 2008] Joonas Paalasmaa and Mika Ranta. *Detecting heartbeats in the ballistocardiogram with clustering*. In Proceedings of the ICML/UAI/COLT 2008 Workshop on Machine Learning for Health-Care Applications, Helsinki, Finland, volume 9, 2008. (Cited on pages 32 and 36.)
- [Paalasmaa 2012] J. Paalasmaa, M. Waris, H. Toivonen, L. Leppäkorpi and M. Partinen. *Unobtrusive online monitoring of sleep at home*. In 2012 Annual International Conference of the IEEE Engineering in Medicine and Biology Society, pages 3784–3788, Aug 2012. (Cited on pages 32 and 36.)
- [Paalasmaa 2015] J. Paalasmaa, H. Toivonen and M. Partinen. *Adaptive Heartbeat Modeling for Beat-to-Beat Heart Rate Measurement in Ballistocardiograms*. IEEE Journal of Biomedical and Health Informatics, vol. 19, no. 6, pages 1945–1952, Nov 2015. (Cited on pages 32 and 36.)
- [Park 2018] Kwang Suk Park and Heenam Yoon. *Ballistocardiography*, pages 127–155. Springer International Publishing, Cham, 2018. (Cited on pages 6 and 65.)

- [Peppard 2013] Paul E. Peppard, Terry Young, Jodi H. Barnet, Mari Palta, Erika W. Hagen and Khin Mae Hla. *Increased Prevalence of Sleep-Disordered Breathing in Adults*. American Journal of Epidemiology, vol. 177, no. 9, pages 1006–1014, 2013. (Cited on page 83.)
- [Percival 2006] Donald B Percival and Andrew T Walden. Wavelet methods for time series analysis, volume 4. Cambridge university press, 2006. (Cited on pages 76, 77 and 78.)
- [Pinheiro 2009] Eduardo Pinheiro, Octavian Postolache and Pedro Girão. *Blood pressure and heart rate variabilities estimation using ballistocardiography*. In Proceedings of the 7th Conf. on. Telecom, pages 125–128, 2009. (Cited on pages 38 and 41.)
- [Pinheiro 2010a] E. C. Pinheiro, O. A. Postolache and P. S. Girão. *Online heart rate estimation in unstable ballistocardiographic records*. In 2010 Annual International Conference of the IEEE Engineering in Medicine and Biology, pages 939–942, Aug 2010. (Cited on pages 38, 41 and 69.)
- [Pinheiro 2010b] Eduardo Pinheiro, Octavian Postolache and Pedro Girão. *Theory and developments in an unobtrusive cardiovascular system representation: ballistocardiography*. The open biomedical engineering journal, vol. 4, page 201, 2010. (Cited on pages xv, xix, 28 and 30.)
- [Pinheiro 2012] Eduardo Pinheiro, Octavian Postolache and Pedro Girão. *Study on ballistocardiogram acquisition in a moving wheelchair with embedded sensors*. Metrology and Measurement Systems, vol. 19, no. 4, pages 739–750, 2012. (Cited on pages 33 and 36.)
- [Pino 2015] E. J. Pino, J. A. P. Chávez and P. Aqueveque. *Noninvasive ambulatory measurement system of cardiac activity*. In 2015 37th Annual International Conference of the IEEE Engineering in Medicine and Biology Society (EMBC), pages 7622–7625, Aug 2015. (Cited on pages 39 and 41.)
- [Pino 2016] E. J. Pino, C. Larsen, J. Chavez and P. Aqueveque. *Non-invasive BCG monitoring for non-traditional settings*. In 2016 38th Annual International Conference of the IEEE Engineering in Medicine and Biology Society (EMBC), pages 4776–4779, Aug 2016. (Cited on pages 39 and 41.)
- [Poeggel 2015] Sven Poeggel, Daniele Tosi, DineshBabu Duraibabu, Gabriel Leen, Deirdre McGrath and Elfed Lewis. *Optical Fibre Pressure Sensors in Medical Applications*. Sensors, vol. 15, no. 7, pages 17115–17148, 2015. (Cited on page 50.)
- [Rashidi 2013] P. Rashidi and A. Mihailidis. *A Survey on Ambient-Assisted Living Tools for Older Adults*. IEEE Journal of Biomedical and Health Informatics, vol. 17, no. 3, pages 579–590, May 2013. (Cited on page 4.)

- [Ricart 2017] Ender Ricart, Thomas F. Osborne, Leonid A. Gavrilov and Gavin W. Hougham. *Current Major Challenges in Aging and Targets for Technology*. In Diane Chau and Thomas Osborne, editors, *Using Technology to Improve Care of Older Adults*, chapter 1, pages 1–18. Springer Publishing Company, New York, 1 édition, 2017. (Cited on pages 3, 4 and 5.)
- [Rilling 2003] G. Rilling, P. Flandrin and P. Gonçalves. *On empirical mode decomposition and its algorithms*. In *Proceedings of IEEE-EURASIP Workshop on Nonlinear Signal and Image Processing NSIP-03, Grado (Italy)*, June 2003. (Cited on pages 71 and 72.)
- [Rogers 2010] K. Rogers. *The respiratory system. Human body*. Britannica Educational Pub., 2010. (Cited on page 12.)
- [Rosales 2012] L. Rosales, M. Skubic, D. Heise, M. J. Devaney and M. Schaumburg. *Heartbeat detection from a hydraulic bed sensor using a clustering approach*. In *2012 Annual International Conference of the IEEE Engineering in Medicine and Biology Society*, pages 2383–2387, Aug 2012. (Cited on pages 47, 48 and 49.)
- [Rosales 2017] Licet Rosales, Bo Yu Su, Marjorie Skubic and KC Ho. *Heart rate monitoring using hydraulic bed sensor ballistocardiogram1*. *Journal of Ambient Intelligence and Smart Environments*, vol. 9, no. 2, pages 193–207, 2017. (Cited on pages 48 and 49.)
- [Russo 2015] Kathryn Russo, Balaji Goparaju and Matt T Bianchi. *Consumer sleep monitors: is there a baby in the bathwater?* *Nature and science of sleep*, vol. 7, page 147, 2015. (Cited on pages 19 and 21.)
- [Sadek 2015] I. Sadek, J. Biswas, V. F. S. Fook and M. Mokhtari. *Automatic heart rate detection from FBG sensors using sensor fusion and enhanced empirical mode decomposition*. In *2015 IEEE International Symposium on Signal Processing and Information Technology (ISSPIT)*, pages 349–353, Dec 2015. (Cited on pages 69 and 101.)
- [Sadek 2016] I. Sadek, J. Biswas, Z. Yongwei, Z. Haihong, J. Maniyeri, C. Zhihao, T. J. Teng, N. S. Huat and M. Mokhtari. *Sensor data quality processing for vital signs with opportunistic ambient sensing*. In *2016 38th Annual International Conference of the IEEE Engineering in Medicine and Biology Society (EMBC)*, pages 2484–2487, Aug 2016. (Cited on page 64.)
- [Sadek 2017a] I. Sadek, J. Biswas, B. Abdulrazak, Z. Haihong and M. Mokhtari. *Continuous and unconstrained vital signs monitoring with ballistocardiogram sensors in headrest position*. In *2017 IEEE EMBS International Conference on Biomedical Health Informatics (BHI)*, pages 289–292, Feb 2017. (Cited on pages 7, 90 and 101.)

- [Sadek 2017b] Ibrahim Sadek, Joaquim Bellmunt, Martin Kodyš, Bessam Abdulrazak and Mounir Mokhtari. Novel unobtrusive approach for sleep monitoring using fiber optics in an ambient assisted living platform, pages 48–60. Springer International Publishing, Cham, 2017. (Cited on page 1.)
- [Sadek 2018a] I. Sadek, E. Seet, J. Biswas, B. Abdulrazak and M. Mokhtari. *Non-intrusive Vital Signs Monitoring for Sleep Apnea Patients: A Preliminary Study*. IEEE Access, vol. 6, pages 2506–2514, 2018. (Cited on page 91.)
- [Sadek 2018b] Ibrahim Sadek. *Nonintrusive Vital Signs Monitoring for Sleep Apnea Patients: A Preliminary Study*. <https://www.codeocean.com/>, January 2018. (Cited on page 107.)
- [Sanchez 2017] Veralia Gabriela Sanchez, Carlos F Pfeiffer and Nils-Olav Skeie. *A Review of Smart House Analysis Methods for Assisting Older People Living Alone*. Journal of Sensor and Actuator Networks, vol. 6, no. 3, page 11, 2017. (Cited on page 27.)
- [Scarborough 1956] William R Scarborough, Samuel A Talbot, John R Braunstein, Maurice B Rappaport, William Dock, WF Hamilton, John E Smith, John L Nickerson and Isaac Starr. *Proposals for ballistocardiographic nomenclature and conventions: revised and extended*. Circulation, vol. 14, no. 3, pages 435–450, 1956. (Cited on pages xix and 30.)
- [Scholten 2011] Johan Scholten and Pascal Bakker. *Opportunistic Sensing in Train Safety Systems*. International journal on advances in networks and services, vol. 4, no. 3-4, pages 353–362, 2011. (Cited on page 64.)
- [Schumm 2010] Johannes Schumm. Quality assessment of physiological signals during ambulatory measurements. Ph.D. dissertation, ETH Zurich, 2010. (Cited on page 64.)
- [Seebo 2017] Seebo. *Smart Sleep: Using Smart Technology to Monitor and Improve Sleep*. <https://blog.seebo.com/smart-sleep-monitor-tracking/>, October 2017. (Accessed on 10/10/2017). (Cited on page 15.)
- [Sela 2016] I. Sela, Z. Shinar and K. Tavakolian. *Measuring left ventricular ejection time using under-the-mattress sensor*. In 2016 Computing in Cardiology Conference (CinC), pages 665–668, Sept 2016. (Cited on pages 35 and 36.)
- [Senaratna 2017] Chamara V. Senaratna, Jennifer L. Perret, Caroline J. Lodge, Adrian J. Lowe, Brittany E. Campbell, Melanie C. Matheson, Garun S. Hamilton and Shyamali C. Dharmage. *Prevalence of obstructive sleep apnea in the general population: A systematic review*. Sleep Medicine Reviews, vol. 34, pages 70 – 81, 2017. (Cited on page 83.)
- [Seo 2017] Youngmin Seo, Yunyoung Choi and Jeongwoo Choi. *River Stage Modeling by Combining Maximal Overlap Discrete Wavelet Transform, Support Vector*

- Machines and Genetic Algorithm*. Water, vol. 9, no. 7, page 525, 2017. (Cited on page 77.)
- [Shin 2006] Jaehyuk Shin, Youngjoon Chee and Kwangsuk Park. *Long-term sleep monitoring system and long-term sleep parameters using unconstrained method*. In Intl. Special Topic Conf. on Info. Tech. in BME, Ioannina-Epirus, Greece, 2006. (Cited on pages 40 and 43.)
- [Shin 2010] J. H. Shin, Y. J. Chee, D. U. Jeong and K. S. Park. *Nonconstrained Sleep Monitoring System and Algorithms Using Air-Mattress With Balancing Tube Method*. IEEE Transactions on Information Technology in Biomedicine, vol. 14, no. 1, pages 147–156, Jan 2010. (Cited on pages 42, 43 and 89.)
- [Starr 1939] Isaac Starr, AJ Rawson, HA Schroeder and NR Joseph. *Studies on the estimation of cardiac output in man, and of abnormalities in cardiac function, from the heart's recoil and the blood's impacts; the ballistocardiogram*. American Journal of Physiology–Legacy Content, vol. 127, no. 1, pages 1–28, 1939. (Cited on pages xv and 28.)
- [Starr 1940] Isaac Starr and Henry A Schroeder. *Ballistocardiogram. II. Normal standards, abnormalities commonly found in diseases of the heart and circulation, and their significance*. Journal of Clinical Investigation, vol. 19, no. 3, page 437, 1940. (Cited on pages xv and 28.)
- [Story 2017] L. Story. Pathophysiology: A practical approach. Jones & Bartlett Learning, 2017. (Cited on page 11.)
- [Su 2012] B. Y. Su, K. C. Ho, M. Skubic and L. Rosales. *Pulse rate estimation using hydraulic bed sensor*. In 2012 Annual International Conference of the IEEE Engineering in Medicine and Biology Society, pages 2587–2590, Aug 2012. (Cited on pages 47, 48 and 49.)
- [Tal 2017] Asher Tal, Zvika Shinar, David Shaki, Shlomi Codish and Aviv Goldbart. *Validation of contact-free sleep monitoring device with comparison to polysomnography*. J Clin Sleep Med, vol. 13, no. 3, pages 517–522, 2017. (Cited on page 24.)
- [Tiberghien 2011] Thibaut Tiberghien, Mounir Mokhtari, Hamdi Aloulou, Jit Biswas, Jiaqi Zhu and Vwen Yen Lee. *Handling User Interface Plasticity in Assistive Environment: UbiSMART Framework*. In Bessam Abdulrazak, Sylvain Giroux, Bruno Bouchard, H el ene Pigot and Mounir Mokhtari, editors, Toward Useful Services for Elderly and People with Disabilities: 9th International Conference on Smart Homes and Health Telematics, ICOST 2011, Montreal, Canada, June 20-22, 2011. Proceedings, pages 256–260. Springer Berlin Heidelberg, Berlin, Heidelberg, 2011. (Cited on page 60.)
- [Torres 2011] M.E. Torres, M.A. Colominas, G. Schlotthauer and P. Flandrin. *A complete ensemble empirical mode decomposition with adaptive noise*. In

- Acoustics, Speech and Signal Processing (ICASSP), 2011 IEEE International Conference on, pages 4144–4147, May 2011. (Cited on page 71.)
- [Tortora 2008] G.J. Tortora and B.H. Derrickson. Principles of anatomy and physiology. John Wiley & Sons, 2008. (Cited on pages 10 and 11.)
- [United Nations 2017] Department of Economic United Nations and Population Division (2017) Social Affairs. *World Population Prospects: The 2017 Revision, Key Findings and Advance Tables. ESA/P/WP/248*, 2017. (Cited on page 2.)
- [van Hoof 2011] J. van Hoof, H.S.M. Kort, P.G.S. Rutten and M.S.H. Duijnste. *Ageing-in-place with the use of ambient intelligence technology: Perspectives of older users*. International Journal of Medical Informatics, vol. 80, no. 5, pages 310 – 331, 2011. (Cited on page 4.)
- [Vehkaoja 2013] Antti Vehkaoja, Satu Rajala, Pekka Kumpulainen and Jukka Leikkala. *Correlation approach for the detection of the heartbeat intervals using force sensors placed under the bed posts*. Journal of Medical Engineering & Technology, vol. 37, no. 5, pages 327–333, 2013. (Cited on pages 45 and 46.)
- [Vogt 2012] Emelie Vogt, David MacQuarrie and John Patrick Neary. *Using ballistocardiography to measure cardiac performance: a brief review of its history and future significance*. Clinical Physiology and Functional Imaging, vol. 32, no. 6, pages 415–420, 2012. (Cited on page 29.)
- [Waltisberg 2017] D. Waltisberg, O. Amft, D. P. Brunner and G. Tröster. *Detecting Disordered Breathing and Limb Movement Using In-Bed Force Sensors*. IEEE Journal of Biomedical and Health Informatics, vol. 21, no. 4, pages 930–938, July 2017. (Cited on page 85.)
- [Wang 2002] J.Y. Wang. *A new method for evaluating ECG signal quality for multi-lead arrhythmia analysis*. In Computers in Cardiology, 2002, pages 85–88, Sept 2002. (Cited on page 64.)
- [Wang 2003] Feng Wang, Mami Tanaka and Seiji Chonan. *Development of a PVDF Piezopolymer Sensor for Unconstrained In-Sleep Cardiorespiratory Monitoring*. Journal of Intelligent Material Systems and Structures, vol. 14, no. 3, pages 185–190, 2003. (Cited on pages 31 and 36.)
- [Wang 2007] Feng Wang, Yanhui Zou, Mami Tanaka, Tadashi Matsuda and Seiji Chonan. *Unconstrained cardiorespiratory monitor for premature infants*. International Journal of Applied Electromagnetics and Mechanics, vol. 25, no. 1-4, pages 469–475, 2007. (Cited on pages 31 and 36.)
- [Wang 2017] Zhu Wang, Xingshe Zhou, Weichao Zhao, Fan Liu, Hongbo Ni and Zhiwen Yu. *Assessing the severity of sleep apnea syndrome based on ballistocardiogram*. PloS one, vol. 12, no. 4, page e0175351, 2017. (Cited on page 84.)

- [Watanabe 2004] T. Watanabe and K. Watanabe. *Noncontact method for sleep stage estimation*. IEEE Transactions on Biomedical Engineering, vol. 51, no. 10, pages 1735–1748, Oct 2004. (Cited on pages 40 and 89.)
- [Watanabe 2005] K. Watanabe, T. Watanabe, H. Watanabe, H. Ando, T. Ishikawa and K. Kobayashi. *Noninvasive measurement of heartbeat, respiration, snoring and body movements of a subject in bed via a pneumatic method*. IEEE Transactions on Biomedical Engineering, vol. 52, no. 12, pages 2100–2107, Dec 2005. (Cited on pages 40 and 43.)
- [Wiard 2011] Richard M. Wiard, Omer T. Inan, Brian Argyres, Mozziyar Etemadi, Gregory T. A. Kovacs and Laurent Giovangrandi. *Automatic detection of motion artifacts in the ballistocardiogram measured on a modified bathroom scale*. Medical & Biological Engineering & Computing, vol. 49, no. 2, pages 213–220, Feb 2011. (Cited on page 44.)
- [Wiles 2012] Janine L. Wiles, Annette Leibing, Nancy Guberman, Jeanne Reeve and Ruth E. S. Allen. *The Meaning of “Aging in Place” to Older People*. The Gerontologist, vol. 52, no. 3, pages 357–366, 2012. (Cited on page 3.)
- [Wu 2009a] Zhaohua Wu and Norden E Huang. *Ensemble empirical mode decomposition: a noise-assisted data analysis method*. Advances in adaptive data analysis, vol. 1, no. 01, pages 1–41, 2009. (Cited on page 71.)
- [Wu 2009b] Zhaohua Wu and Norden E Huang. *Ensemble empirical mode decomposition: a noise-assisted data analysis method*. Advances in adaptive data analysis, vol. 1, no. 01, pages 1–41, 2009. (Cited on page 99.)
- [Xin 2016] Yi Xin, Chao Guo, Xiaohui Qi, Hongying Tian, Xiang Li, Qiang Dai, Shuhong Wang and Cheng Wang. *Wearable and unconstrained systems based on PVDF sensors in physiological signals monitoring: A brief review*. Ferroelectrics, vol. 500, no. 1, pages 291–300, 2016. (Cited on page 31.)
- [Zaunseder 2017] S. Zaunseder, A. Henning, D. Wedekind, A. Trumpp and H. Malberg. *Unobtrusive acquisition of cardiorespiratory signals*. Somnologie, vol. 21, no. 2, pages 93–100, Jun 2017. (Cited on page 22.)
- [Zheng 2014] Y. L. Zheng, X. R. Ding, C. C. Y. Poon, B. P. L. Lo, H. Zhang, X. L. Zhou, G. Z. Yang, N. Zhao and Y. T. Zhang. *Unobtrusive Sensing and Wearable Devices for Health Informatics*. IEEE Transactions on Biomedical Engineering, vol. 61, no. 5, pages 1538–1554, May 2014. (Cited on page 5.)
- [Zhu 2013] Y. Zhu, H. Zhang, M. Jayachandran, A. K. Ng, J. Biswas and Z. Chen. *Ballistocardiography with fiber optic sensor in headrest position: A feasibility study and a new processing algorithm*. In 2013 35th Annual International Conference of the IEEE Engineering in Medicine and Biology Society (EMBC), pages 5203–5206, July 2013. (Cited on pages 51 and 54.)

- [Zhu 2014] Y. Zhu, V. F. S. Fook, E. H. Jianzhong, J. Maniyeri, C. Guan, H. Zhang, E. P. Jiliang and J. Biswas. *Heart rate estimation from FBG sensors using cepstrum analysis and sensor fusion*. In 2014 36th Annual International Conference of the IEEE Engineering in Medicine and Biology Society, pages 5365–5368, Aug 2014. (Cited on pages 52, 54 and 81.)
- [Zhu 2015] Y. Zhu, J. Maniyeri, V. F. S. Fook and H. Zhang. *Estimating respiratory rate from FBG optical sensors by using signal quality measurement*. In 2015 37th Annual International Conference of the IEEE Engineering in Medicine and Biology Society (EMBC), pages 853–856, Aug 2015. (Cited on pages 52 and 54.)
- [Zink 2015] Matthias Daniel Zink, Christoph Brüser, Patrick Winnersbach, Andreas Napp, Steffen Leonhardt, Nikolaus Marx, Patrick Schauerte and Karl Mischke. *Heartbeat cycle length detection by a ballistocardiographic sensor in atrial fibrillation and sinus rhythm*. BioMed research international, vol. 2015, 2015. (Cited on pages 39 and 41.)
- [Zink 2017] Matthias Daniel Zink, Christoph Brüser, Björn-Ole Stüben, Andreas Napp, Robert Stöhr, Steffen Leonhardt, Nikolaus Marx, Karl Mischke, Jörg B Schulz and Johannes Schiefer. *Unobtrusive Nocturnal Heartbeat Monitoring by a Ballistocardiographic Sensor in Patients with Sleep Disordered Breathing*. Scientific Reports, vol. 7, no. 1, page 13175, 2017. (Cited on pages 39 and 41.)